Department of Biomedical and Biotechnological Sciences

Ph.D. in Biotechnology

Curriculum in Pharmaceutical Biotechnology

XXXV Cycle

CRISTINA TORRISI

DESIGN, PREPARATION AND CHARACTERIZATION OF NANOPARTICLE SYSTEMS AS CARRIERS OF BIOLOGICALLY ACTIVE SUBSTANCES

Ph.D. Thesis

Tutor: *Prof.ssa Maria Grazia Sarpietro*

Coordinator: *Prof. Vito De Pinto*

ACADEMIC YEARS 2019/2022

SOMMARIO

I polifenoli costituiscono una delle più grandi famiglie di molecole organiche naturali, largamente presenti nel regno vegetale, ma ottenibili anche per semisintesi. Dal punto di vista chimico, essi sono caratterizzati dalla presenza di uno o più gruppi fenolici che, in funzione dei loro legami e dei sostituenti, conferiscono alle molecole una diversa attività biologica. Negli ultimi anni i ricercatori hanno dimostrato il loro contributo nel ridurre diversi disturbi quali: ipertensione, asma, osteoporosi, aterosclerosi, disturbi neurologici e oculari. Tuttavia, il loro utilizzo è limitato a causa della loro bassa stabilità all'esposizione all'ambiente esterno, bassa solubilità e permeabilità ma, soprattutto, rapido metabolismo. Una strategia per superare questi problemi è data dall'utilizzo di carriers che siano in grado di proteggere le molecole e veicolarle nei siti di interesse, aumentandone così la loro biodisponibilità: tra essi, i sistemi lipidici nanoparticellari si sono particolarmente distinti grazie alla loro elevata biocompatibilità e biodegradabilità, inoltre le dimensioni modulabili li rendono adatti ad essere impiegati attraverso svariate vie di somministrazione. L'obiettivo di questo lavoro di tesi è stato quello di ottimizzare Solid Lipid Nanoparticles (SLN) e Nanostructured Lipid Carriers (NLC) per incapsulare diverse molecole appartenenti alla classe dei polifenoli; tali carrier lipidici sono stati disegnati, preparati e caratterizzati da un punto di vista chimico-fisico, biologico e termotropico.

ABSTRACT

Polyphenols are one of the largest families of natural organic molecules, widely present in the plant kingdom, but also obtainable from semisynthetic ways. From a chemical perspective, they are characterized by one or more phenolic moieties which, based on their bonds and substituents, confer to the compounds a different biological activity. Recently, most research have underlined the potential beneficial influence of polyphenols on various disorders such as: hypertension, asthma, osteoporosis, atherosclerosis, neurological diseases and eye disorders. However, their use is limited due to their low stability to external environmental factors (namely light and oxidation), insufficient aqueous solubility, scarce permeability and rapid metabolism. These problems are overridden by the employment of carriers which protect the molecules and transport them to the targeted site, thus increasing their bioavailability: among them, the lipid nanocarriers have distinguished themselves thanks to their high biocompatibility and biodegradability, furthermore the modular dimensions make them suitable for usage through various routes of administration. The aim of this thesis is to optimize Solid Lipid Nanoparticles (SLN) and Nanostructured Lipid Carriers (NLC) to encapsulate different actives belonging to the polyphenol class; these lipid carriers have been designed, prepared, through different techniques, and characterized by a chemical-physical, biological and thermotropic standpoint.

KEYWORDS AND ABBREVIATIONS

Keywords:

Polyphenols; Solid Lipid Nanoparticles; Nanostructured Lipid Carriers; Liposomes; Differential Scanning Calorimetry; Biomembrane models; Benzo[k,l]xanthene lignans; Mangiferin; Human Foreskin Fibroblast; Topical application.

Abbreviations:

PC	Phenolic compounds
PAs	Phenolic acids
BXLs	Benzo[k,l]xanthene lignans
SLN	Solid Lipid Nanoparticles
NLC	Nanostructured Lipid Carriers
DSC	Differential Scanning Calorimetry
MLV	Multilamellar Vesicles
DMPC	Dimyristoylphosphatidylcholine
MGN	Mangiferin
HFF-1	Human Foreskin Fibroblast
PDI	Polydispersity index
ZP	Zeta Potential
HPH	High Pressure Homogenization

AFFILIATIONS

2019-2022 – PhD Student

Laboratory of Thermal Analysis, Department of Drug and Health Sciences, University of Catania, Viale Andrea Doria 6, 95125 Catania, Italy;

July 2022 – Visiting student

Laboratory of Pharmaceutical Technology, Department of Drug Sciences, Faculty of Pharmacy, University of Porto, Rua de Jorge Viterbo Ferreira, 228, 4050-313, Porto, Portugal.

INDEX

1. PROJECT SUMMARY

1.1. General introduction

1.1.1. Phenolic compounds

In the last decade, researchers have placed their attention on natural products due to their safe toxicological profile, numerous biological applications, and their probable role in the prevention of various diseases[1]. One of the most diverse groups of bioactive molecules in nature are phenolic compounds (PC) widespread in vegetables, fruits and cereals. PC are a class of secondary metabolites in plants, in which they are responsible for pigmentation and protection against UV light, parasites and insects; they also represent a panacea for human health. In recent years, numerous studies have reported the diverse biological effects of PC and their contribution in reducing the risk of insurgence of several conditions as atherosclerosis, hypertension, stroke, prostate cancer, asthma, osteoporosis, eye and neurological diseases[2]. From the chemical point of view, these molecules are characterized by one or more aromatic rings with one or more hydroxyl moieties which allow to classify them in two main groups: flavonoids (e.g., anthocyanins, flavanols, flavanones, flavonols, and isoflavones) and non-flavonoids (e.g., phenolic acids, xanthones, stilbenes, lignans, and tannins)[3]. The structure of PC play an important role for the biological activities because many of them can be attributed to the potent properties as free radical scavengers (e.g. ROS/RNS) and metal-ion chelators[4].

Flavonoids

Flavonoids are the most abundant family of polyphenols present in human diet. Their structure is constituted of two aromatic rings linked through three carbons, that frequently form an oxygenated heterocycle. Different arrangements in the basic structure define the different subgroups of flavonoids as shown in Fig.1. The characteristic structure is able to support the scavenging of free radicals and the chelation of redox-active metals, so the benefits of flavonoids are certainly to be attributed to this ability. It was reported that they can be highly functional in pathological situation associated with high free radical production such as hypertension and cardiovascular diseases[5].

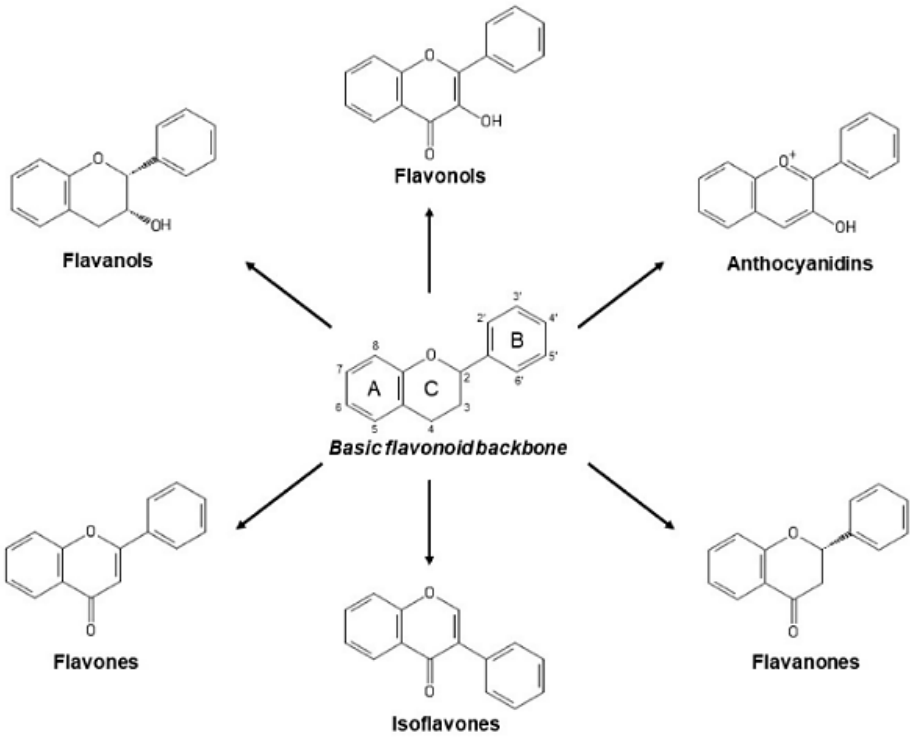

Figure 1: Structure of flavonoids

Phenolic acids

Phenolic acids (PAs) are a class of phenolic compounds characterized by a carboxylic acid group. They are mainly divided into two sub-groups: hydroxybenzoic and hydroxycinnamic acids. Ferulic, caffeic, p-coumaric and sinapic acids are the four most common hydroxycinnamic acids widely present in food; p-hydroxybenzoic, protocatechuic, vanillic, and syringic acids are the four commons hydroxybenzoic acids. As compared to hydroxycinnamic acids, hydroxybenzoic acids are generally found in low concentration in red fruits, onions and black radish[6]. PAs are the most widespread bioactive molecules in the plant kingdom in which they have an important role in growth, reproduction, and defence against environmental stress and microorganisms. Among the biological activities, the most prevalent is certainly the antioxidant activity but numerous studies have also reported anti-inflammatory, anticancer, hepatic and cardio protective activities[7].

Xanthones, stilbenes, lignans, and tannins

Xanthones present a distinctive chemical structure composed of a tricyclic aromatic system (C6-C3-C6) which, based on its tricyclic scaffold and the nature and/or position

of the substituents, shows different biological activities such as anticancer, anti-bacterial, anti-inflammatory, and antidiabetic[8].

Stilbenes show a characteristic structure constituted of two benzene rings connected by double bond, according to which, they are divided into the isomers Z and E. The most important isomer is E and changing the isomerization type generally makes its biological activity to decrease.

Lignans have a chemical structure composed of the combination of two phenylpropanoid (C6-C3) units linked by the central carbons to the side chains, and belong to the group of phytoestrogens[9]. They are widely distributed in beverages, vegetables and cereals and a lot of studies have shown a large spectrum of health-promoting effects, such as protective effects against cancer, osteoporosis, and coronary heart diseases due to their antitumoral, antioxidant, and antiestrogenic properties[10].

Tannins are defined as water soluble phenolic compounds, due to the large number of hydroxyl groups. They can be classified into two subclasses: hydrolysable and non-hydrolysable or condensed tannins. The first group is composed of a mix of simple phenols conjugated with carbohydrates, in fact after hydrolyzation they produce phenolic acids and carbohydrate molecules. Condensed tannins are more complex molecules composed of flavan-3-ol nuclei which form oligomers or polymers[11].

The beneficial properties of polyphenolic compounds above mentioned are usually observed *in vitro*; when the experiments are extended *in vivo*, the use of PC is limited by many factors such as low stability to external physical effects (light and oxidation), low solubility, low permeability and rapid metabolism. In order to overcome these limitations, polyphenols can be loaded into various carriers to enhance their bioavailability[12], [13]. In recent years, a lot of nano-drug-delivery systems (NDDS) have been developed for the delivery of polyphenolic compounds, including liposomes, polymeric and lipid nanoparticles. NDDS demonstrated impressive features in improving drug therapy due to their ability to increase drug stability, to solubilize poorly soluble drugs and to achieve the controlled delivery and targeting of different compounds[14].

1.1.2. Lipid based nanoparticles

Lipid based nanoparticles are safe carriers, made from natural or synthetic lipids, in the range of 30 to 1000 nm. The most used lipids are fatty acids (i.e., palmitic, myristic, and

stearic acids), glycerides (i.e., glyceryl monostearate and caprate), complex glyceride mixtures or even waxes which make vehicles to have excellent biodegradability and biocompatibility; for these reasons they can be considered ideal candidates for drug delivery systems in biomedical applications[15]. Lipid nanoparticles are suitable carriers for both hydrophilic and lipophilic drugs and, based on the composition of lipid matrix, they can be classified into two types: a first generation called Solid Lipid Nanoparticles (SLNs) and a second one called Nanostructured Lipid Carriers (NLCs)[16] (Fig. 2).

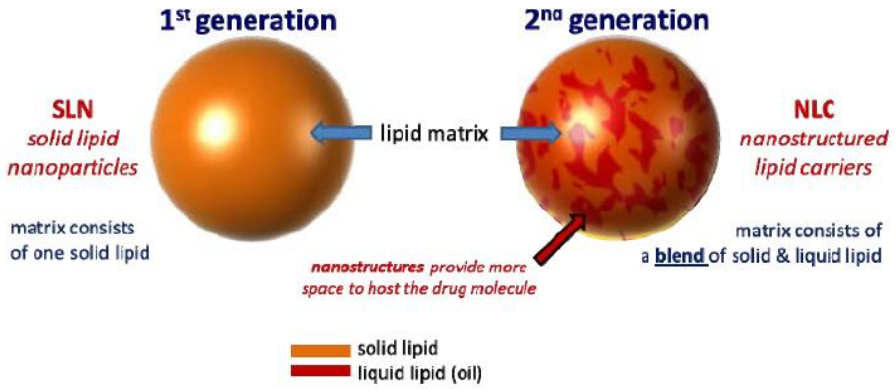

Figure 2: Representation of SLN and NLC

1.1.2.1. Solid Lipid Nanoparticles (SLN)

SLN were introduced in 1990 as alternative carrier systems to emulsions, liposomes, and polymeric nanoparticles due to their ability to combine advantages of the traditional carriers and avoid some of their major disadvantages. SLN are colloidal systems consisting of a mixture of one or more solid lipids at room and body temperature, plus surfactants and water. They are formulated using biodegradable lipids that are Generally Recognized As Safe (GRAS), in fact one of their major benefits is the absence of toxicity; they also possess excellent physical stability, chemical versatility, biocompatibility and biodegradability, low cost and suitability for high scale production. The lipid concentration employed is usually in a range 0.1 - 30% while the surfactants' one is between 0.5 and 5%. The most used surfactants are poloxamers, polysorbates, soybean and egg lecithin[17]. SLN are able to encapsulate both hydrophilic and lipophilic compounds, controlling their delivery and protecting them from degradation. According to the data published by the group of Mehnert[18], SLN have a highly organized crystalline structure defined as a "symmetric brick wall model" in which drugs can be encapsulated in different ways, obtaining three different morphologies (Fig. 3):

- Homogeneous matrix model: the drug is dispersed in the solid solution;
- Drug-enriched shell model: the drug is bound to the shell of the nanoparticles;
- Drug-enriched core model: the drug is mainly localized in the lipid core.

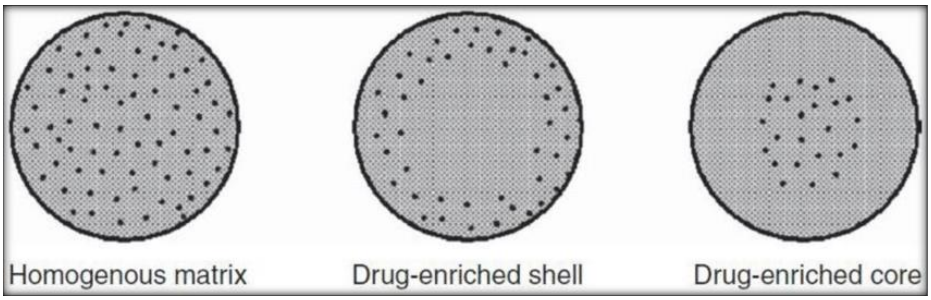

Figure 3: Types of SLN: Homogeneous matrix model (a), drug-enriched shell model (b), drug-enriched core model (c).

Although SLN represent innovative and excellent drug delivery systems, sometimes the crystalline structure can lead to potential limitations that have been overcome with the second generation of lipid nanoparticles, NLC[19].

1.1.2.2. Nanostructured lipid carriers (NLC)

NLC were developed to solve some problems associated with SLN such as minor drug loading capacity and prominent drug expulsion during storage. They are produced from a mixture of solid and liquid lipids, surfactants and water. Liquid oils typically used for NLC are Mygliol, paraffin oil, 2-octyl dodecanol, propylene glycol dicaprylocaprate (Labrafac®), isopropyl myristate and squalene. The addition of a liquid lipid to the solid matrix leads to the formation of an amorphous structure defined as "welsh natural stone wall model". This structure improves the solubility of the drugs because the solubility of compounds is usually higher in liquid lipids, compared with solid lipid, and allow the drug to have a better accommodation in the structure itself minimizing its expulsion. Three kinds of NLC structures have been proposed: imperfect (type I), amorphous (type II), and multiple (type III) (Fig. 4). The first kind of structure is obtained mixing solid lipids with small amounts of liquid lipids. The addition of liquid lipids creates a disorder in the crystalline structure and generate imperfections which are able to increase the drug loading. The second structure, called the amorphous model, is created mixing solid lipids with special liquid lipids (i.e. hydroxyoctacosanyl hydroxystearate and isopropyl myristate) which do not recrystallize after homogenization and cooling. The lack of a

crystalline structure can reduce the leakage of the loaded drug. The third kind, known as multiple structure, contains a higher liquid lipid concentration than the other structures and it has been developed to improve the loading capacity of several drugs, like the ones whose solubility in liquid lipids is higher than in solid lipids. So, NLC type III can achieve a better drug loading and slower drug release[20].

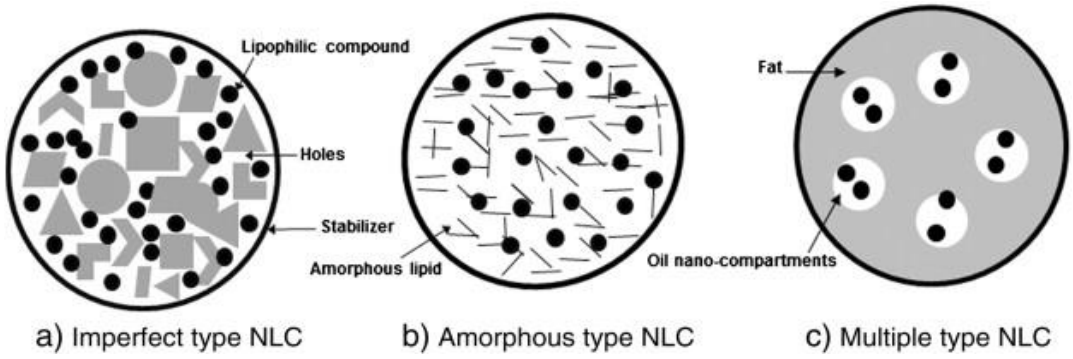

Figure 4: Types of NLC - imperfect (type I), amorphous (type II), and multiple (type III)

1.1.2.3. Preparation of lipid nanoparticles

Different approaches for the preparation of lipid nanoparticles have been reported since these carriers were first described in 1990s[18]. These methods can be divided into two groups: techniques which require a high energy approach such as high-pressure homogenization, high sheer homogenization and/or ultrasonication and techniques which undergo a low energy approach such as solvent-based techniques and phase inversion temperature technique. The preparation method represents an important factor which influences the performance and the characteristics of lipid nanoparticles; it is chosen according to the physicochemical properties of the drug to be incorporated and to the desired nanoparticle characteristics[21].

High pressure homogenization

High pressure homogenization (HPH) technology is an established and potent technique for large-scale production of lipid nanoparticles. The operating mechanism of high-pressure homogenizers is to firstly push a liquid with high pressure (100–2000 bar) through a narrow gap (in the range of a few microns); then the fluid accelerates in a very short distance at high velocity (over 1000 km/h) and the strong shear stress and cavitation forces disrupt the particles down to the sub-micron dimensions. This technique has several advantages including large-scale production, absence of organic solvents,

improved product stability and loading of drugs[22]. Two homogenization approaches have been developed: the hot homogenization and the cold homogenization. In both cases, the pharmaceutical compound is dissolved or dispersed in the melted lipid before the HPH.

In the hot homogenization technique, a pre-emulsion is first prepared and then submitted to HPH at temperatures above the melting point of lipids. In general, the quality of pre-emulsion and the temperature have an influence on the final product. Usually, higher temperatures give lower particle sizes[23].

In the cold homogenization, more suitable for thermolabile compounds, the melted lipid containing drug is rapidly cooled with dry ice or liquid nitrogen and milled in microparticles in the range of 50-100 microns. The solid lipid microparticles are then dispersed in a cold emulsifier solution and subjected to high pressure homogenization at temperatures below the melting point of the lipid. In general, cold homogenization gives larger particle sizes and a broader size distribution compared to hot homogenization[24].

High Shear Homogenization and/or Ultrasound

High shear homogenization and ultrasonication are dispersing techniques in which the solid lipid is primarily heated to approximately 5–10 °C above its melting point and then dispersed in an aqueous surfactant solution at the same temperature under high-speed stirring to form an emulsion. The latter is subsequently submitted to sonication to reduce the size of the particles. Afterwards, the samples are cooled to room temperature or lower temperatures to form the lipid nanoparticles by lipid crystallization. However, there are some disadvantages of these methods, such as a low dispersion of nanoparticles due to the presence of microparticles in the HSH technique or the metal contamination from probe erosion during sonication which can affect the physical stability of the SLN[25].

Solvent based methods

Solvent based methods, thanks to the mild operating temperatures, are often used for the encapsulation of thermosensitive drugs which have problems of stability and bioavailability; although one of the limiting aspects is the toxicity of the solvents[26].

They can be divided in:

• Solvent injection;

• Solvent evaporation/diffusion from emulsions;

In the first method, the lipid and the drug are dissolved in a water-miscible organic solvent (ethanol, acetone, isopropanol) and the final solution is injected through a syringe needle in water under stirring. Nanoparticles will be formed by precipitation of the lipid in water[27].

In the second one, the lipid is initially dissolved in an organic solvent (cyclohexane, chloroform, ethyl acetate) and emulsified in an aqueous solution of surfactant to yield an organic solvent-in-water emulsion. A lipid nanoparticle dispersion is then formed after the removing of the solvent either by evaporation (solvent evaporation technique for volatile solvents) or by water dilution (solvent diffusion technique for partially water miscible solvents)[28],[29].

Phase Inversion Temperature (PIT) method

The PIT is one of the most common methods for the preparation of nano emulsions based on the ability of some polyethoxylated surfactants to modify their affinities for water and oil as a function of the temperature. This leads to the switch from O/W macroemulsion to a W/O emulsion when temperature is above the PIT, and to the formation of a O/W nano emulsion when the temperature is below the PIT[30].

The lipid and the aqueous phase are separately heated at temperature above the melting point of the main lipid; then the aqueous phase is added dropwise, at constant temperature and under agitation, to the lipid phase, in order to obtain a W/O emulsion. At the PIT, the turbid mixture becomes clear, then below the PIT an O/W nano emulsion is formed. The mixture is then cooled to room temperature under slow and continuous stirring. The main advantage of this technique is certainly the absence of the use of any kind of solvent[31].

1.1.2.4. Characterization of lipid nanoparticles

The lipid nanoparticles can be characterized in terms of size, distribution, surface charge and stability. An appropriate characterization of these formulations is required to allow the development of dispersions with the desired properties for an intended application[25].

Dynamic light scattering (DLS), also referred to as Photon Correlation Spectroscopy (PCS), is one of the most popular methods used to determine the particle size in a colloidal

suspension and to detect the possible presence of agglomerates, by measuring the random changes in the intensity of light scattered from a sample as function of time[32]. In this technique, a monocromatic beam of light passes through the suspension in which small particles undergo random thermal motions known as Brownian motions; in general, large particles have slow speed while small particles are faster. Brownian motions of particles are analysed by a correlator and converted into particles size using the Stokes-Einstein equation (eq.1):

$$D = \frac{kT}{6\pi\eta Rh} \tag{1}$$

in which *D* is diffusion coefficient, *k* is Boltzmann's constant, *T* is temperature, η is solvent viscosity, and *Rh* is the rheodynamic radius of particle solution[33].

For this analysis, a disposable polystyrene cuvette filled with an appropriate dilution of formulation is placed in a Zetasizer Nano-ZS (Malvern Panalytical Ltd.) or in an equivalent instrument. Particle size is a critical parameter of lipid nanoparticles, which affects stability, encapsulation efficiency, bio-distribution, mucoadhesion and cellular uptake.

The polydispersity index (PDI) is another key parameter that describes the distribution of size populations of particles into a sample. It is defined as the standard deviation of the particle diameter distribution divided by the mean particle diameter (eq.2) and it is used to evaluate the uniformity of a nanoparticle suspension[34].

$$PdI = \left(\frac{\sigma}{2a}\right)^2 \tag{2}$$

The numerical value of PDI ranges from 0.0 to 1.0. The lowest extreme indicates a perfectly uniform sample with respect to the particle size while the highest one indicates a very polydispersed sample with different particle size populations. Values around 0.5 are acceptable for lipid vesicles, while 0.3 and below are considered the optimum[35].

Zeta potential is a measure of nanoparticles' surface charge. It is determined by the technique of Electrophoretic Light Scattering (ELS), also referred as Laser Doppler

Microelectrophoresis, which measures the electrophoretic mobility of particles in an aqueous medium. When nanoparticles are immersed in a solvent, an electric double layer (EDL) develops instantly. The EDL is composed of a double coating; the inner one, also called the Stern layer, consists of opposite charged ions strongly bound to the core of the central particle, while the outermost layer comprises both opposite and equally charged ions. Zeta potential reflects the difference between the EDL and external aqueous environment[36]. It is measured by filling with the sample a cuvette that contains two gold electrodes. When a voltage is applied to the electrode, the charged particles will move towards the electrode with the opposite charge and their velocity is measured and expressed in unit field strength as their electrophoretic mobility, which is then converted into zeta potential (ב) through Henry's equation (eq. 3):

$$U_E = \frac{2\varepsilon ב(ka)}{3\eta} \tag{3}$$

where ε is the dielectric constant of the dispersant, ב *(ka)* is the Henry function and η is the viscosity[37]. The zeta potential is usually used to predict the long-term stability of a colloidal system and the interaction of the system with a surface.

1.1.2.5. Applications of lipid nanoparticles

Oral administration

Oral route is one of the most preferred ways of administration due to significant convenience, less pain and patient's high compliance. However, sometimes the bioavailability of orally administered drugs is limited by different factors such as low drug solubility, poor gastrointestinal absorption, rapid metabolism, high fluctuation of drug plasma levels, and drug-drug and/or drug-food interactions[24]. To overcome these problems, researchers have introduced lipid nanoparticles as potential carriers for oral drug delivery, since they are able to increase the bioavailability and reduce the erratic absorption and the intestinal degradation of the encapsulated drug. Some of the advantages associated with the use of lipid nanoparticles are the delivery of poorly water-soluble drugs and the targeting to a specific site of gastrointestinal tract[38].

Parenteral administration

Lipid nanoparticles have been introduced as carriers for systemic delivery because of the biocompatible and biodegradable nature of the formulation's constituents. They can be injected intramuscularly, subcutaneously, intravenously, directly adjacent to the target organs and are able to maintain constant the serum levels of the drugs[39].

Ocular administration

The topical administration of drugs into the eye is the most common route for the ophthalmic molecules; however, it must overcome different challenges such as ocular blood barrier, corneal epithelium and tear drainage. Usually, the bioavailability of the drugs is less than 3-5% of the administered dose. Lipid nanoparticles have the ability to increase the bioavailability of the encapsulated drug because the lipidic components improve the interaction with the lipid layer of the tear film[40].

Pulmonary administration

Pulmonary delivery is a non-invasive administration route for the treatment of local and systemic disorders; it benefits from the large epithelial surface area, the high organ vascularization, the thin nature of the alveolar epithelium and the immense capacity for solute exchange. However, one of the main challenges is to develop drugs with sufficient stability, appropriate size and ideal blood/air partition coefficient. Lipid nanoparticles have been considered attractive and efficient carriers for the pulmonary delivery of drugs for their small size, biocompatible composition and deep-lung deposition ability. The major goal of these systems is to allow a more specific targeting of the drug and/or a controlled drug release, leading to improved therapeutic efficacy with reduced drug dosage and dosing frequency. They can also limit side effects and ameliorate patient compliance[41].

Brain administration

Drug delivery to the brain is one of the most important challenges in pharmaceutical sciences because of the presence of a semi-impermeable blood brain barrier (BBB) and efflux of transported drugs from brain to blood circulation. Lipid nanoparticles, through their lipophilicity and their small particle size, have been considered good carriers for specific targeting of brain tissues. They have the advantage of increasing drug retention

time in blood of brain capillaries and inducing a drug gradient from blood to brain tissues, the latter opening tight junctions to facilitate passage from BBB and transcytosis of drug-loaded lipid nanoparticles through the endothelium layer[42].

Topical administration

Among the different routes of administration for lipid nanoparticles, the topical one seems to be one of the most promising for therapeutic and cosmetic use. The cutaneous use of lipid nanoparticles has several advantages: chemical protection of the incorporated substances, allowing the skin application of labile molecules that are difficult to transport in other formulations; the possibility to improve and modulate the drug bioavailability and release, respectively. The strategic mechanism behind the topical application of lipid nanoparticles is the formation of an occlusive film at stratum corneum (SC) surface that prevents water loss and improves the skin lipid film barrier by nanoparticles adhesion to the SC[43]. Topical drug delivery systems are an attractive approach for the treatment of many diseases such as inflammatory disorders and cutaneous infections.

1.1.2.6. Liposomes

Liposomes are spherical vesicular systems consisting of phospholipids, suspended in aqueous solutions, arranged to form one or more lipid bilayers which entrap water in their compartments; the polar heads of the phospholipids are oriented towards both the exterior and interior aqueous phases, while the acyl chains are dispose in a more-or-less ordinated bilayer depending on the chemical traits of the lipids: these two components are hold together by glyceryl esterification[44].

Based on the number of bilayers and size, they can be divided into three classes[45] (Fig.5):

- Small Unilamellar Vesicles (SUV) consisting of a single lipid bilayer of 20–100 nm in diameter;
- Large Unilamellar Vesicles (LUV), which display a 100nm -1µm diameter ranges, or Giant Unilamellar Vesicles (GUV), if the diameter exceeds 1µm;
- Multi Lamellar Vesicles (MLV), consisting of several lipid bilayers interspersed with aqueous phases, that show a mean diameter around 0,5µm-10µm.

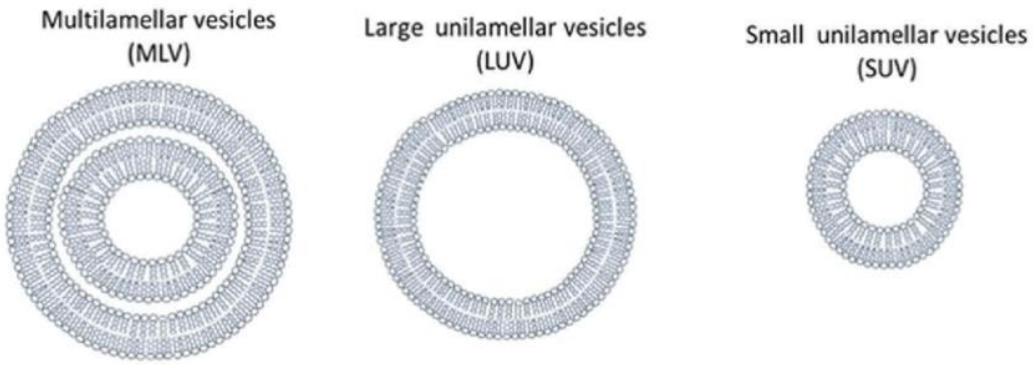

Figure 5: Representation of MLV, LUV and SUV

Lipophilic bilayer components determine the degree of rigidity; phospholipids with long acyl chains such as distearoyl phosphatidylcholine (DSPC) establish more rigid, rather impermeable bilayer structures than shorter chains, whereas unsaturated fatty acids of the same length, like dioleoyl phosphatidylcholine (DOPC), which cannot achieve the all-trans packed disposition due to the presence of said insaturations, give out much more permeable and less stable bilayers. The polar phospholipidic heads instead influence the net charge of liposomes and their interaction with the target: positively charged groups like phosphatidylcholine (PC) augments affinity for more electronegative substrates (i.e. bacteria and tumoral cells), while neutral, ionizable groups like phosphatidylethanolamine (PE) can modify the liposomal bilayer, depending on the target pH, by an additional inverted hexagonal conformation happening after the lamellar distribution[46]. Phospholipidic composition influences which preparation method is better to employ for a specific mixture; traditional preparation methods (e.g. Thin-Film Hydration) are suitable for most phospholipids but, since its first passages are based on the dissolution of lipids in organic solvents followed by their evaporation, even minimal organic solvent residues inside the liposome's structure could result in toxicity and hindered vesicular stability – moreover these methods usually produce MLV, which have then to undergo extrusion to obtain LUV or SUV or high pressure homogenization/ultrasound sonication to obtain SUV[47]. Most modern methods, such as Mozafari's, skip these first steps and, instead of resuspending the dried phospholipids in water, directly disperse the lipidic mixture in an appropriate aqueous phase along with surfactants to obtain unilamellar nanoliposomes; however, formulative obstacles can show up when working with highly lipophilic phospholipids and active compounds[48].

Liposomes are extensively used as carriers for numerous molecules in cosmetic and pharmaceutical applications thanks to their biocompatibility, biodegradability, low toxicity, and capacity of encapsulate both lipophilic and hydrophilic compounds[49]. Hydrophilic compounds can be entrapped in the aqueous compartments while the hydrophobic ones can be associated with the bilayers. Compounds with intermediate logP effortlessly partition between the lipid and aqueous phases, both in the bilayer and in the aqueous core.

In addition to be efficient carriers, during the last few decades liposomes have attracted great interest as ideal models for biological membranes[31]. The interaction between drugs and biomembrane is a complex mechanism which have a great influence on the pharmacokinetic and pharmacodynamic of drugs. A lot of molecules have to cross or bind to the lipid membrane to exert their therapeutic effect. So, one of the factors which determines the interaction with cell membrane is the hydrophilic/lipophilic character of the molecules. The most accepted theory to describe the structure of plasma membranes is the fluid mosaic model, developed in 1972. Based on this theory, a cell membrane consists of a fluid double layer of phospholipids containing other components like proteins, carbohydrates and cholesterol (CHOL)[50]. The fluid liquid crystal-state is achieved when the aqueous medium's temperature is above the melting temperature (*Tm*) of the main phospholipidic component (Fig.6), while the solid gel-phase is predominant when the temperature is lower than the *Tm* – all depending from the disposition and additional chemical properties (like insaturations) of the acyl chains; other key factors are the percentage of cholesterol, the degree of hydration, the phospholipid polar head groups and the pH[51].

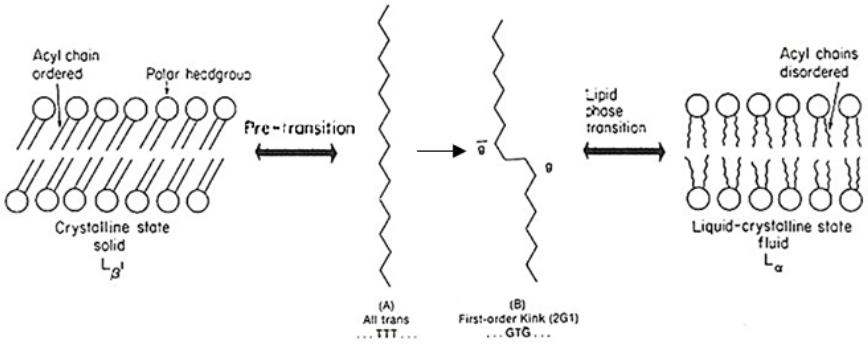

Figure 6: Main phospholipidic transitions

This model can be evaluated with differential scanning calorimetry (DSC).

1.1.3. Differential scanning calorimetry

Differential scanning calorimetry (DSC) is the most common thermoanalytical technique, introduced in the 1960s, which measures the changes in peak temperatures and in heat flow which occur during thermal transitions in a material. The procedure is based on the application of a linear heating or cooling to a sample and the subsequent measurement of the temperature and energy associated with different events such as melting, crystallization, glass transitions and decomposition reactions[52].

DSC can be based on one of these two different approaches: heat flux and power compensation[53].

Heat flux DSC (Fig.7) is the simpler mechanism between the two ones. Generally, two crucibles (one containing the sample and the other as reference) are placed symmetrically on a thermocouple within a furnace, placed in close contact with each other. The differential in heat capacity (*Cp*) between the sample and reference pans, in function of the difference in temperature is measured by area thermocouples, and the resultant heat flow is calculated by the equation (eq.4):

$$\frac{dQ}{dT} = \frac{\Delta T}{R} \tag{4}$$

where Q = heat, t = time, ΔT = temperature difference between the sample and the reference, and R = thermal resistance of the heat path between the furnace and the crucible. From the equation is possible to deduce that the differential heat flow is a direct measure of the properties of the sample, since the contribution from the reference is subtracted.

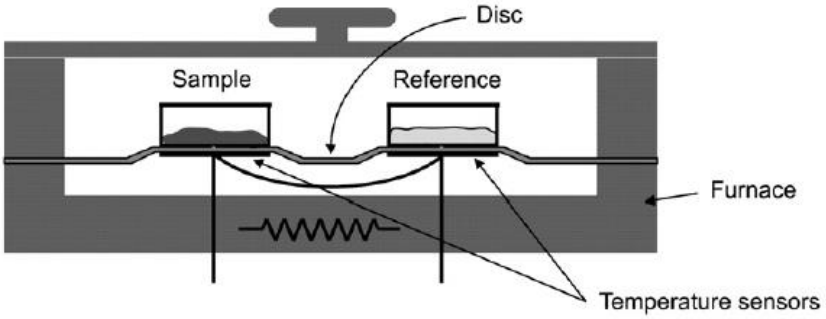

Figure 7: Heat Flux DSC

In the power compensation method (Fig.8), the sample and the reference are completely isolated from each other, and both their crucibles have their own heating and temperature sensing elements. Sample and reference are set to go through the same temperature program. When thermotropic changes occur, more or less (for an endothermic or an exothermic event, respectively) heat will be needed to maintain the set temperature and thus no difference between sample and reference. This power difference is recorded by the instrument and transformed in a thermogram. Power compensated DSC has lower sensitivity than heat flux DSC, but its response time is more rapid.

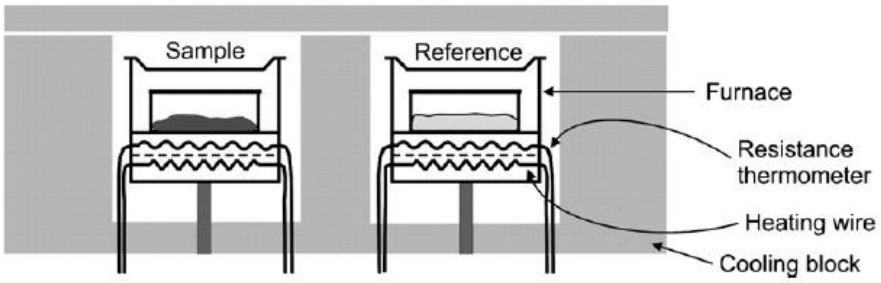

Figure 8: Power compensation DSC

The result of a DSC experiment is a curve of heat flux versus temperature or versus time which can be used to extrapolate the enthalpy, calculated by integrating the peak corresponding to a given transition: in mathematical terms, these results are obtained from the following equation (eq.5):

$$\frac{dQ}{dt} = Cp \times \frac{dT}{dt} \tag{5}$$

where *dQ/dt* is the heat flow, *dT/dt* is the heating rate and *Cp* is the heat capacity that, for traditional DSC measurement and enthalpy extraction, is relying on the relationship (eq.6):

$$Cp = \frac{K\Delta Y}{b} \tag{6}$$

where K is the calorimetric sensitivity, ΔY is the difference between the sample's and reference's baselines and b is the heating rate.

Calorimetric sensitivity (*K*) is a property unique to the instrument and it is determined by calibration with a pure standard reference which can properly regain its crystalline structure after undergoing ample temperature-shifting programs, such as Indium. Heating rate (*b*) is chosen by the operator and mostly influences sensitivity and accuracy of the instrument, the two key parameters which should be balanced to obtain precise and well-resolved peaks.

The principal values that should be read and then commented when analysing a thermogram (Fig.9) are the extrapolated onset temperature (T_{onset}), the peak temperature (T_{peak}) and the calorimetric enthalpy (ΔH) extracted by integrating the area under the peak.

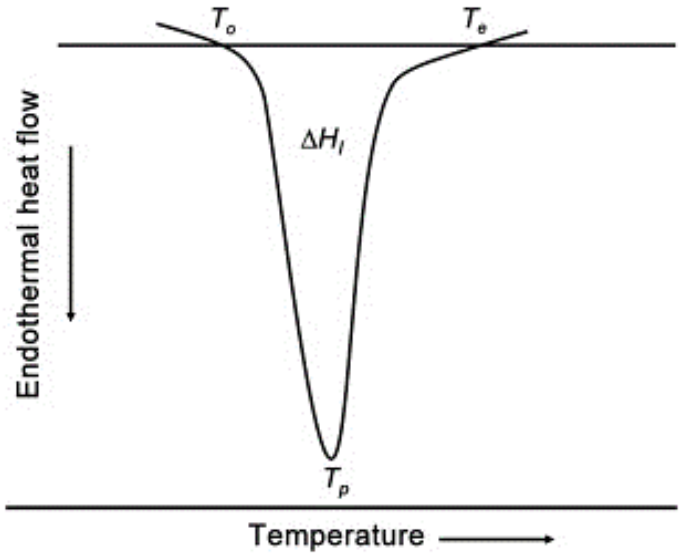

Figure 9: Example of thermogram with key values reported

The thermograms can be influenced by different factors depending on the instrument (furnace heating rate and atmosphere; recording speed; sensitivity of the recording system; composition of sample containers) or the characteristics of the sample (nature and amount of the sample; heat reactions; thermal conductivity)[54].

In the last decades the interest in DSC employment to study the thermotropic behaviour of phospholipid bilayers, which act as a model of biological membranes, is exponentially increased[55].

Phospholipid, when suspended in aqueous medium, form bilayer structures which have a specific lyotropic behaviour based on the lipid mixture used. The main transition of phospholipid bilayers, when thermal energy is gradually added, occurs between the gel (ordered) and fluid (disordered) state due to the diminished effect of the van der Waals

interactions between hydrocarburic chains, consequently increasing their mobility; other smaller transitions, like the gauche pre-transition from the all-trans (ordered) state, can be observed and quantified. The amount of energy provided is directly proportional to the reversible phase transitions of phospholipids occurring at different peak temperatures, and intrinsically to the conformation properties of the phospholipid mix, which chemical nature affects the stability of the system. The enthalpy of these transition is calculated using calorimetric techniques such as DSC and then normalized as enthalpy per mg of lipid. The polymorphic behaviour (Fig.10) is related to the numerous, minor transitions occurring between the gel and the liquid crystalline phase[56].

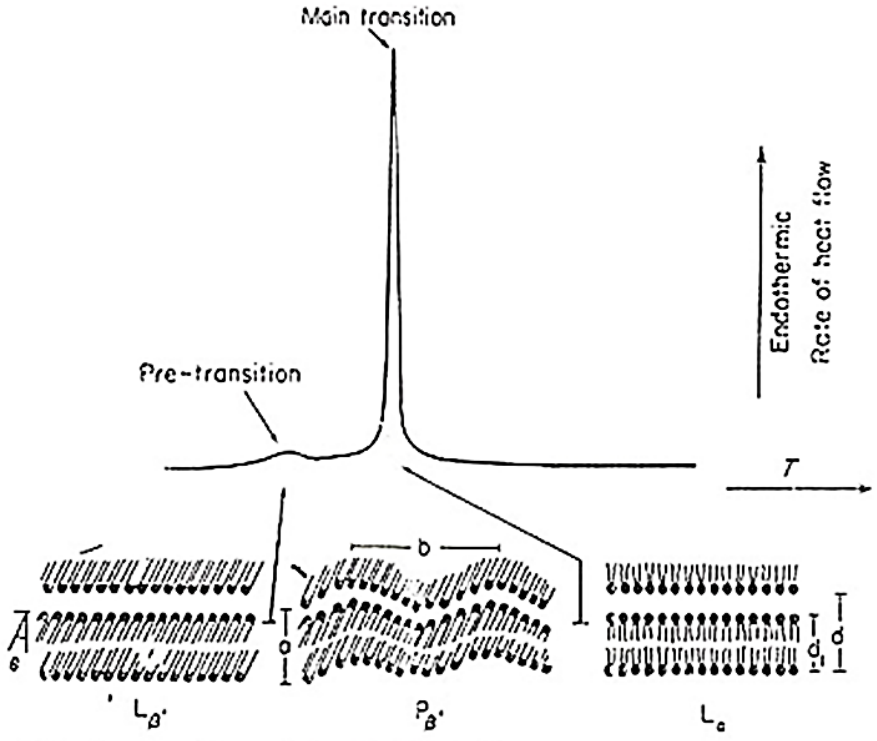

Figure 10: Phospholipidic polymorphism

1.2. Aims of my PhD project and general conclusions

The aim of this thesis was to design, prepare and characterize lipid nanoparticles in order to find the ideal formulation for encapsulating active molecules belonging to polyphenols, thus increasing their bioavailability and amplifying their actions. Employed molecules were benzo[k,l]xanthene lignans and mangiferin.

Benzo[k,l]xanthene lignans are a subgroup of polyphenols, found in plant kingdom, which show a large range of biological activities such as antioxidant, anti-inflammatory, antifungal, antibacterial and antiproliferative. Their low availability in nature has led researchers to develop a simple and biomimetic methodology for their synthesis, in order to better investigate their actions. Two semisynthetic molecules of benzo[k,l]xanthene lignans (BXL and BXL-A2) were encapsulated into Solid Lipid Nanoparticles (SLN) and Nanostructured Lipid Carriers (NLC).

- SLN containing BXL were prepared by PIT method and characterized in terms of size, PDI, ZP, encapsulation efficiency and thermotropic behaviour. The final formulation showed appreciable chemical-physical characteristics, but unpromising biological activity on the *in vitro* model; so, the same molecule (BXL) was then encapsulated within another formulation, sporting a different composition and prepared by a combination of PIT and ultrasonication methods, which demonstrated excellent chemical-physical characteristics and biological activity, too. This last formulation is undergoing further studies to be incorporated in a Carbopol-based hydrogel for the treatment of topical affections.
- BXL-A2 has been subjected to preliminary studies; SLN and NLC, both empty and with BXL-A2, were prepared with the employment of the high pressure – hot homogenization method and characterized in terms of size, PDI, ZP, thermotropic behaviour, encapsulation efficiency and IR spectrum. An excellent encapsulation efficiency was obtained for both SLN-BXL-A2 and NLC-BXL-A2, probably due to the prominent lipophilicity of the active compound, and the successful incorporation was additionally proved by the means of FT-IR. Other studies will be performed to confirm these data and evaluate the possible biological activities.

Mangiferin (MGN) is a natural compound with anti-inflammatory and antioxidant activities, assessed for a potential treatment of various eye diseases. The poor

physicochemical features of MGN (low solubility and high instability) justify its encapsulation into nanostructured lipid carriers (NLC) to improve its ocular bioavailability. MGN-NLC were prepared by high shear homogenization coupled with ultrasonication method (HSH−US): good technological parameters suitable for ocular administration were obtained. Moreover, the ORAC assay demonstrated the higher antioxidant activity of MGN-NLC compared to the free compound and *in ovo* studies (HET-CAM) revealed that the formulation can be considered non-irritant.

1.3. References

[1] H.-K. Biesalski *et al.*, «Bioactive compounds: Definition and assessment of activity», *Nutrition*, vol. 25, n. 11–12, pagg. 1202–1205, nov. 2009, doi: 10.1016/j.nut.2009.04.023.

[2] A. E. Q. Sauceda *et al.*, «Biological Actions of Phenolic Compounds», in *Fruit and Vegetable Phytochemicals*, E. M. Yahia, A c. di Chichester, UK: John Wiley & Sons, Ltd, 2017, pagg. 125–138. doi: 10.1002/9781119158042.ch6.

[3] A. Durazzo *et al.*, «Polyphenols: A concise overview on the chemistry, occurrence, and human health», *Phytother. Res.*, vol. 33, n. 9, pagg. 2221–2243, set. 2019, doi: 10.1002/ptr.6419.

[4] J.-M. Lü, P. H. Lin, Q. Yao, e C. Chen, «Chemical and molecular mechanisms of antioxidants: experimental approaches and model systems», *J. Cell. Mol. Med.*, vol. 14, n. 4, pagg. 840–860, apr. 2010, doi: 10.1111/j.1582-4934.2009.00897.x.

[5] M. Galleano, S. V. Verstraeten, P. I. Oteiza, e C. G. Fraga, «Antioxidant actions of flavonoids: Thermodynamic and kinetic analysis», *Arch. Biochem. Biophys.*, vol. 501, n. 1, pagg. 23–30, set. 2010, doi: 10.1016/j.abb.2010.04.005.

[6] N. Kumar e N. Goel, «Phenolic acids: Natural versatile molecules with promising therapeutic applications», *Biotechnol. Rep.*, vol. 24, pag. e00370, dic. 2019, doi: 10.1016/j.btre.2019.e00370.

[7] V. Saibabu, Z. Fatima, L. A. Khan, e S. Hameed, «Therapeutic Potential of Dietary Phenolic Acids», *Adv. Pharmacol. Sci.*, vol. 2015, pagg. 1–10, 2015, doi: 10.1155/2015/823539.

[8] O. Mazimba, F. Nana, V. Kuete, e G. S. Singh, «Xanthones and Anthranoids from the Medicinal Plants of Africa», in *Medicinal Plant Research in Africa*, Elsevier, 2013, pagg. 393–434. doi: 10.1016/B978-0-12-405927-6.00011-4.

[9] S. Sang e Y. Zhu, «Bioactive Phytochemicals in Wheat Bran for Colon Cancer Prevention», in *Wheat and Rice in Disease Prevention and Health*, Elsevier, 2014, pagg. 121–129. doi: 10.1016/B978-0-12-401716-0.00010-6.

[10] B. Pastor-Villaescusa, E. Sanchez Rodriguez, e O. D. Rangel-Huerta, «Polyphenols in Obesity and Metabolic Syndrome», in *Obesity*, Elsevier, 2018, pagg. 213–239. doi: 10.1016/B978-0-12-812504-5.00011-8.

[11] K.-T. Chung, T. Y. Wong, C.-I. Wei, Y.-W. Huang, e Y. Lin, «Tannins and Human Health: A Review», *Crit. Rev. Food Sci. Nutr.*, vol. 38, n. 6, pagg. 421–464, ago. 1998, doi: 10.1080/10408699891274273.

[12] B. Yang, Y. Dong, F. Wang, e Y. Zhang, «Nanoformulations to Enhance the Bioavailability and Physiological Functions of Polyphenols», *Molecules*, vol. 25, n. 20, pag. 4613, ott. 2020, doi: 10.3390/molecules25204613.

[13] A. Borges, V. de Freitas, N. Mateus, I. Fernandes, e J. Oliveira, «Solid Lipid Nanoparticles as Carriers of Natural Phenolic Compounds», *Antioxidants*, vol. 9, n. 10, pag. 998, ott. 2020, doi: 10.3390/antiox9100998.

[14] C. Carbone, S. Cupri, A. Leonardi, G. Puglisi, e R. Pignatello, «Lipid-based nanocarriers for drug delivery and targeting: a patent survey of methods of production and characterization», *Pharm. Pat. Anal.*, vol. 2, n. 5, pagg. 665–677, set. 2013, doi: 10.4155/ppa.13.43.

[15] S. Bochicchio, G. Lamberti, e A. A. Barba, «Polymer–Lipid Pharmaceutical Nanocarriers: Innovations by New Formulations and Production Technologies», *Pharmaceutics*, vol. 13, n. 2, pag. 198, feb. 2021, doi: 10.3390/pharmaceutics13020198.

[16] D. Patel, R. Kesharwani, e S. Gupta, «D EV ELO PM EN T & SC R EEN IN G A PPR O A C H FO R LIPID N A N O PA R TIC LE:A R EV IEW», pag. 7, 2013.

[17] J. Pardeike, A. Hommoss, e R. H. Müller, «Lipid nanoparticles (SLN, NLC) in cosmetic and pharmaceutical dermal products», *Int. J. Pharm.*, vol. 366, n. 1–2, pagg. 170–184, gen. 2009, doi: 10.1016/j.ijpharm.2008.10.003.

[18] W. Mehnert, «Solid lipid nanoparticles Production, characterization and applications», *Adv. Drug Deliv. Rev.*, vol. 47, n. 2–3, pagg. 165–196, apr. 2001, doi: 10.1016/S0169-409X(01)00105-3.

[19] B. Fonseca-Santos, P. B. Silva, R. B. Rigon, M. R. Sato, e M. Chorilli, «Formulating SLN and NLC as Innovative Drug Delivery Systems for Non-Invasive Routes of Drug Administration», *Curr. Med. Chem.*, vol. 27, n. 22, pagg. 3623–3656, giu. 2020, doi: 10.2174/0929867326666190624155938.

[20] S. Shidhaye, R. Vaidya, S. Sutar, A. Patwardhan, e V. Kadam, «Solid Lipid Nanoparticles and Nanostructured Lipid Carriers – Innovative Generations of Solid Lipid Carriers», *Curr. Drug Deliv.*, vol. 5, n. 4, pagg. 324–331, ott. 2008, doi: 10.2174/156720108785915087.

[21] P. Ganesan e D. Narayanasamy, «Lipid nanoparticles: Different preparation techniques, characterization, hurdles, and strategies for the production of solid lipid nanoparticles and nanostructured lipid carriers for oral drug delivery», *Sustain. Chem. Pharm.*, vol. 6, pagg. 37–56, dic. 2017, doi: 10.1016/j.scp.2017.07.002.

[22] R. H. MuÈller, K. MaÈder, e S. Gohla, «Solid lipid nanoparticles (SLN) for controlled drug delivery ± a review of the state of the art», *Eur. J. Pharm. Biopharm.*, pag. 17, 2000.

[23] S. A. Wissing, O. Kayser, e R. H. Müller, «Solid lipid nanoparticles for parenteral drug delivery», *Adv. Drug Deliv. Rev.*, vol. 56, n. 9, pagg. 1257–1272, mag. 2004, doi: 10.1016/j.addr.2003.12.002.

[24] S. Das e A. Chaudhury, «Recent Advances in Lipid Nanoparticle Formulations with Solid Matrix for Oral Drug Delivery», *AAPS PharmSciTech*, vol. 12, n. 1, pagg. 62–76, mar. 2011, doi: 10.1208/s12249-010-9563-0.

[25] R. Shah, D. Eldridge, E. Palombo, e I. Harding, *Lipid Nanoparticles: Production, Characterization and Stability*. Cham: Springer International Publishing, 2015. doi: 10.1007/978-3-319-10711-0.

[26] L. Battaglia *et al.*, «Techniques for the Preparation of Solid Lipid Nano and Microparticles», in *Application of Nanotechnology in Drug Delivery*, A. D. Sezer, A c. di InTech, 2014. doi: 10.5772/58405.

[27] M. Schubert, «Solvent injection as a new approach for manufacturing lipid nanoparticles – evaluation of the method and process parameters», *Eur. J. Pharm. Biopharm.*, vol. 55, n. 1, pagg. 125–131, gen. 2003, doi: 10.1016/S0939-6411(02)00130-3.

[28] S. Mukherjee, S. Ray, e R. S. Thakur, «Solid Lipid Nanoparticles: A Modern Formulation Approach in Drug Delivery System», *Indian J. Pharm. Sci.*, pag. 10, 2009.

[29] M. Trotta, F. Debernardi, e O. Caputo, «Preparation of solid lipid nanoparticles by a solvent emulsification–diffusion technique», *Int. J. Pharm.*, vol. 257, n. 1–2, pagg. 153–160, mag. 2003, doi: 10.1016/S0378-5173(03)00135-2.

[30] K. Shinoda e H. Saito, «The Stability of O/W type emulsions as functions of temperature and the HLB of emulsifiers: The emulsification by PIT-method», *J. Colloid Interface Sci.*, vol. 30, n. 2, pagg. 258–263, giu. 1969, doi: 10.1016/S0021-9797(69)80012-3.

[31] L. Montenegro *et al.*, «*In vitro* evaluation of idebenone-loaded solid lipid nanoparticles for drug delivery to the brain», *Drug Dev. Ind. Pharm.*, vol. 37, n. 6, pagg. 737–746, giu. 2011, doi: 10.3109/03639045.2010.539231.

[32] N. Raval, R. Maheshwari, D. Kalyane, S. R. Youngren-Ortiz, M. B. Chougule, e R. K. Tekade, «Importance of Physicochemical Characterization of Nanoparticles in Pharmaceutical Product Development», in *Basic Fundamentals of Drug Delivery*, Elsevier, 2019, pagg. 369–400. doi: 10.1016/B978-0-12-817909-3.00010-8.

[33] P. M. Carvalho, M. R. Felício, N. C. Santos, S. Gonçalves, e M. M. Domingues, «Application of Light Scattering Techniques to Nanoparticle Characterization and Development», *Front. Chem.*, vol. 6, pag. 237, giu. 2018, doi: 10.3389/fchem.2018.00237.

[34] K. N. Clayton, J. W. Salameh, S. T. Wereley, e T. L. Kinzer-Ursem, «Physical characterization of nanoparticle size and surface modification using particle scattering diffusometry», *Biomicrofluidics*, vol. 10, n. 5, pag. 054107, set. 2016, doi: 10.1063/1.4962992.

[35] M. Danaei *et al.*, «Impact of Particle Size and Polydispersity Index on the Clinical Applications of Lipidic Nanocarrier Systems», *Pharmaceutics*, vol. 10, n. 2, pag. 57, mag. 2018, doi: 10.3390/pharmaceutics10020057.

[36] M. Kaszuba, J. Corbett, F. M. Watson, e A. Jones, «High-concentration zeta potential measurements using light-scattering techniques», *Philos. Trans. R. Soc. Math. Phys. Eng. Sci.*, vol. 368, n. 1927, pagg. 4439–4451, set. 2010, doi: 10.1098/rsta.2010.0175.

[37] A. V. Delgado, F. González-Caballero, R. J. Hunter, L. K. Koopal, e J. Lyklema, «Measurement and Interpretation of Electrokinetic Phenomena (IUPAC Technical Report)», *Pure Appl. Chem.*, vol. 77, n. 10, pagg. 1753–1805, gen. 2005, doi: 10.1351/pac200577101753.

[38] M. Plaza-Oliver, M. J. Santander-Ortega, e M. Victoria. Lozano, «Current approaches in lipid-based nanocarriers for oral drug delivery», *Drug Deliv. Transl. Res.*, vol. 11, n. 2, pagg. 471–497, apr. 2021, doi: 10.1007/s13346-021-00908-7.

[39] M. D. Joshi e R. H. Müller, «Lipid nanoparticles for parenteral delivery of actives», *Eur. J. Pharm. Biopharm.*, vol. 71, n. 2, pagg. 161–172, feb. 2009, doi: 10.1016/j.ejpb.2008.09.003.

[40] Z. Qamar *et al.*, «Nano-Based Drug Delivery System: Recent Strategies for the Treatment of Ocular Disease and Future Perspective», *Recent Pat. Drug Deliv. Formul.*, vol. 13, n. 4, pagg. 246–254, apr. 2020, doi: 10.2174/1872211314666191224115211.

[41] C. Jaafar-Maalej, A. Elaissari, e H. Fessi, «Lipid-based carriers: manufacturing and applications for pulmonary route», *Expert Opin. Drug Deliv.*, vol. 9, n. 9, pagg. 1111–1127, set. 2012, doi: 10.1517/17425247.2012.702751.

[42] A. R. Neves, J. F. Queiroz, B. Weksler, I. A. Romero, P.-O. Couraud, e S. Reis, «Solid lipid nanoparticles as a vehicle for brain-targeted drug delivery: two new strategies of functionalization with apolipoprotein E», *Nanotechnology*, vol. 26, n. 49, pag. 495103, dic. 2015, doi: 10.1088/0957-4484/26/49/495103.

[43] A. Garcês, M. H. Amaral, J. M. Sousa Lobo, e A. C. Silva, «Formulations based on solid lipid nanoparticles (SLN) and nanostructured lipid carriers (NLC) for cutaneous use: A review», *Eur. J. Pharm. Sci.*, vol. 112, pagg. 159–167, gen. 2018, doi: 10.1016/j.ejps.2017.11.023.

[44] A. Akbarzadeh *et al.*, «Liposome: classification, preparation, and applications», *Nanoscale Res. Lett.*, vol. 8, n. 1, pag. 102, dic. 2013, doi: 10.1186/1556-276X-8-102.

[45] N. V. Katre, «Liposome-based depot injection technologies», *Am. J. Drug Deliv.*, vol. 2, n. 4, pagg. 213–227, 2004.

[46] R. N. Lewis, D. A. Mannock, e R. N. McElhaney, «Membrane lipid molecular structure and polymorphism», in *Current Topics in Membranes*, vol. 44, Elsevier, 1997, pagg. 25–102.

[47] H. Zhang, «Thin-film hydration followed by extrusion method for liposome preparation», in *Liposomes*, Springer, 2017, pagg. 17–22.

[48] J.-C. Colas, W. Shi, V. M. Rao, A. Omri, M. R. Mozafari, e H. Singh, «Microscopical investigations of nisin-loaded nanoliposomes prepared by Mozafari method and their bacterial targeting», *Micron*, vol. 38, n. 8, pagg. 841–847, 2007.

[49] H. R. A. Ashtiani, P. Bishe, N.-A. Lashgari, M. A. Nilforoushzadeh, e S. Zare, «Liposomes in cosmetics», *J. Skin Stem Cell*, vol. 3, n. 3, 2016.

[50] P. Eichman, «From the lipid bilayer to the fluid mosaic: a brief history of membrane models», *Resour. Cent. Sociol. Hist. Philos. Sci. Teach.-Teach. Netw. News*, vol. 9, n. 2, pag. 1, 1999.

[51] K. M. G. Taylor e R. M. Morris, «Thermal analysis of phase transition behaviour in liposomes», *Thermochim. Acta*, vol. 248, pagg. 289–301, gen. 1995, doi: 10.1016/0040-6031(94)01884-J.

[52] D. Q. Craig e M. Reading, *Thermal analysis of pharmaceuticals*. CRC press, 2006.

[53] G. W. H. Höhne, K.-H. Breuer, e W. Eysel, «Differential scanning calorimetry: comparison of power compensated and heat flux instruments», *Thermochim. Acta*, vol. 69, n. 1–2, pagg. 145–151, 1983.

[54] T. Kousksou, A. Jamil, K. El Omari, Y. Zeraouli, e Y. Le Guer, «Effect of heating rate and sample geometry on the apparent specific heat capacity: DSC applications», *Thermochim. Acta*, vol. 519, n. 1–2, pagg. 59–64, 2011.

[55] C. Carbone e R. Pignatello, «DSC in drug–biomembrane interaction studies», in *Drug-Biomembrane Interaction Studies*, Elsevier, 2013, pagg. 213–236.

[56] M. J. Janiak, D. M. Small, e G. G. Shipley, «Nature of the thermal pretransition of synthetic phospholipids: dimyristoyl-and dipalmitoyllecithin», *Biochemistry*, vol. 15, n. 21, pagg. 4575–4580, 1976.

2. CHARACTERIZATION AND INTERACTION WITH BIOMEMBRANE MODEL OF BENZO[K,L]XANTHENE LIGNAN LOADED SOLID LIPID NANOPARTICLES

Cristina Torrisi[1], Nunzio Cardullo[2], Vera Muccilli[2], Corrado Tringali[2], Francesco Castelli[1] and Maria Grazia Sarpietro[1,]*

[1]Department of Drug and Health Sciences, University of Catania, Viale Andrea Doria 6, 95125 Catania, Italy; torrisi.cristina@hotmail.it (C.T.); fcastelli@unict.it (F.C.)

[2] Department of Chemical Sciences, University of Catania, Viale Andrea Doria 6, 95125 Catania, Italy; ncardullo@unict.it (N.C.); v.muccilli@unict.it (V.M.); ctringali@unict.it (C.T.)

*correspondence: mg.sarpietro@unict.it

Membranes 2022, 12, 615. https://doi.org/ 10.3390/membranes12060615

2.1. Introduction

Benzo[k,l]xanthene lignans (BXLs) are a group of rare natural products belonging to the class of polyphenols. To date, only six naturally occurring BXLs have been discovered: rufescidride [1], mongolicumin A [2] and its dimethyl ester [3], yunnaneic acid H [4], chiliantin D [5], and dodegranoside [6]. Because of their limited availability in nature, the biological activities of natural BXLs have been almost unexplored for years. In 2009, a simple and biomimetic methodology for the synthesis of BXLs was published [7], and a variety of synthetic benzoxanthenes have since been obtained and evaluated as antioxidant [8], anti-inflammatory [9], selective copper-chelators [10], antifungal [11], antibacterial [12], antiproliferative agents [13,14]. Additionally, BXLs are reported to induce autophagy towards tumour cells [15] and act as antiangiogenic [16], pro-apoptotic agents [17], DNA-binders [12,17], proteasome inhibitors [18], all targets involved in tumorigenesis, and which are useful for the development of anticancer drugs. These studies highlighted the promising biological activities of this class of lignans as potential chemotherapeutic agents. Nevertheless, the lipophilic character of the xanthene core [14] makes these molecules difficult to use in an aqueous medium, limiting their employment in in vivo studies for pharmaceutical applications. One of the approaches to overcome this problem is the employment of a drug-delivery system able to improve the stability and bioavailability of the candidate drug. In recent years, solid lipid nanoparticles (SLN) have attracted the attention of numerous researchers as carriers for lipophilic molecules such as BXLs. SLN are colloidal systems composed of solid lipids at room and body temperature and are stabilized by surfactants. They represent an alternative option to the traditional colloidal drug-delivery systems, such as emulsions, liposomes, polymeric micro- and nanoparticles, because of the reduced problems related to industrial production scale-up and mid-term storage. Some of their main advantages are related to their nanometric size, between 50 and 1000 nm, which allows them to be used for different routes of administration and in the presence of biocompatible lipids that make them safe and efficient delivery vehicles. As described in the literature, SLN can be produced by different methods and using various lipid compositions that strongly affect their drug-loading capacity and drug release profile [19,20]. In this preliminary study, a bioactive benzoxanthene (BXL) has been included in SLN. Unloaded and BXL-loaded SLN have been prepared using the Phase Inversion Temperature (PIT) method and characterized in terms of size, zeta potential, entrapment

efficiency and stability. Their thermotropic behaviour and interaction with biomembrane models, made of dimyristoylphosphatidylcholine multilamellar vesicles (MLV), was evaluated using differential scanning calorimetry. The release profile of bioactive compound from BXL-loaded SLN was evaluated with an in vitro model. Finally, two spectroscopic assays were performed to evaluate the effect of drug encapsulation on BXL's antioxidant activity.

2.2. Materials and methods

2.2.1. Materials

Precirol® ATO 5 (Glyceryl distearate) was kindly donated by Gattefossé (Saint-Pries, France). TEGIN® O (Glyceryl oleate) and Oleth-20 were obtained from A.C.E.F. S.p.a (Piacenza, Italy). Dimyristoylphosphatidylcholine (DMPC) was obtained from Genzyme (Liestal, Switzerland). Caffeic acid and Mn(OAc)3* 2 H2O were purchased from Sigma Aldrich (Milan, Italy). Purified water from Millipore-Q® Gradient A10TMultra-pure water system (Millipore, Guyancourt, France) was used throughout the study.

2.2.2. Synthesis of BXL

The benzoxanthene lignan diethyl 6,9,10-trihydroxybenzo[k,l]xanthene-1,2-dicarboxylate (to the follow simply BXL) was synthesized according to the methodology previously reported [14]. Briefly, caffeic acid (400 mg, 2.2 mmol) was refluxed with an excess of EtOH (70 mL) and a catalytic amount of concentrated H2SO4 (0.2 mL) for 24 h. The mixture was concentrated, diluted with 50 mL of EtOAc and partitioned with a saturated $NaHCO_3$ solution (50 mL). The aqueous phase was partitioned with EtOAc (3 × 50 mL), and the combined organic layers were dried over anhydrous Na_2SO_4, filtered and taken until dry. The caffeic acid ethyl ester was recovered from the organic phase with 92% yield without further purification. The ester (475 mg, 2.0 mmol) was solubilized in $CHCl_3$ (50 mL) and a suspension of $Mn(OAc)_3$ (2.170 gr, 8.0 mmol; 50 mL of $CHCl_3$) was added. The mixture was stirred for 12 h and then a saturated ascorbic solution (40 mL) was added to quench the reaction. The two phases were partitioned, and the aqueous layer was partitioned again with CH_2Cl_2 (3 × 40 mL). The recovered organic layer was subjected to column chromatography on diol silica gel eluting with CH_2Cl_2:MeOH (100:0 → 95:5), thus affording BXL with 58% yield (Scheme 1). NMR data were in perfect agreement with those previously reported [14].

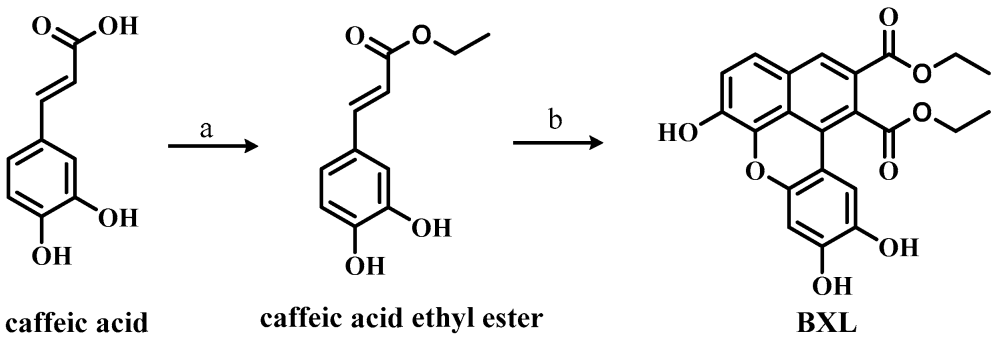

Scheme 1. Synthesis of BXL (a) $H2SO_4$, ethanol, reflux, 12 h; (b) $Mn(OAc)_3$, $CHCl_3$, rt, 3 h

2.2.3. Preparation of SLN

Unloaded and BXL-loaded SLN, whose composition is reported in Table 1, were prepared using the PIT method. Briefly, the lipid phase containing Precirol ATO 5, the emulsifiers (Oleth-20 and Tegin-O) and the aqueous phase were separately heated on a magneto–thermal plate at 75–80 °C. When the two phases reached the same temperature, the aqueous phase was added drop by drop, at constant temperature and under agitation, to the oil phase. The opaque formulation became transparent, realizing the phase reversal from an A/O system to an O/A system. After that, the formulation was taken to room temperature under stirring. BXL was added to the oil phase.

Table 1 Composition of unloaded and BXL-loaded SLN.

	SLN	**SLN 4**	**SLN 8**
BXL (mg)	-	4	8
PrecirolATO 5 (mg)	200	200	200
Tegin-O (mg)	126	126	126
Oleth-20 (mg)	246	246	246
H_2O	up to 20 ml	up to 20 ml	up to 20 ml

2.2.4. SLN physicochemical characterization

The average size (Z-Ave) and polydispersity index (PDI) of SLN were measured by Dynamic Lights Scattering (DLS) method, using a Zeta Sizer Nano-ZS90 (Malvern Instrument Ltd., Worcs, England). The instrument was equipped with a laser whose nominal power was 4.5 mW with a maximum power of 5 mW at 670 nm. The analysis was performed using a 90◦ scattering angle at 25 ± 0.2 ◦C. Before the measurements, 40

µL of each sample suspension was diluted in 1 mL of deionized water. Measurements were performed in triplicate and the calculated mean values were used. The zeta potential (ZP, ξ) was measured by Electrophoretic Light Scattering (ELS) using a Zeta Sizer Nano-ZS90 (Malvern Instrument Ltd., Worcs, England). Each measurement was recorded at 25°C.

2.2.5. Determination of the entrapment efficiency

Two different procedures were used for the entrapment efficiency determination: (1) SLN preparation (0.4 mL) was purified by size-exclusion liquid chromatography. Sephadex-LH20 (1.0 × 10 cm) was employed as a stationary phase, eluted in sequence with water (15 mL), water:EtOH (50:50; 10 mL), EtOH (10 mL) and acetone (10 mL). This latter eluate allowed for the recovery of unentrapped (free) BXL, while the aqueous eluate contained the entrapped BXL. The fraction eluted with water was treated with acetone in order to destroy the SLN and release the BXL [21]. (2) The SLN preparation (3 mL) was centrifuged at 105,000×g at 4 °C for 90 min using an Ultima TL Ultracentrifuge (Beckman, Milan, Italy). The amount of the free BXL present in the suspension was determined from the supernatant properly diluted with acetone (1:3). The entrapped BXL was determined from the pellet, employing acetone (2 mL) to destroy the nanoparticles. Both trapped and free BXL recovered with the two above-described approaches (performed in triplicate) was detected by HPLC-UV (Agilent, Series 1100, Milan, Italy) equipped with a diode array detector set at 280 and 390 nm; a Luna C-18 (Phenomenex; 5 µm, 250 mm × 4.60 mm) was employed as column. The mobile phase consisted of a gradient of CH_3CN (solvent A) in water (solvent B) with a flow rate of 1.0 mL/min: t0A = 10%, t13A = 100%, t15A = 100%, t25A = 10%. In these conditions, BXL eluted at about tR = 11.99 min. The concentration of BXL was calculated by external standard calibration, comparing the area of the peak of BXL in selected samples with BXL standard solutions of known concentrations. The entrapment efficiency % (EE%) was calculated indirectly and directly according to Equations (1) and (2), respectively [22]:

$$EE\% = [(mg_{BXLtot} - mg_{BXLfree}) \div mg_{BXLtot}] \times 100 \quad (1)$$

$$EE\% = (mg_{BXLentrapped} \div mg_{BXLtot}) \times 100 \quad (2)$$

2.2.6. *In vitro* release study of BXL from SLN

The in vitro release study of BXL was carried out for one week. Briefly, 1 mL of SLN formulation containing BXL equivalent to 0.4 mg/mL was placed into a dialysis tube with a molecular weight cut-off of 3.5 kDa (Spectra/Pro, Spectrum Lab., Rancho Dominguez, Ca, USA) and dispersed in a beaker containing 30 mL of H_2O/EtOH 80:20 mixture. The solution was stirred at 200 rpm at 37 ± 0.5 ◦C. At pre-determined intervals, 1 mL of the release medium was withdrawn and replaced with an equal volume of fresh release medium. The concentration of BXL was determined by HPLC.

2.2.7. Antioxidant activity determination

2.2.7.1. DPPH• scavenging assay

The 2,2-diphenyl-1-picrylhydrazyl radical scavenging activity (DPPH•) of BXL and BXL-loaded SLN (SLN 8) samples was determined with the procedure previously reported [23]. A 150 mM DPPH• solution (in MeOH) was freshly prepared and added (200 µL) to 96-well plate, then, aliquots (10, 20, and 30 µL) of samples (1.2 mM) were added to the 96-well plate. The mixtures were stored in the dark at 25 °C, and the OD was acquired with Synergy H1 microplate reader (Agilent, Milan, Italy) at 517 nm after 30 min. Quercetin was employed as reference compound, and all the experiments were performed in triplicate. Aliquots (10, 20, and 30 µL) of MeOH were added to DPPH• solution and these samples were employed as negative control. The percentage of DPPH• quenched was calculated according to equation (3):

$$quenched\ DPPH\cdot\ \% = \frac{(OD_{ctrl} - OD_{sample})}{OD_{crtl}} \times 100 \quad (3)$$

where OD_{ctrl} and OD_{sample} are the optical density of the DPPH• solution without and in presence of the samples, respectively. EC_{50} is the effective concentration (µM) required to quench the 50% of DPPH• present in solution, and it was calculated by regression analysis of quenched DPPH• %.

2.2.7.2. Oxygen Radical Absorption Capacity (ORAC) assay

The ORAC assay was performed as previously reported [23]. All the regents used were freshly prepared. Trolox (used as the standard in the range 5–50 µM), quercetin (used as positive reference; 2.4 mM) or samples (diluted to gain several concentrations: 1.2, 0.6

and 0.1 mM) were added (25 µL) to a black walled 96-well plate. Then, fluorescein (8.16 × 10−5 mM in 75 mM phosphate buffer, pH = 7.4; 150 µL) was added to the multi-well plate and this was shaken at 37 °C for 10 min. The reaction started with the addition of a 153 mM 2,2'-azobis(2-methylpropionamidine) dihydrochloride solution (25 µL). Fluorescence intensity was measured every 1 min for 31 cycles at λEx = 485 nm, λEm = 528 nm, GAIN 50. Tris-HCl buffer solutions (10–80 µM) were used for the negative control. The data acquired in triplicate for each sample were elaborated as the area under the curve (AUC), and Trolox was used as the standard to obtain a calibration curve (R2 = 0.9971), in order to determine the ORAC value of the samples as Trolox equivalents (TE) with Equation (4):

$$ORAC = \frac{(AUC_{sample} - AUC_{blank})}{(slope\ AUC_{Trolox})} \times \frac{1}{(molarity\ sample)} \quad (4)$$

2.2.8. Stability studies

To investigate the stability, SLN were stored in hermetically sealed bottle at room temperature for three months. Technological parameters (particle sizes, PDI and ZP values) were determined after 24 h, a week and at the end of the 1st, 2nd and 3rd months.

2.2.9. Preparation of MLV

MLV were prepared both in the absence and the presence of BXL at different molar fractions (0.003; 0.015; 0.03; 0.045; 0.06; 0.09 and 0.12). DMPC was dissolved in Chloroform/Methanol (1:1, v:v) while BXL was dissolved in Acetone. Aliquots of the DMPC solution containing 7 mg of DMPC were delivered into glass tubes in which aliquots of the BXL solution were added in order to have the exact molar fraction of the compound with respect to DMPC. The solvents were evaporated under nitrogen flow (in a water bath at 37 °C) to obtain the lipid films that were freeze dried overnight. The films were hydrated with 168 µL of 50 mM TRIS (hydroxymethyl)-aminomethane solution (pH = 7.4), heated in a water bath at 37 °C for 1 min, vortexed for 1 min (the procedure was repeated three times) and kept at 37 °C for 1 h [24].

2.2.10. Differential scanning calorimetry

Calorimetric analysis was performed using a Mettler Toledo STARe thermoanalytical system (Greifensee, Switzerland) equipped with a DSC1 calorimetric cell. A Mettler Toledo STARe software (version 16.00) was used to obtain and analyse data. The

sensitivity was automatically chosen as the maximum possible by the calorimetric system. The calorimeter was calibrated using Indium (99.95%), based on the setting of the instrument. Aluminum calorimetric pans of 160 µL were used. Enthalpy changes were calculated from the peak areas.

2.2.10.1. Unloaded and BXL-loaded-SLN

Analysis The thermotropic behaviour of the SLN was evaluated submitting the samples to DSC analysis under N_2 flow (60 mL/min) as follows: a heating scan from 5 to 85 °C, at 2 °C/min; a cooling scan from 85 to 5 °C, at 4 °C/min; for at least three times to confirm the reproducibility of data.

2.2.10.2. Unloaded and BXL-loaded-MLV analysis

Aliquots of 120 µL of MLV at different molar fractions of BXL (0.003; 0.015; 0.03; 0.045; 0.06; 0.09; 0.12) were situated in 160 µL DSC aluminium pans, which were hermetically sealed and subjected to calorimetric analysis under N_2 flow (60 mL/min) as follows: a heating from 5 °C to 37 °C, at 2 °C/min; a cooling from 37 °C to 5 °C, at 4 °C/min. The process was repeated three times to check the reproducibility of results. Unloaded MLV were also analysed to be used as reference [25].

2.2.10.3. MLV/SLN interaction

An amount of 60 µL of MLV and 60 µL of SLN or BXL-loaded-SLN was placed in a 160µL DSC aluminum pan, which was hermetically sealed and subjected to calorimetric analysis under N_2 flow (60 mL/min) as follows: (1) a heating scan between 5 and 85 °C at the rate of 2 °C/min; (2) a cooling scan between 85 and 37 °C at the rate of 4 °C/min; (3) an isothermal period of one hour at 37 °C and (4) a cooling scan between 37 and 5 °C (4 °C/min). This procedure was repeated eight times.

2.3. Results and discussion

2.3.1. Formulation and characterization of SLN

Natural products and their derivatives have played an important role in treating and preventing human diseases since ancient times and they still represent a significant source of modern drugs. However, their efficacy can be limited due to their low hydrophilicity and instability. In addition, they can show scarce absorption, poor pharmacokinetics and poor bioavailability. Novel nanoformulations based on drug-delivery systems could overcome these limitations. Nanoparticles have emerged as versatile, biodegradable, biocompatible carriers for the delivery of drugs [26,27]. From many studies, nanoformulations with sustained release and improved bioavailability at much lower doses than conventional preparations, and in many cases presenting a better safety profile, have been obtained. In this context, we designed SLN using PrecirolATO 5, Tegin-O and Oleth-20 for the encapsulation of BXL to overcome its biopharmaceutical limitations. The components were selected for their wide use, biocompatibility, biodegradability, and versatility [19,26] and on the basis of a series of preliminary experiments. The formulated SLN showed appreciated consistency. As reported in Table 2, unloaded SLN, SLN 4 and SLN 8 showed a mean diameter of around 300 nm, and a polydispersity index within the acceptable range (<0.5) [28]. Zeta potential values were in the range −29 to −25 mV; the magnitude of zeta potential offers a signal of the stability of colloidal preparations. The surface charge of developed nanoparticles will allow their dispersion, since the range obtained is above the threshold values for agglomeration, i.e., ± 15 mV [29,30]. Thus, this surface charge is sufficient to confer physical stability to nanosuspension. The stability of BXL at the temperature used to prepare SLN has been confirmed by HPLC analysis.

Table 2: Dimension (Z-Ave), polydispersity index (PDI) and zeta potential (ZP) of unloaded SLN, SLN4 and SLN8.

	Z-Ave (nm ± SD)	**PDI (-) ± SD**	**ZP (mV ± SD)**
Unloaded-SLN	305.4 ± 1.3	0.360 ± 0.04	-24.9 ± 0.1
SLN 4	296.1 ± 10.3	0.395 ±0.07	-25.6 ± 0.1
SLN 8	300.2 ± 6.9	0.368 ± 0.06	-28.9 ± 0.1

The measurement of the sizes and the polydispersity index during the three months showed that the nanoparticle systems remained stable over the indicated period. The stability of the investigated SLN could be attributed to a steric stabilization due to the presence on the nanoparticle surface of long polyoxyethylene chains of Oleth-20 used to prepare such SLN.

2.3.2. Entrapment Efficiency (EE)

The EE% of the SLN was determined by HPLC-UV, applying two different methodologies [19,20], thus allowing the quantification of both entrapped and free BXL after the preparation of SLN. Precisely, SLN preparation was loaded onto a Sephadex-LH20 column to afford an aqueous eluate containing the SLN and an acetone eluate containing the free BXL (method 1). The former eluate was diluted with acetone to destroy the SLN for the quantification of entrapped BXL. Alternatively, free BXL was determined after ultrafiltration from the permeate, whereas entrapped BXL in SLN was quantified from the retentate (method 2). The details are reported in the Experimental section. The entrapment efficiency (see Table 3) was calculated indirectly and directly according to Equations (1) and (2). The results achieved with both the methodologies agree with each other, thus confirming the reliability of the entrapment procedure. The results indicated an entrapment efficiency between 54.5 and 61.7% when SLN were loaded with 4 mg of BXL (SLN4) and between 62.8 and 68.7% when nanoparticles were loaded with twice the amount of BXL (SLN8).

Table 3: Entrapment efficiency (EE) determination of BXL in SLN4 and SLN8. Data are reported as mean (n = 3) ± SD.

sample	**Method**	**EE%***	
SLN 4	Sephadex-LH20	$59.3\pm2.0^{a,b}$	(Eq.1)
		$61.7\pm1.8^{a,c}$	(Eq.2)
	Centrifugation	$54.5\pm2.7^{b,c}$	(Eq.1)
		$58.7\pm0.9^{a,d}$	(Eq.2)
SLN 8	Sephadex-LH20	$62.8\pm4.1^{b,d}$	(Eq.1)
		$66.1\pm2.7^{c,d}$	(Eq.2)
	Centrifugation	$65.5\pm1.4^{a,e}$	(Eq.1)
		$68.7\pm3.9^{b,e}$	(Eq.2)

* Each determination was performed in triplicate. EE% was calculated with indirect method according to Equation (1) and with direct method according to Equation (2). a–e Different letters indicate statistical differences at $p < 0.01$ (Tukey test).

2.3.3. *In vitro* release

The in vitro release of BXL from SLN in H_2O/EtOH 80:20 was evaluated by a dialysis method. An amount of 1 mL of medium was removed at predetermined time intervals and the released BXL was assayed by HPLC-UV [31]. The concentration of BXL released from the SLN was reported as a percentage respect to the total compound present in SLN and this value was plotted as a function of time in Figure 1. In figure, the BXL release taking into account the encapsulation efficiency (black line) and the BXL release from the SLN formulation (red line) are shown. The BXL is released faster within the 60h followed by a slow-release phase. Taking into account the encapsulation efficiency, the percentage of drug released reached 15.7% at 6 h and then it slowly increased up to 20.2% at 54 h, stabilizing at 21% for the remaining time (from 54 h up to 168 h). The percentage of drug released from the total SLN formulation reached the 60 % between 48 and 54 h and increased up to 70% within 168 h.

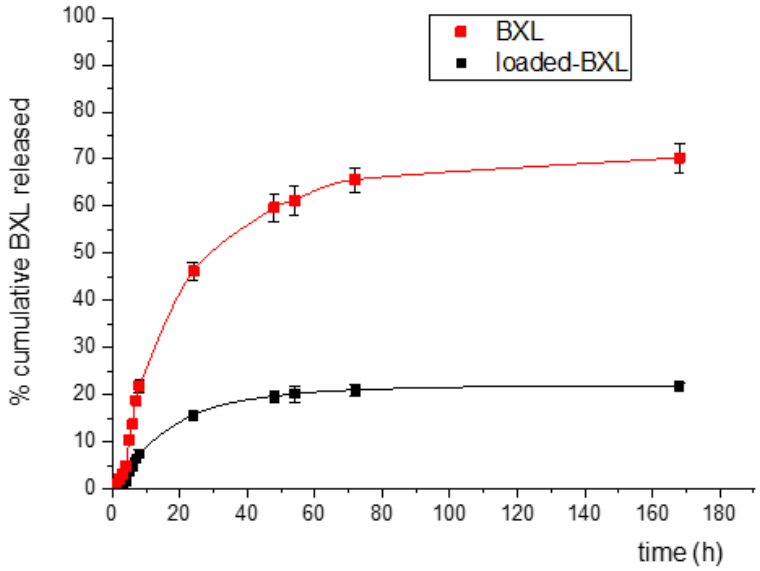

Figure 1: In vitro BXL release profile. In red is reported the quantification of BXL released from the formulation, while in black the quantification of BXL released based on the entrapment efficiency. The data plotted are means (n = 3) ± SD.

Similar values have been obtained for the polyphenolic quercetin [32,33]. The sustained release of BXL SLN could reveal the applicability of these SLN as a drug-delivery system which could permit the accumulation of the drug in the cells and allow the delivery of BXL for a long timeframe.

2.3.4. Antioxidant activity determination

Benzoxanthene lignans are reported for a variety of biological activities, including antioxidant activity [8]. In order to determine the capability of pure BXL and BXL-loaded in SLN to scavenge reactive oxygen species, two in vitro assays were employed. Usually, the most commonly employed methods to measure the antioxidant activity are split into assays based on hydrogen atom transfer (HAT) such as the ORAC assay, and others based on single electron transfer (SET) such as DPPH radical scavenging assay. The results of the two tests are reported in Table 4. DPPH radical scavenging activity is expressed as the concentration of sample quenching the 50% of radical (EC_{50}), thus the lower the EC_{50} values the higher the activity. ORAC results are reported referring to the antioxidant standard Trolox (TE; µmol Trolox equivalent), namely, higher TE value corresponds to higher antioxidant activity. Quercetin was employed as positive reference in both the assays. According to the results, BXL maintains its antioxidant activity even when it is loaded in SLN, and DPPH and ORAC values (Table 4) are similar to those of the free active compound. These results are in agreement with the findings on similar SLN formulations [34] and encourage future studies with BXL-SLN aimed at in vivo evaluation of antioxidant activity with a potential prolonging of the antioxidant effect.

Table 4 Antioxidant activity determination of BXL and SLN8. EC50 values refer to DPPH radical scavenging activity; TE values refer to ORAC assay.

Sample	DPPH (EC_{50})[1]	ORAC (TE)[2]
BXL	68.7 ± 12.4^{a,b}	6.2 ± 0.3 ^{a,d}
SLN 8	83.1 ± 7.3 ^{a,c}	4.4 ± 0.2^{b,d}
Quercetin	17.9 ± 4.3 ^{b,c}	15.4 ± 2.3 ^{c,d}
MeOH[3]	>350	-
Tris-HCl[3]		0.05 ± 0.01^{a,e}

[1] Results are reported in µM as mean ± SD (n = 3). 2 Results are reported as Trolox equivalent (TE) in µmol as mean ± SD (n = 3). 3 Negative controls. a–e Different letters indicate statistical differences at $p < 0.05$ (Tukey test).

2.3.5. Differential scanning calorimetry

DSC has an important role in the characterization of lipid nanoparticles and their interactions with biological membrane models. It is able to measure the heat exchanges associated with structural alterations of materials and allows us to obtain information about the structural properties of the samples [35]. In this study, DSC was used to

characterize unloaded and loaded SLN and to study their interactions with liposomes of 1,2-dimyristoyl-sn-glycero-3-phosphocholine (DMPC). In addition, DSC was used to study the effect of BXL on the DMPC MLV.

2.3.5.1. Unloaded and BXL-loaded-SLN analysis

Calorimetric curves of Precirol, unloaded SLN, SLN 4 and SLN 8 are shown in Figure 2. Precirol exhibits a peak at 55.06 °C and an enthalpy variation of 125 J/g. Unloaded SLN are characterized by a peak at around 51 °C and an enthalpy variation of −90.39 J/g. SLN melting temperature was about 4 °C lower than that of Precirol, which could be due to an increase in surface area resulting from SLN colloidal sizes and due to interactions between solid lipid and surfactant molecules that led to a less ordered structure. The enthalpy variation decreases and the $\Delta T_{1/2}$ increase are an indication that, during the melting, a lower cooperation among the lipid molecules occurs. The loading of BXL inside SLN did not produce significant variation of the melting temperature but it produced the appearance of a small shoulder at lower temperature; the shoulder was more accentuated when the concentration of BXL was higher. BXL also caused a slight decrease in the enthalpy variation and an increase in the $\Delta T_{1/2}$ (Table 5). The variation of the calorimetric curve of loaded SLN compared to unloaded SLN, as well as to the enthalpy variation and $\Delta T_{1/2}$, are an indication of the incorporation of BXL into the SLN structure. The presence of the shoulder suggests that BXL could be incorporated in the SLN not homogeneously. The SLN exhibit melting points (>50 °C) above body temperature, which is a prerequisite for retaining the solid state of the nanoparticles. In fact, many of the claimed advantages of SLN as drug carrier systems are related to the solid state of their lipid matrix [36].

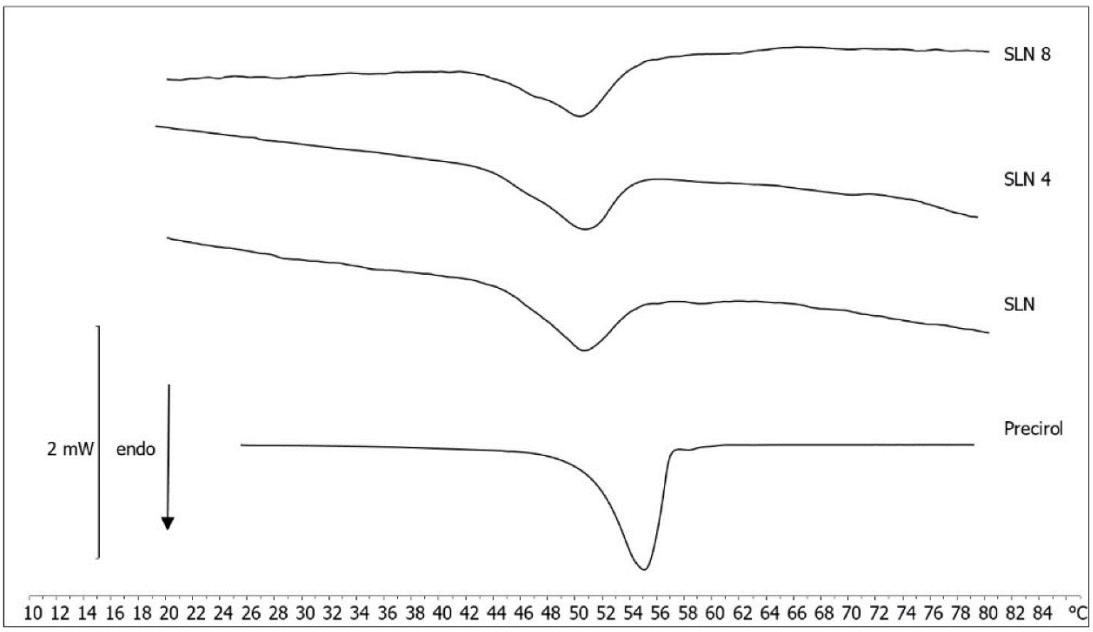

Figure 2: Calorimetric curves, in heating mode, of Precirol, SLN, SLN 4 and SLN 8.

Table 5 Transition temperature (Tm), enthalpy variation (ΔH) and peak width at half height (ΔT1/2) of Precirol, SLN, SLN4 and SLN8.

Sample	T_m (°C)	ΔH (J/gr Precirol)	$\Delta T_{1/2}$ (°C)
Precirol	55.06	-125.00	3.65
SLN	50.60	-90.39	5.79
SLN 4	50.63	-76.32	5.92
SLN 8	50.44	-73.31	6.13

2.3.5.2. Unloaded and BXL-loaded-MLV analysis

Calorimetric curves of MLV without and with BXL at different molar fractions (0.00; 0.015; 0.03; 0.045; 0.06; 0.09; 0.12) are reported in Figure 3. The calorimetric curve of unloaded MLV is characterized by a pre-transition peak at about 17 °C (related to the transition from the lamellar gel phase to the ripple phase) and a transition peak at about 25 °C (related to the transition from the ripple phase to liquid crystalline phase) [37]. The increased concentration of BXL led to significant variation in the calorimetric curve of MLV; in fact, the pre-transition peak decreased and completely disappeared starting from the molar fraction of 0.03. The main transition peak shifted to a lower temperature and its intensity decreased. These data indicate that BXL affected the thermotropic behaviour of MLV. It caused a fluidization of the MLV as well as a decrease in the cooperativity among the phospholipids during their melting. The presence of a unique peak indicates that BXL is homogenously incorporated in the DMPC MLV.

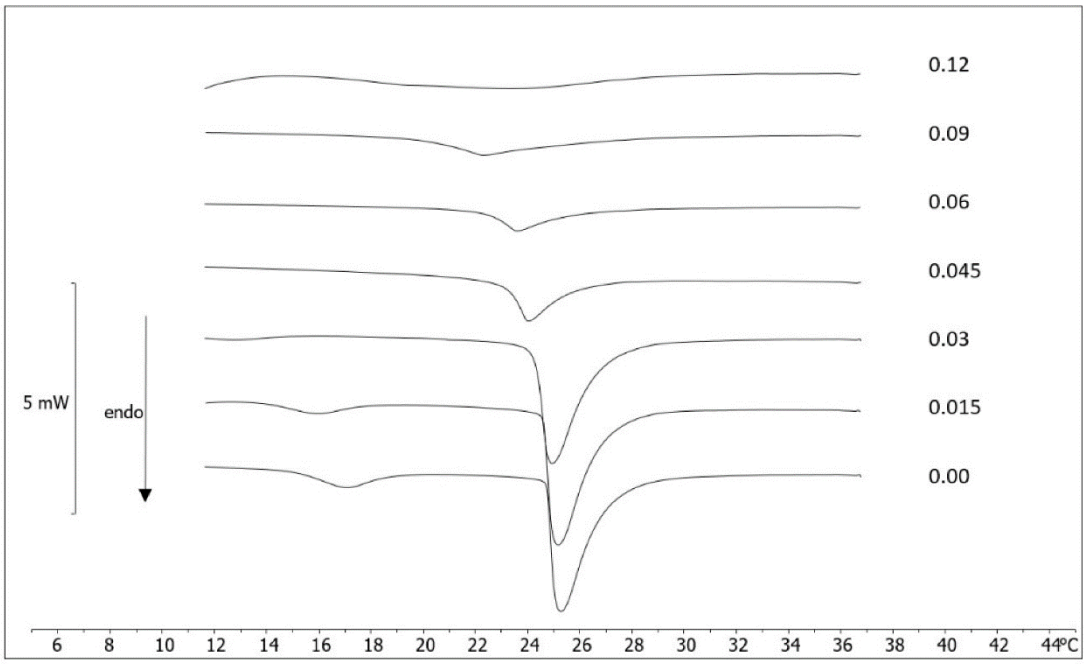

Figure 3: Calorimetric curves, in heating mode, of MLV prepared without and with BXL at different molar fractions.

2.3.5.3. MLV/SLN Interaction

This intricacy of the cell membrane structure makes the interactions with drugs and drug-delivery systems very difficult to investigate. Therefore, simplified artificial membrane systems, which mimic the natural bilayer lipid membrane, have been developed. In this article, DMPC MLV are used as a simplified system that mimics many biological membrane properties [38]. DSC was used to evaluate the interaction between SLN and MLV. Before evaluating this eventual interaction, we studied the ability of BXL to be incorporated into MLV when put in contact with them. For this reason, BXL and MLV were put in contact in a calorimetric pan and submitted to DSC analysis. The calorimetric curves are shown in Figure 4. If BXL was able to be incorporated into the MLV, a variation of the calorimetric curve should be seen. In the figure, it is evident that only the pre-transition peak slightly varies, whereas the main peak remains unchanged during all the contact time with BXL. This result suggests that BXL does not affect the thermotropic behaviour of MLV and it is not able to cross the aqueous medium, reach the MLV surface and go inside the MLV structure, probably due to its low water solubility.

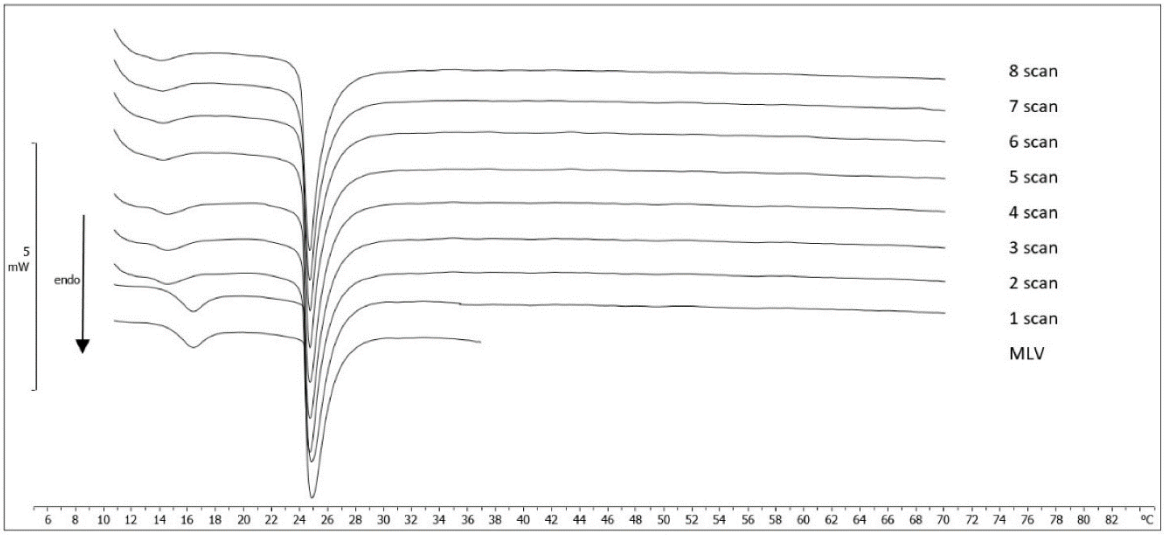

Figure 4: Calorimetric curves, in heating mode, of MLV put in contact with BXL at increasing incubation time. There are 68 min between one scan and the next one.

To evaluate the interaction between MLV and unloaded SLN or BXL-loaded SLN, the samples were put in contact in the calorimetric pan and submitted to analysis over a period of time. The interaction between MLV and SLN is highlighted by the variation of the calorimetric curves with respect to the calorimetric curve of the samples recorded before the contact. The calorimetric curves of the interaction between MLV and unloaded SLN show important features (Figure 5). First, we will consider the peaks of the MLV: the pre-transition peak decreases and then disappears; the main peak slightly shifts to a lower temperature and its intensity decreases. The peak of unloaded SLN shifts and the intensity decreases. These features are a sign of the interaction between MLV and SLN. In Figure 6, the calorimetric curves related to the interaction between MLV and SLN 8 are shown. As far as the MLV are concerned, the pre-transition peak vanishes from the first scan and the main peak slightly moves to a lower temperature and its intensity decreases. As the alteration of the phase behaviour of MLV and SLN is due the presence of a perturbing agent in their structure, we can hypothesize that MLV and SLN 8 interact. Let us compare the results obtained with SLN and SLN8. In Figure 7a, the transition temperature variation of MLV is reported as a function of calorimetric scans. A decrease in this parameter is evident and the decrease is more evident in the experiment run with SLN 8. The results related to the enthalpy variation as a function of the calorimetric scans, shown in Figure 7b, clearly indicate a decrease in the parameter and that the decrease is more pronounced in the experiment run with SLN 8. This information, together with the results of the MLV prepared with BXL, provide us with important information. We saw that BXL interacts

with MLV. SLN and SLN 8 interact and affect the thermotropic behaviour of MLV with SLN 8 exerting a more pronounced effect that can be due both to SLN and to BXL (SLN and BXL could exert an additive effect on MLV); in other words, SLN could enter the MLV and release BXL. The results of our research on the interactions between BXL-loaded SLN and a biological membrane model pointed out that SLN could be able to penetrate into the biomembrane, thus facilitating BXL permeation into the biomembrane itself. Therefore, SLN interactions with biomembranes could account for their ability to allow the penetration of BXL into cell membranes improving its uptake by the cells and, hence, its bioavailability.

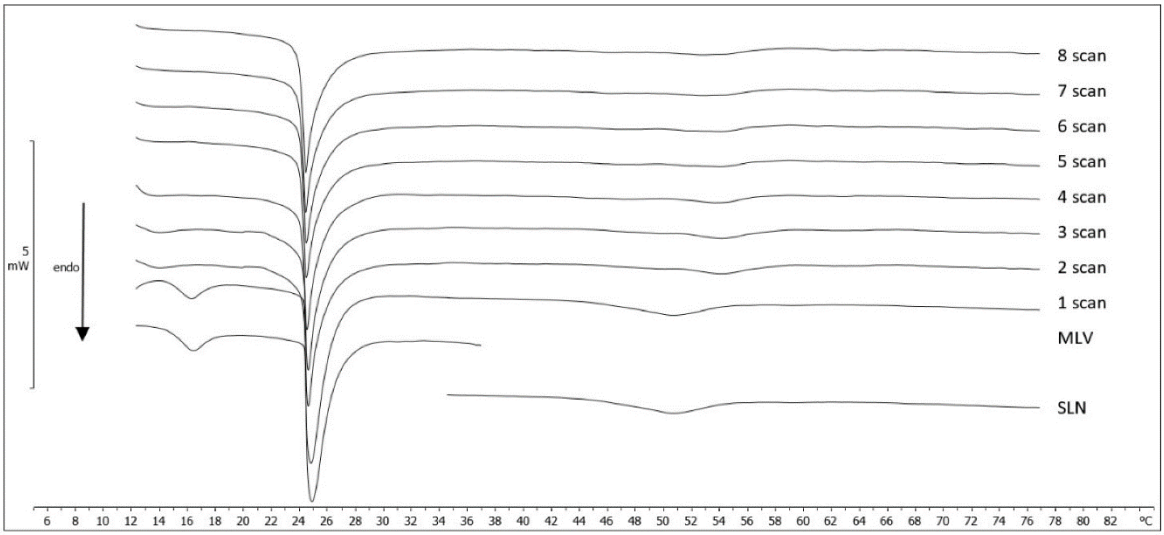

Figure 5: Calorimetric curves, in heating mode, of MLV put in contact with SLN, at increasing incubation time. There are 68 min between one scan and the next.

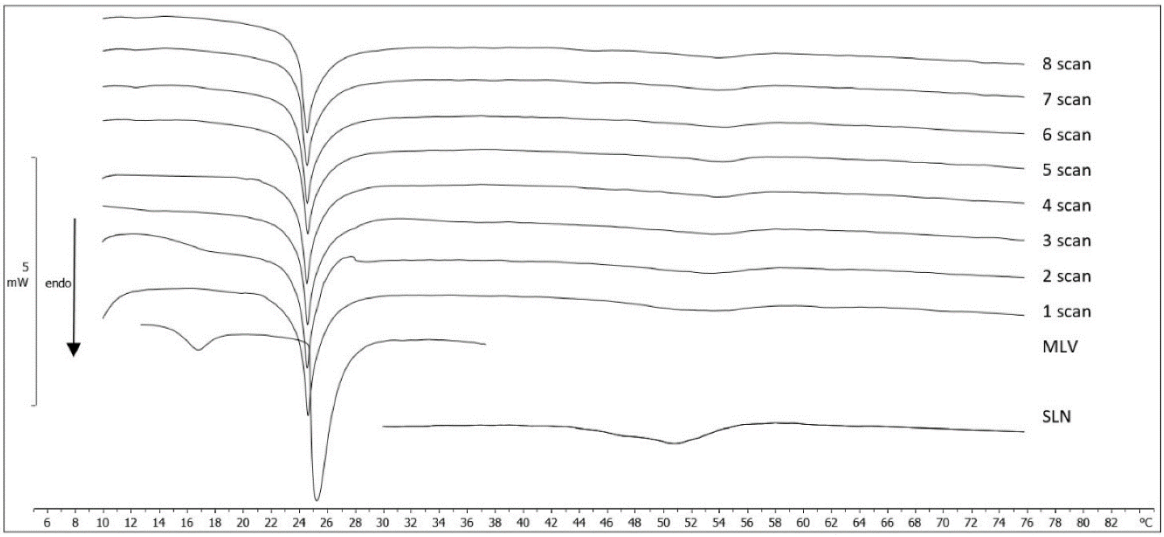

Figure 6: Calorimetric curves, in heating mode, of MLV put in contact with SLN 8 at increasing incubation time. There are 68 minutes between one scan and the next.

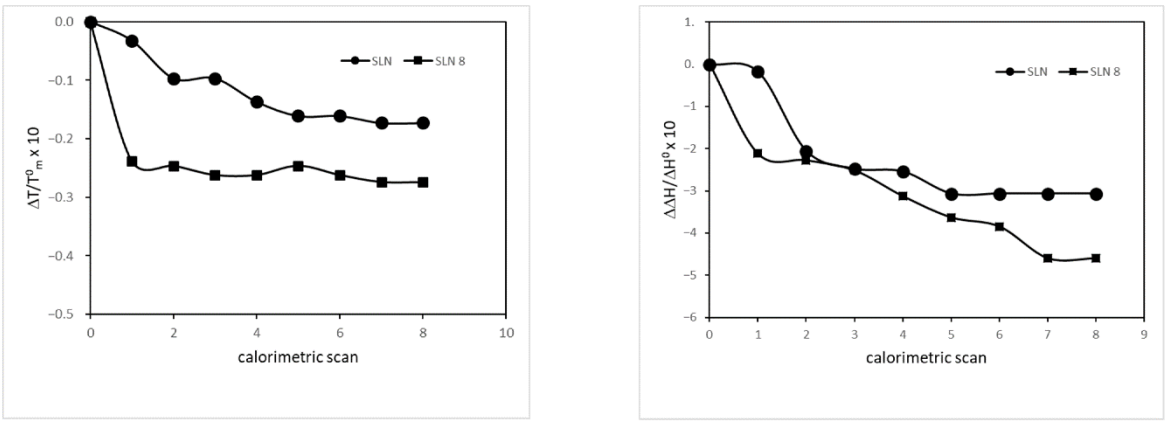

(a) (b)

Figure 7: (a) Transition temperature variation of MLV left in contact with SLN and SLN 8, as a function of the calorimetric scans. There are a 68 min between one scan and the next. The transition temperature variation is reported as $\Delta T/T^0m$ ($\Delta T = Tm - T^0m$, where Tm is the transition temperature of the MLV left in contact with SLN or SLN 8 and T^0m is the transition temperature of MLV. (b) Transition enthalpy variation of MLV left in contact with SLN and SLN 8, as a function of the calorimetric scans. There are 68 min between one scan and the next. The transition enthalpy variation is reported as $\Delta\Delta H/\Delta H^0$ ($\Delta\Delta H = \Delta H - \Delta H^0$, where ΔH is the transition enthalpy variation of the MLV left in contact with SLN or SLN 8 and $\Delta H0$ is the transition enthalpy variation of MLV).

2.4. Conclusions

In this work, a bioactive benzoxanthene was included in SLN, prepared by the Phase Inversion Temperature (PIT) method, which produced promising results in terms of size, zeta potential, entrapment efficiency and stability. The percentage of benzoxanthene released from SLN was about 70%. The DPPH and ORAC tests indicated that BXL maintains its antioxidant activity even when it is loaded in SLN. Differential scanning calorimetry was used to study the SLN thermotropic behaviour and interaction with biomembrane models represented by multilamellar vesicles of dimyristoylphosphatidylcholine. The obtained data suggest that SLN could interact and release the benzoxanthene into the biomembrane model. The results obtained in this study suggest the potential use of SLN as a delivery system for benzoxanthene.

Author Contributions: Conceptualization, M.G.S.; methodology, C.T. (Cristina Torrisi), N.C., V.M. and M.G.S.; software, N.C.; validation, N.C. and V.M.; formal analysis, C.T. (Cristina Torrisi), N.C., and V.M.; investigation, M.G.S.; resources, C.T. (Corrado Tringali), F.C. and M.G.S.; data curation, N.C., V.M. and M.G.S.; writing—original draft preparation, C.T. (Cristina Torrisi), N.C., V.M. and M.G.S.; writing—review and editing, N.C., V.M., C.T. (Corrado Tringali) and M.G.S.; visualization, C.T. (Cristina Torrisi) and F.C.; supervision, F.C., C.T. (Corrado Tringali) and M.G.S.; project administration, M.G.S.; funding acquisition, V.M. All authors have read and agreed to the published version of the manuscript.

Funding: This research was funded by MIUR ITALY PRIN 2017 (Project No. 2017A95NCJ).

Institutional Review Board Statement: Not applicable.

Informed Consent Statement: Not applicable.

Data Availability Statement: Data were generated at the Department of Drug and Health Sciences and at the Department of Chemical Sciences, University of Catania. Data supporting the results of this study are available from the corresponding authors on request.

Acknowledgments: The authors gratefully acknowledge the Bio-Nanotech Research and Innovation Tower of the University of Catania (BRIT; project PONa3_00136) financed by the Italian Ministry for Education, University and Research MIUR) for making available the Synergy H1 microplate reader.

Conflicts of Interest: The authors declare no conflict of interest.

2.5. References

1. Da Silva, S.A.S.; Souto, A.L.; Agra, M.D.; da-Cunha, E.V.L.; Barbosa, J.M.; da Silva, M.S.; Braz Filho, R. *A new arylnaphthalene type lignan from Cordia rufescens A. DC. (Boraginaceae).* *Arkivoc*, 2004, 54-58. https://doi.org/10.3998/ark.5550190.0005.607.
2. Shi, S.; Zhang, Y.; Huang, K.; Liu, S.; Zhao, Y. Application of preparative high-speed counter-current chromatography for separation and purification of lignans from Taraxacum mongolicum. *Food Chem.* 2008, *108*, 402-406. https://doi.org/10.1016/j.foodchem.2007.10.069.
3. Qu, Z.Y.; Zhang, Y.W.; Yao, C.L.; Jin, Y.P.; Zheng, P.H.; Sun, C.H.; Wang, Y.P. Chemical constituents from Orobanche cernua Loefling. *Biochem. Systematics Ecol.* 60, *2015*, 199-203. https://doi.org/10.1016/j.bse.2015.04.028.
4. Tanaka, T.; Nishimura, A.; Kouno, I.; Nonaka, G.; Yang, C.R. Four new caffeic acid metabolites, yunnaneic acids E-H, from Salvia yunnanensis. *Chem. Pharmac. Bull.* 1997, *45*, 1596-1600.
5. Jiang, Z.H.; Tanaka, T.; Kouno, I. Chilianthins A-F, six triterpene esters having dimeric structures from Rhioptelea chiliantha Diels et Hand-Mazz. *Chem. Pharm. Bull.* 1996, *44*, 1669-1675.
6. Kumar, M.; Rawat, P.; Rahuja, N.; Srivastava, A.K.; Maurya, R. Antihyperglycemic activity of phenylpropanoyl esters of catechol glycoside and its dimers from Dodecadenia grandiflora. *Phytochem.* 2009, *70*, 1448-1455. https://doi.org/10.1016/j.phytochem.2009.07.029.
7. Daquino, C.; Rescifina, A.; Spatafora, C.; Tringali, C. Biomimetic synthesis of natural and "unnatural" lignans by oxidative coupling of caffeic esters. *Eur. J. Org. Chem.* 2009, *36*, 6289-6300. https://doi.org/10.1002/ejoc.200900804.
8. Spatafora, C.; Daquino, C.; Tringali, C.; Amorati, R. Reaction of benzoxanthene lignans with peroxyl radicals in polar and non-polar media: cooperative behaviour of OH groups. *Org. Biomol. Chem.* 2013, *11*, 4291-4294. https://doi.org/10.1039/c3ob40723c.
9. Gerstmeier, J.; Kretzer, C.; Di Micco, S.; Miek, L.; Butschek, H.; Cantone, V.; Pace, S. Novel benzoxanthene lignans that favorably modulate lipid mediator biosynthesis:

A promising pharmacological strategy for anti-inflammatory therapy. *Biochem. Pharmacol.* 2019, *165*, 263-274. https://doi.org/10.1016/j.bcp.2019.03.003.

10. Floresta, G.; Cardullo, N.; Spatafora, C.; Rescifina, A.; Tringali, C. A rare natural benzo k,l xanthene as a turn-off fluorescent sensor for Cu2+ Ion. *Int. J. Mol. Sci.* 2020, *21*. https://doi.org/10.3390/ijms21186933.
11. Genovese, C.; Pulvirenti, L.; Cardullo, N.; Muccilli, V.; Tempera, G.; Nicolosi, D.; Tringali, C. Bioinspired benzoxanthene lignans as a new class of antimycotic agents: synthesis and Candida spp. growth inhibition. *Nat. Prod. Res.* 2020, *34*, 1653-1662. https://doi.org/10.1080/14786419.2018.1525375.
12. Tumir, L.M.; Zonjic, I.; Zuna, K.; Brkanac, S.R.; Jukic, M.; Hudek, A.; Stojkovic, M.R. Synthesis, DNA/RNA-interaction and biological activity of benzo k,l xanthene lignans. *Bioorg. Chem.* 2010, *104*. https://doi.org/10.1016/j.bioorg.2020.104190.
13. Di Micco, S.; Mazue, F.; Daquino, C.; Spatafora, C.; Delmas, D.; Latruffe, N.; Bifulco, G. Structural basis for the potential antitumour activity of DNA-interacting benzo kl xanthene lignans. *Org. Biomol. Chem.* 2011, *9*, 701-710. https://doi.org/10.1039/c0ob00480d.
14. Spatafora, C.; Barresi, V.; Bhusainahalli, V.M.; Di Micco, S.; Musso, N.; Riccio, R.; Tringali, C. Bio-inspired benzo k,l xanthene lignans: synthesis, DNA-interaction and antiproliferative properties. *Org. Biomol. Chem.* 2014, *12*, 2686-2701. https://doi.org/10.1039/c3ob42521e.
15. Vijayakurup, V.; Spatafora, C.; Tringali, C.; Jayakrishnan, P.C.; Srinivas, P.; Gopala, S. Phenethyl caffeate benzoxanthene lignan is a derivative of caffeic acid phenethyl ester that induces bystander autophagy in WiDr cells. *Mol. Biol. Rep.* 2014, *41*, 85-94. https://doi.org/10.1007/s11033-013-2840-8.
16. Basini, G.; Baioni, L.; Bussolati, S.; Grasselli, F.; Daquino, C.; Spatafora, C.; Tringali, C. Antiangiogenic properties of an unusual benzo k,l xanthene lignan derived from CAPE (Caffeic Acid Phenethyl Ester). *Investigational New Drugs* 2012, *30*, 186-190. https://doi.org/10.1007/s10637-010-9550-z.
17. Vijayakurup, V.; Spatafora, C.; Daquino, C.; Tringali, C.; Srinivas, P.; Gopala, S. Phenethyl caffeate benzo kl xanthene lignan with DNA interacting properties induces DNA damage and apoptosis in colon cancer cells. *Life Sci.* 2012, *91*, 1336-1344. https://doi.org/10.1016/j.lfs.2012.10.013.

18. Capolupo, A.; Tosco, A.; Mozzicafreddo, M.; Tringali, C.; Cardullo, N.; Monti, M.C.; Casapullo, A. proteasome as a new target for bio-inspired benzo k,l xanthene lignans. *Chem. Eur. J.* 2017, *23*, 8371-8374. https://doi.org/10.1002/chem.201701095.
19. Mehnert, W.; Mäder, K. Solid lipid nanoparticles production, characterization and applications. *Adv. Drug Del. Rev.* 2001, *47*, 165 –196
20. Gordillo-Galeano, A.; Mora-Huertas, C.E. Solid lipid nanoparticles and nanostructured lipid carriers: A review emphasizing on particle structure and drug release. *Eur. J. Pharm. Biopharm.* 2018, *133*, 285–308.
21. Ji, P.; Yu, T.; Liu, Y.; Jiang, J.; Xu, J.; Zhao, Y.; Wu, C. Naringenin-loaded solid lipid nanoparticles: preparation, controlled delivery, cellular uptake, and pulmonary pharmacokinetics. *Drug Design Development and Therapy* 2016, *10*, 911-925. https://doi.org/10.2147/dddt.s97738
22. Goncalves, L.M.D.; Maestrelli, F.; Manelli, L.D.; Ghelardini, C.; Almeida, A.J.; Mura, P. Development of solid lipid nanoparticles as carriers for improving oral bioavailability of glibenclamide. *Eur. J. Pharm. Biopharm.* 2016, *102*, 41-50. https://doi.org/10.1016/j.ejpb.2016.02.012.
23. Cardullo, N.; Floresta, G.; Rescifina, A.; Muccilli, V.; Tringali, C. Synthesis and in vitro evaluation of chlorogenic acid amides as potential hypoglycemic agents and their synergistic effect with acarbose. *Bioorg. Chem.* 2021, *117*, 105458
24. Sarpietro, M.G.; Torrisi, C.; Di Sotto, A.; Castelli, F. Interaction of limonene, terpineol, and 1,8 cineol with a model of biomembrane: a DSC study. *Thermochim. Acta* 2021, *700*, 178938.
25. Torrisi, C.; Malfa, G.A.; Acquaviva, R.; Castelli, F.; Sarpietro, M.G. Effect of protocatechuic acid ethyl ester on biomembrane models: multilamellar vesicles and monolayers. *Membranes* 2022, *12*, 283. https://doi.org/10.3390/membranes12030283
26. Andersen, F.A. Final Report on the Safety Assessment of Oleth-2, -3, -4, -5, -6, -7, -8, -9, -10, -11, -12, -15, -16, -20, -23, -25, -30, -40, -44, and -501. *Int. J. Toxicol.* 1999, *18(Suppl. 2)*, 17-24.
27. Graverini, G.; Piazzini, V.; Landucci, E.; Pantano, D.; Nardiello, P.; Casamenti, F.; Pellegrini-Giampietro, D.E.; Bilia, A.R.; Bergonzi, M.C. Solid lipid nanoparticles for

delivery of andrographolide across the blood-brain barrier: in vitro and in vivo evaluation. *Coll. Surf. B: Biointerfaces* 2018, *16*1, 302-313.

28. Aditya, N.P.; Macedo, A.S.; Doktorovova, S.; Souto, E.B.; Kim, S.; Chang, P.-S.; Ko, S. Development and evaluation of lipid nanocarriers for quercetin delivery: A comparative study of solid lipid nanoparticles (SLN), nanostructured lipid carriers (NLC), and lipid nanoemulsions (LNE). *LWT - Food Sci. Technol.* 2014, *59*, 115e121116
29. Sharma, A.K.; Sahoo, P.K.; Majumdar, D.K.; Sharma, N.; Sharma, R.K.; Kumar, A. Fabrication and evaluation of lipid nanoparticulates for ocular delivery of a COX-2 inhibitor. *Drug Deliv.* 2016, *23*, 3364–3373.
30. Samimi, S.; Maghsoudnia, N., Eftekhari, R.B.; Dorkoosh, F. Lipid-Based Nanoparticles for Drug Delivery Systems. In *Characterization and biology of nanomaterials for drug delivery*; 2019; pp. 47-76.
31. Pandita, D.; Kumar, S.; Poonia, N., Lather, V. Solid lipid nanoparticles enhance oral bioavailability of resveratrol, a natural polyphenol. *Food Res. Int.* 2014, *62*, 1165-1174.
32. Bose, S.; Du, Y.; Takhistov, P.; Michniak-Kohn, B. Formulation optimization and topical delivery of quercetin from solid lipid based nanosystems. *Int. J. Pharm.* 2013, *441*, 56–66.
33. Vijayakumar, A.; Baskaran, R.; Jang, Y.S.; Oh, S.H.; Yoo, B.K. Quercetin-loaded solid lipid nanoparticle dispersion with improved physicochemical properties and cellular uptake. *AAPS PharmSciTech*, 2016, DOI: 10.1208/s12249-016-0573-4
34. Montenegro, L.; Modica, M.N., Salerno, L.; Panico, A.M.; Crascì, L.; Puglisi, G.; Romeo, G. In vitro antioxidant activity of idebenone derivative-loaded solid lipid nanoparticles. *Molecules* 2017, *22*, 887. doi:10.3390/molecules22060887
35. Bunjes, H.; Unruh, T.S. Characterization of lipid nanoparticles by differential scanning calorimetry, X-ray and neutron scattering. *Adv. Drug Deliv. Rev.* 2007, *59*, 379-402.
36. Barbosa, R.M.; Ribeiro, L.N.M.; Casadei, B.R.; da Silva, C.M.G.; Queiróz, V.A.; Duran, N.; de Araújo, D.R.; Severino, P; de Paula, E. Solid lipid nanoparticles for dibucaine sustained release. *Pharmaceutics* 2018, *10*, 231; doi:10.3390/pharmaceutics10040231

37. Walde, P. Preparation of vesicles (liposomes). In *ASP Encyclopedia of Nanoscience and Nanotechnology*; Nalwa, H.S., Ed.; American Scientific Publishers: Stevenson Ranch, CA, USA, 2004; Volume 9, pp. 43–79.
38. Wisniewska-Becker, A.; Gruszecki,W.I. Biomembrane models. In *Drug-Biomebrane Interaction Studies: The Application of Calorimetric Techniques*; Pignatello, R., Ed.; Woodhead Publishing Limited: Cambridge, UK, 2013; pp. 46–95.

3. BENZO[K,L]XANTHENE LIGNAN-LOADED SOLID LIPID NANOPARTICLES FOR TOPICAL APPLICATION: A PRELIMINARY STUDY

Cristina Torrisi[1], Nunzio Cardullo[2], Stefano Russo[1], Alfonsina La Mantia[1], Rosaria Acquaviva[1], Vera Muccilli[2], Francesco Castelli[1] and Maria Grazia Sarpietro[1,]*

[1]Department of Drug and Health Sciences, University of Catania, Viale Andrea Doria 6, 95125 Catania, Italy; torrisi.cristina@hotmail.it (C.T.); fcastelli@unict.it (F.C.)

[2] Department of Chemical Sciences, University of Catania, Viale Andrea Doria 6, 95125 Catania, Italy; ncardullo@unict.it (N.C.); v.muccilli@unict.it (V.M.); ctringali@unict.it (C.T.)

*correspondence: mg.sarpietro@unict.it

Molecules 2022, *27*, 5887. https:// doi.org/10.3390/molecules27185887

3.1. Introduction

Skin is the largest organ and covers the entire surface of the human body. Anatomically, it is composed of different layers-epidermis, dermis, and hypodermis- of which the outermost is the stratum corneum (SC). The latter represents the first protective human physical barrier: it prevents the loss of water and electrolytes, reduces the penetration of chemical substances, and protects against pathogenic microorganisms [1]. Skin has, historically, been used for the topical delivery of compounds since it reduces the risk of systemic side effects and allows the drug to remain concentrated in the targeted tissue. However, skin is composed of alternated hydrophobic and hydrophilic layers (ranging from the perspiratio insensibilis to the adipocytes), and the particular structure of SC is comparable to a brick wall made of these sheets, so it is not surprising that only a few substances, with an ideal n-octanol/water partition ratio (logP), are able to cross the skin [2]. A way to overcome this problem, and improve drug penetration and distribution, is the employment of lipid nanoparticles as carriers of active molecules [3]. Solid lipid nanoparticles (SLN) have been studied as alternative colloidal carriers to the traditional methods, especially for the delivery of lipophilic compounds. They are composed of a solid lipid matrix dispersed in aqueous medium and stabilized by various surfactants. Cutaneous use of SLN exhibits several advantages, such as biocompatibility (since they are composed of physiological and biodegradable lipids), protection of encapsulated compounds sensitive to light, oxidation and hydrolysis, and drug release control [4]. The strategic mechanism behind lipid nanoparticles for topical application is the formation of an occlusive film at the SC surface that prevents water loss and improves the skin lipid barrier, leading to corneocytes packing reduction and inter-corneocyte gaps enlargement, with a consequent increase in drug penetration [5–7]. It was also observed that a better SC occlusion and a greater interaction with skin is obtained with smaller lipid nanoparticles, generally around 200–300 nm [8]. Nowadays, skin is constantly exposed to environmental stresses (ultraviolet radiations, chemical substances, and pathogens) which leads to the formation of ROS species. The latter can activate proliferative and cell survival signals that can alter apoptotic pathways and lead to an extensive number of skin disorders. One way to eliminate or minimize the effects of ROS and/or their products, reducing oxidative damage to cellular constituents, is the use of antioxidant molecules [9].

In the present work, a bioinspired lignan (BXL, Scheme 1), belonging to the rare group of benzoxanthene lignans, was used to prepare SLN formulations that will be used in the preventive treatment of the skin conditions.

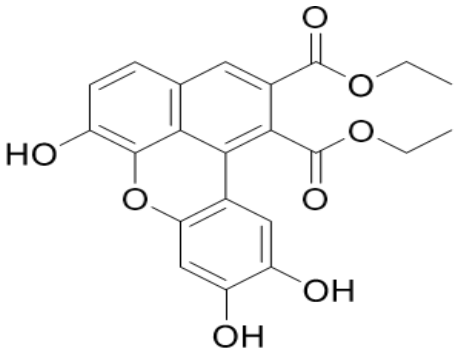

Scheme 1: Structure of BXL

BXL and other analogues show an array of biological properties, including antioxidant, antifungal [10], antibacterial [11], anti-inflammatory [12], anti-proliferative, anti-angiogenic, DNA-binding [13], and proteasome-inhibiting activities [14,15]. However, these bioactive compounds are very lipophilic (BXL: capacity factor 3.24; calculated logP 3.71) [16] and their potential use in pharmacological studies is limited, due to the very low solubility in aqueous media (See Figure S1, Supplementary Material for the predicted physicochemical properties of BXL) [17,18]. The introduction of BXL into SLN produced promising results in terms of size, polydispersity index, zeta potential, stability, and entrapment efficiency, while retaining its antioxidant and anti-inflammatory activity [19]. The interest behind the possible applications of this uncommon family of molecules drove us into further research. In this study, we employ a new SLN formulation with and without BXL, aiming for better encapsulation and less cytotoxicity (compared to the previous formulation), which we tested and validated from the calorimetric, technological, and biochemical perspectives.

3.2. Materials and methods

3.2.1. Materials

Precirol® ATO 5 (Glyceryl Distearate) was kindly donated by Gattefossé (Saint-Pries, France). Tween® 80 (Polysorbate 80) was purchased from Sigma Aldrich Co. (St. Louis, MO, USA). Dimyristoylphosphatidylcholine (DMPC) was obtained from Genzyme (Liestal, Switzerland).

Caffeic acid, Mn(OAc)3* 2 H_2O, 3-(4,5-dimethyl-2-thiazolyl)-2,5-diphenyl-2H-tetrazolium bromide (MTT), Dulbecco's modified Eagle's medium, foetal bovine serum, glucose, penicillin– streptomycin, interleukin-2 (IL-2), and 2′,7′-dichlorofluorescein diacetate were purchased from Sigma Aldrich (Milan, Italy).

Human foreskin fibroblast (HFF-1) cells were obtained from ATCC® SCRC-1041 TM(ATCC, Manassas, VA, USA). Purified water from Millipore-Q® Gradient A10TM ultra-pure water system (Millipore, Guyancourt, France) was used throughout the study. In the manuscript, the benzoxanthene lignan (diethyl-6,9,10-trihydroxybenzo[k,l]xanthene-1,2-dicarboxylate, indicated as BXL) employed in the formulations was obtained as described previously, and 1H NMR and HPLC–UV analyses established its purity [16].

3.2.2. SLN preparation

SLN were prepared by combined PIT and ultrasonication methods, following the procedures reported elsewhere [29–31]. Briefly, lipid phase (consisting of 1.5% w/w Precirol® ATO 5 for empty SLN; 1.5% w/w Precirol® ATO 5 plus 0.06% w/w BXL for SLN-BXL) and aqueous phase (consisting of 0.5% w/w Tween® 80 in water) was separately heated at 75 °C on a magnetic heat plate, then the aqueous phase was added drop by drop, at constant temperature and under stirring (300–400 rpm), to the oil phase. The obtained pre-emulsion was ultrasonicated using a UP400S (Ultra-Schallprozessor, Dr. Hielscher GmbH, Teltow, Germany) for 5 min at amplitude of 70%.

3.2.3. SLN characterization

Mean particles size (Z-Average) and polydispersity index (PDI) of the prepared formulations (SLN and SLN-BXL) were determined by dynamic light scattering using a Zetasizer Nano-ZS90 (Malvern Instrument Ltd., Worcs, UK), equipped with a solid-state laser, with a nominal power of 4.5 mW with a maximum output of 5 mW at 670 nm. Analyses were performed using a 90° scattering angle at 25±0.2 °C. Zeta potential (ZP) was determined using the electrophoretic light scattering (ELS) technique, which measures the electrophoretic mobility of particles in a dispersed system, indicating its stability. For measurements, each sample were prepared diluting 100 µL of SLN suspension with 900 µL of distilled water. Each value was measured at least in triplicate.

3.2.4. Encapsulation Efficiency (EE)

SLN-BXL preparations (0.4 mL) were loaded onto a Sephadex LH20 column (1.0 10 cm) eluted in sequence with: water (15 mL), H_2O:EtOH (50:50; 10 mL), EtOH (10 mL), and acetone (10 mL). In these conditions, the aqueous fraction contains the entrapped BXL, whereas the acetone fraction contains the unentrapped (free) BXL. The entrapped and free BXL were quantified by HPLC–UV (Agilent, Series 1100) equipped with a diode array detector set at 280 and 390 nm. The chromatographic separation occurred in a Luna C-18 (Phenomenex; 5 µM, 250 mm 4.60 mm) column employing the conditions previously adopted [19]. The entrapment efficiency % (EE%) was determined according to Equations (1) and (2):

$$EE\% = [(mgBXL_{tot} - mgBXL_{free}) \div mgBXL_{tot}] \times 100 \quad (1)$$

$$EE\% = (mgBXL_{entrapped} \div mgBXL_{tot}) \times 100 \quad (2)$$

3.2.5. BXL release from the SLN

The in vitro release study of BXL was performed employing dialysis tubes with a molecular weight cut-off of 3.5 kDa (Spectra/Pro, Spectrum Lab., Rancho Dominguez, CA, USA) Briefly, 1 mL of SLN-BXL formulations containing 0.6 mg/mL of BXL were placed into a dialysis tube and dispersed in a beaker containing 20 mL of 50 mM citrate buffer (pH 5), 20 mL of 50 mM TRIS buffer (pH 7.4), or 20 mL of H2O/EtOH 80:20 mixture. The solution was stirred at 200 rpm at 37± 0.5°C. At pre-determined intervals within 24 h, 1 mL of the release medium was withdrawn and replaced with an equal volume of the same fresh release medium. The samples were lyophilized and then analysed by HPLC-UV with the same chromatographic conditions employed for the entrapment efficiency determination.

3.2.6. Cell culture

HFF-1 were cultured in Dulbecco's modified Eagle's medium supplemented with 15% foetal bovine serum, 4.5 g/L glucose, 100 U/mL penicillin, and 100 µg/mL streptomycin. Cells were seeded in 96-well microplates at a constant density (8×10^3 cells/well) to obtain identical experimental conditions in the different tests, and to achieve a high accuracy of the measurements. After 24h of incubation in a humidified atmosphere of 5% CO_2 at 37 °C to allow cell attachment, the cells were treated with different concentrations of SLN-

BXL (7.3–14.6–29.2 μM) and/or with the corresponding amount of BLX and empty SLN (SLN 1:200; 1:100; 1:50) for 12 h and 24 h. Four replicates were performed for each sample. At the end of the treatment, the cells were scraped, washed with PBS, and immediately utilized for the analysis.

3.2.7. MTT bioassay

The MTT assay was performed to assess the cells viability. After 24 h of incubation in humidified atmosphere of 5% CO_2 at 37 °C to allow cell attachment, cells were treated with different concentrations of empty SLN (1:200; 1:100; 1:50), of BLX and SLN-BXL (7.3–14.6–29.2 μM). This assay measures the conversion of tetrazolium salt to yield coloured formazan in the presence of metabolic activity. The amount of formazan is proportional to the number of living cells [32]. The optical density was measured with a microplate spectrophotometer reader (Titertek Multiskan, Flow Laboratories, Helsinki, Finland) at λ = 570 nm. Results are expressed as percentage cell viability with respect to control (untreated cells).

3.2.8. ROS determination

The inhibitory effects of SLN on ROS production were investigated on untreated and treated cells using a fluorescent probe 2′,7′-dichlorofluorescein diacetate (DCFH-DA) [33]. This probe, because of its chemical characteristics, diffuses into the cells: intracellular esterases hydrolyse the acetate groups and the resulting DCFH then reacts with intracellular oxidants resulting in the observed fluorescence. The intensity of fluorescence is proportional to the levels of intracellular oxidant species. HFF1 cells, pre-treated with different concentrations of SLN (1.200; 1:100; 1:50), of BLX and SLN-BXL (7.3–14.6–29.2 μM) for 180 min, were stimulated with interleukin-2β (IL-2β) (3 μM) for 12 h. After treatments the culture medium was aspirated, the cells washed with PBS, treated with DCFH-DA (5 μM) and DAPI (5 μM) in PSB, and incubated for 15 min. After the time had elapsed, fluorescence was read with a microplate reader (Multiskan EX-Thermolab System) by selecting the following wavelengths: DCF (λ excitation = 493 nm; λ emission = 523 nm) and DAPI (λ excitation = 358 nm; λ emission = 461 nm). The fluorescence of DCF referred to the amount of ROS normalized for the number of cells by calculating the ratio of DCF fluorescence/DAPI fluorescence, and then the results were expressed as a percentage compared to the untreated control.

3.2.9. Differential scanning calorimetry

Calorimetric analysis was performed using a Mettler Toledo STARe thermoanalytical system (Greifensee, Switzerland) equipped with a DSC822 calorimetric cell. A Mettler TA- STARe software (version 16.00) (Greifensee, Switzerland) was used to obtain and analyse data. The calorimeter was calibrated using Indium (99.95%), based on the setting of the instrument. The sensitivity was automatically chosen as the maximum possible by the calorimetric system. For this, 160 µL aluminium calorimetric pans were used. Enthalpy changes were calculated from the peak areas.

3.2.9.1. Empty SLN and BXL-SLN analysis

To evaluate the thermotropic behaviour of the SLN, the formulation was submitted to DSC analysis under N_2 flow (70 mL/min) as follows: a heating scan from 5 to 85 °C, at 2 °C/min, and a cooling scan from 85 to 5 °C, at 4 °C/min, at least three times to confirm the reproducibility of data [34].

3.2.9.2. MLV/SLN analysis

A total of 30 µL of MLV and 90 µL of SLN or SLN-BXL were placed in a 160 µL DSC aluminium pan, which was hermetically sealed and subjected to calorimetric analysis under N_2 flow (70 mL/min) as follows: (1) a heating scan from 5 to 85 °C at the rate of 2 °C/min, (2) a cooling scan from 85 to 37 °C at the rate of 4 °C/min, (3) an isothermal period of one hour at 37 °C, and (4) a cooling scan from 37 to 5 °C (4 °C/min). This procedure was repeated eight times [35].

3.3. Results and discussions

3.3.1. SLN characterization

In order to characterize and evaluate the physiochemical stability of the produced solid lipid nanoparticles, mean particle size (Figure 1), polydispersity index (PDI) (Figure 2), and zeta potential (Figure 3) were analyzed over three months at 25 °C.

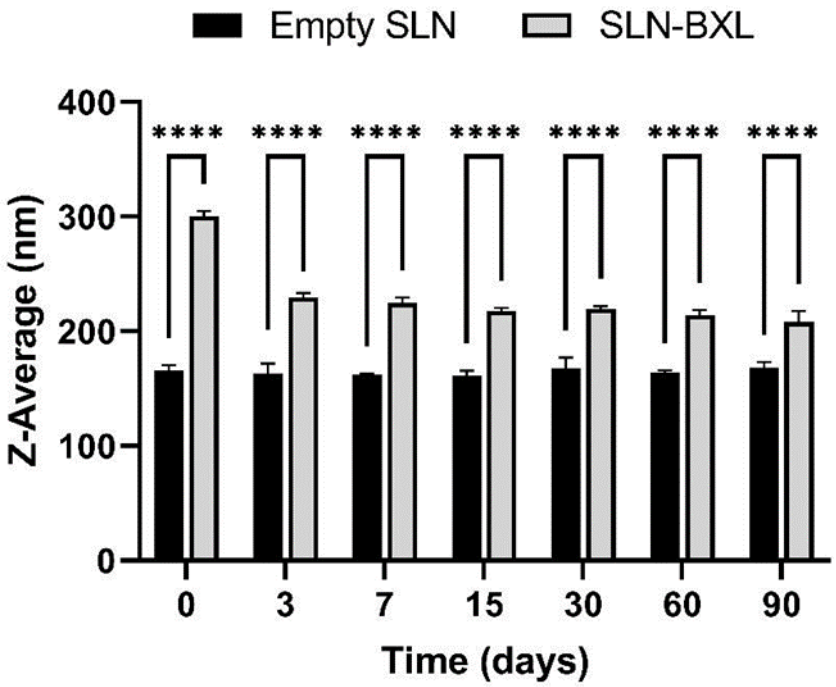

*Figure 1: SLN mean particle size. The results are shown as mean ± standard deviation. Confidence intervals calculated by two-way ANOVA: **** = p < 0.0001.*

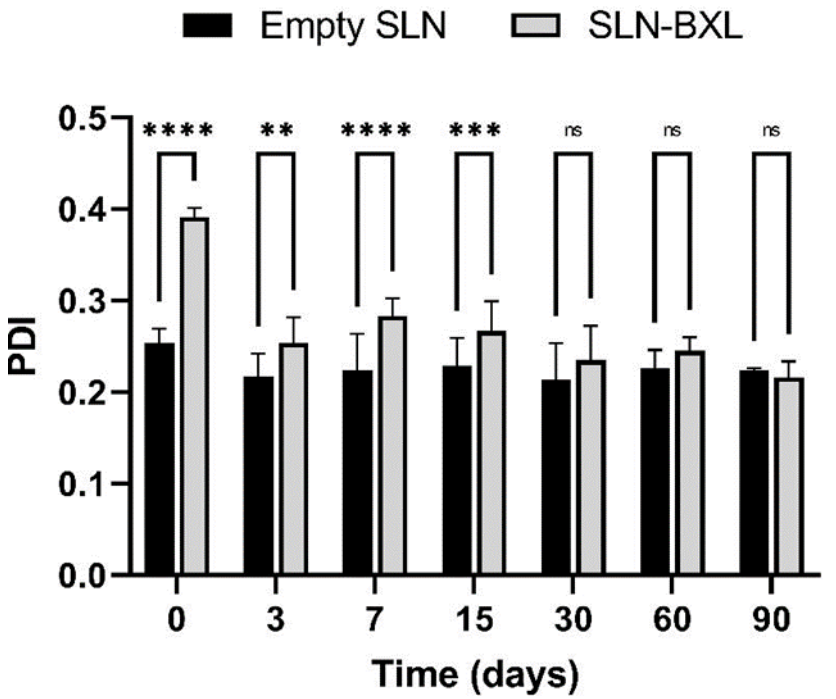

*Figure 2: SLN polydispersity index (PDI). The results are shown as mean ± standard deviation. Confidence intervals calculated by two-way ANOVA: ns = not significant; ** = p < 0.01; *** = p < 0.001; **** = p < 0.0001.*

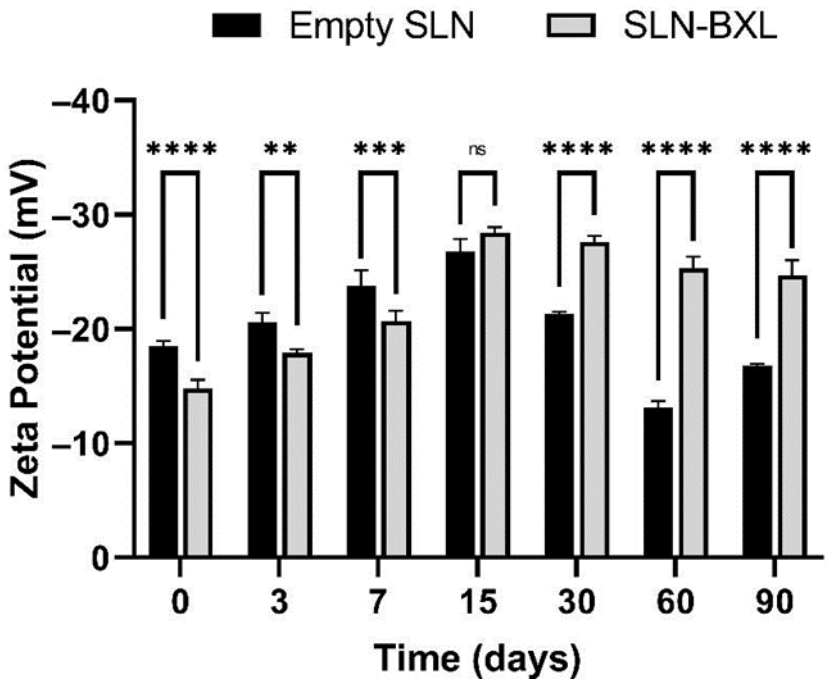

*Figure 3: SLN zeta potential. The results are shown as mean ± standard deviation. Confidence intervals calculated by two-way ANOVA: ns = not significant; ** = $p < 0.01$; *** = $p < 0.001$; **** = $p < 0.0001$.*

Empty SLN exhibit a mean particle size of 165 nm, remain unchanged over the period, while the association with the BXL causes an initial size increase at 300 nm, probably caused by the adsorption [20] of BXL onto the SLN surface, and/or a slow, gradual distribution of the compound into the nanoparticle's matrix; after 3 days, the SLN-BXL z-average stabilizes at 220 nm. The mean particle size values are additionally confirmed by PDI values, which are initially high and then stabilize around 0.2.

Regarding zeta potential, during the first 15 days, both unloaded and loaded SLN show an increment of said absolute value up to -28 mV. Following that day, unloaded SLN undergoes a non-linear decrement of ZP whereas SLN-BXL remains almost unchanged, possibly indicating a balancing effect of BXL on the electrical behaviour of SLN.

The results obtained suggest that the preparation is suitable for BXL encapsulation and delivery from a pharmaceutical technology standpoint, since mean size and PDI are nearly unaffected by the compound inclusion, retaining their ideal small values, while zeta potential is even positively influenced and brought to higher absolute values, causing a net negative charge-driven separation between nanoparticles and, thus, avoiding caking phenomena [21] all in a time period as long as 3 months without usage of preservatives.

3.3.2. Encapsulation efficiency

The previously developed methodology, described in [19], based on Sephadex LH20 column chromatography followed by high pressure liquid chromatography—UV quantitative analysis, allows the determination of the entrapment efficiency (EE%) of the SLN. The details are reported in the experimental section. The EE% can be calculated indirectly (see Equations) by quantification of free BXL eluted with acetone from Sephadex LH20, and directly by recovering the SLN-BXL from aqueous eluate. The results achieved with the two equations agree with each other, as the EE% values are between 69.4 and 74.2%. Of note, the formulation employed in this study leads to an increase in encapsulation efficiency (calculated with Equation (1)) compared to that observed in the previous work. These higher, but not total, encapsulation values provide more control in BXL release over time when in contact with lipophilic matrices such as cellular membranes, diminishing, although not denying, a burst release imputable to free BXL. For a possible therapeutical application, optimal employment of this suspension should be as a whole, so that a rapid onset effect, along with slower long-lasting release, is obtained [22].

3.3.3. Drug release

The in vitro release of BXL from SLN is achieved by dialysis method in citrate buffer (pH 5), TRIS buffer (pH 7.4), and H_2O/EtOH (80:20). The BXL released within 24h was assayed by HPLC–UV. The results are reported in Figure 4 as % of cumulative BXL released vs. time. As shown by the black line, the release in citrate buffer is slow, reaching only 3.7% at 24 h, and the release in TRIS buffer shows nearly the same trend. When BXL-SLN are dispersed in H_2O/EtOH, the release is faster within 24h, reaching up to 38.6%.

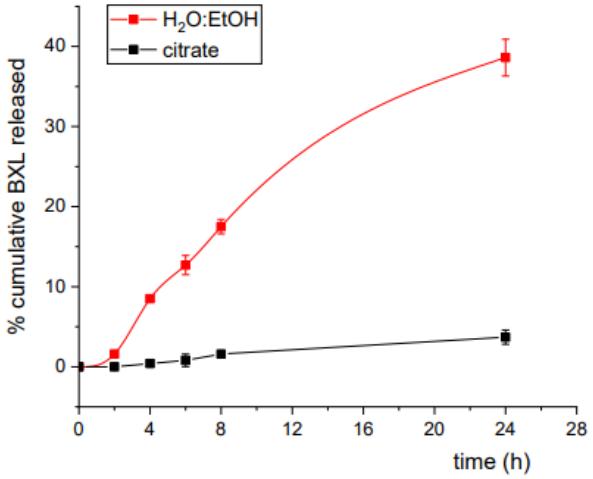

Figure 4: In vitro BXL release profile in citrate buffer (pH 5; black line) and in H_2O:EtOH 80:20 mixture (red line). The data plotted are means (n = 3) ± SD.

Since the whole formulation was used, these data suggest that in strongly hydrophilic environments, such as blood (pH 7.4) and acid urine (pH 5), both encapsulated and free BXL remain in and adsorbed onto nanoparticles, respectively (pointing to a possible higher half- life and slower excretion), whilst a broader, faster release over time is observed when SLN come in contact with slightly more lipophilic substrates, such as the proposed H_2O/EtOH mixture model (needed for sufficient solubility conditions, since both SLN and BXL are not soluble solely in water) [23] or, as we will see successively, the water-suspended biomembrane model based on DMPC MLV.

3.3.4. Cell viability

SLN-BXL treatment does not affect the viability of HFF-1 cells in any concentrations tested after 12 h and 24 h of exposure. BXL and empty SLN also show no toxicity in HFF-1 cells in the same experimental conditions (Figure 5). Since the administration of SLN-BXL, BXL, and empty SLN at 12 h and 24 h induce a similar effect, we have chosen to use 12 h as exposure time for ROS assay.

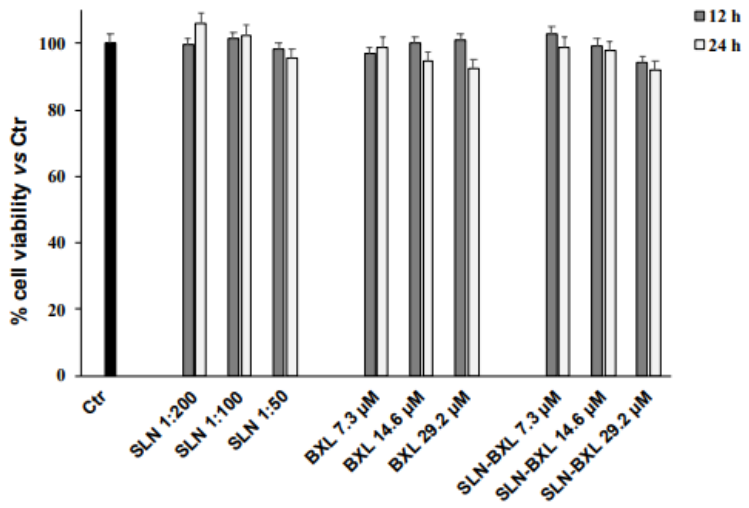

Figure 5: Cell viability in HFF-1 untreated (Ctr) and treated with empty SLN, BXL, and SLN-BXL at different concentrations. Values are expressed as mean ± S.D. of four experiments in triplicate.

3.3.5. ROS determination

Figure 6 shows that exposure of HFF-1 cells to IL-2β (3 µM) for 12 h increases ROS levels by approximately 50% relative to the control, as revealed by the intensity of the fluorescence; pre-treatment with SLN-BXL can induce, in a dose-dependent manner, a decrease in radical species compared to the cells treated with IL-2β and to the control. In particular, SLN-BXL is more effective than BXL alone, and, at a concentration of 29.2 µM, reduces ROS levels by about 50% compared to untreated cells.

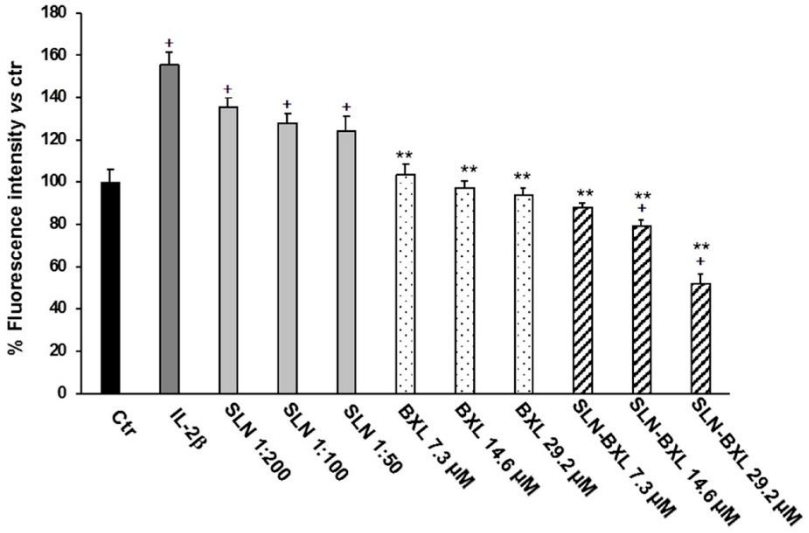

*Figure 6: ROS levels in HFF-1 cells untreated (Ctr), treated with IL-2β (3 µM), and pre-treated with SLN, BXL, and SLN-BXL at different concentrations. Values are expressed as mean ± S.D. of four experiments in triplicate. + Significant vs. untreated control cells $p < 0.001$; ** significant vs. IL-2β-treated cells: $p < 0.001$.*

These results may be due to a possible modification of the surface of SLN that allows a greater release of BXL. Furthermore, the data reported in Figure 6 indicate that empty SLN, while not altering cell viability, slightly increase ROS levels compared to control, unlike SLN-BXL. The SLN-BXL formulation, in fact, is able to block the ROS levels induced by IL-2β, and the encapsulation with SLN enhances the antioxidant effect of BXL.

Recently, it was reported that oxidative stress can induce skin damage due to a decrease in the levels of endogenous antioxidants [24–26]. Increased levels of ROS can, indeed, be responsible for an altered cellular redox state, DNA damage, and release of pro-inflammatory processes. The results of the in vitro experiments confirm that the increased ROS levels due to IL-2β treatment in HFF-1 cells are neutralized by SLN-BXL, which sport a stronger antioxidant activity than BXL alone; SLN can then be used to improve the overall efficacy of the compound.

3.3.6. Empty SLN and SLN-BXL calorimetric analysis

The thermotropic behaviour of the SLN was evaluated by DSC analysis (Figure 7). The calorimetric curve of empty SLN is characterized by a main peak at 54.40 °C and a shoulder on lower temperature. In the SLN-BXL calorimetric curve, as the temperature increases, a smaller shoulder, a secondary peak at 52.80 °C, and the primary peak at 54.60 °C are observed. The prominent differences among the empty and SLN-BXL calorimetric curves suggest that BXL is inside the SLN structure, affecting its response to heat and temperature-based transitions.

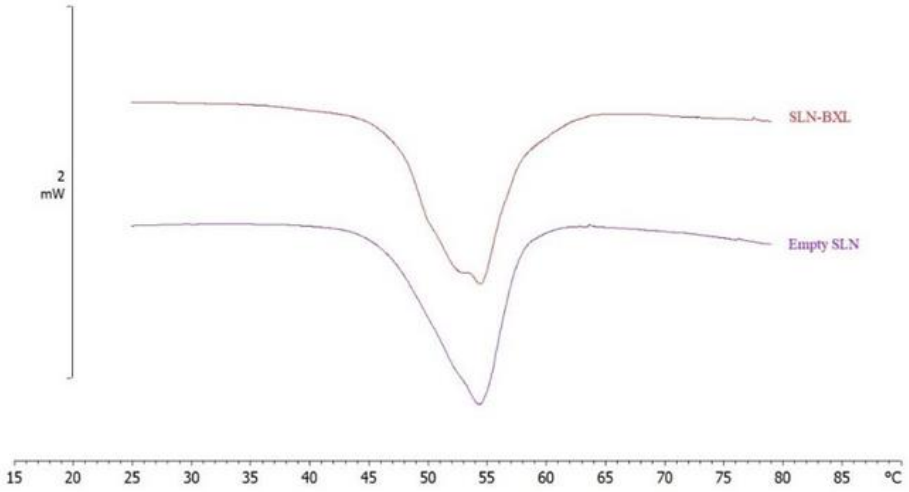

Figure 7: Calorimetric curves, in heating mode, of SLN and SLN-BXL.

3.3.7. MLV/SLN Interaction study

Differential scanning calorimetry was used to evaluate an eventual interaction between a biomembrane model made of DMPC MLV and empty SLN or SLN-BXL.

The interaction was assessed both at pH 5.0 (Figures 8 and 9) and pH 7.4 (Figures 10 and 11). The interaction between MLV and SLN is evidenced by the variation of the calorimetric peaks of MLV and/or SLN. The calorimetric curve of MLV shows a pre-transition peak at about 17 °C, related to the transition from the ordered gel phase to the ripple phase, and a main peak at about 25 °C, related to the transition from the ripple phase to the disordered liquid crystalline phase [27]. The contact of SLN with MLV induces several variations in the calorimetric peaks of MLV and SLN, in both pH conditions.

Regarding the experiment carried out with empty SLN and MLV, the pre-transition peak of MLV disappears and the main peak becomes smaller as the contact time increases; the calorimetric peaks of SLN vary significatively in terms of enthalpy and morphology. In the experiments carried out with SLN-BXL, the calorimetric curve of MLV loses the pre-transition peak, whereas the main peak becomes smaller; the calorimetric curve of SLN-BXL also undergoes evident variations.

Experimental results indicate a strong, pH-independent interaction between both SLN preparations and the MLV biomembrane model that can be supposed to be of penetrative nature, since changes in enthalpy and morphology are far more prominent than temperature-based ones [28]. Moreover, it can be observed, especially at pH 5, that on late scans the calorimetric morphology of both SLN specimens tested becomes gradually similar to practically superimposable, hinting at a complete redistribution of BXL in the MLV matrix and, thus, to a behavioural alignment of SLN-BXL back to empty SLN after the interaction.

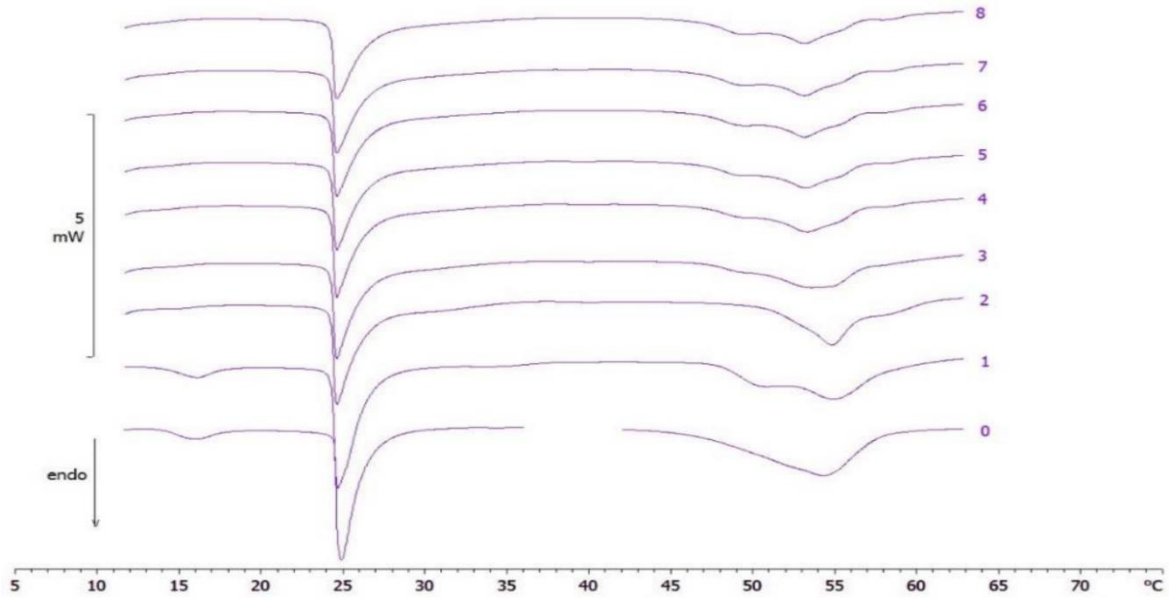

Figure 8: Calorimetric curves, in heating mode, of MLV put in contact with empty SLN, at pH 5, at increasing incubation time. The numbers on the right side of the curves refer to the calorimetric scans. The curves 0 refer to the samples before contact.

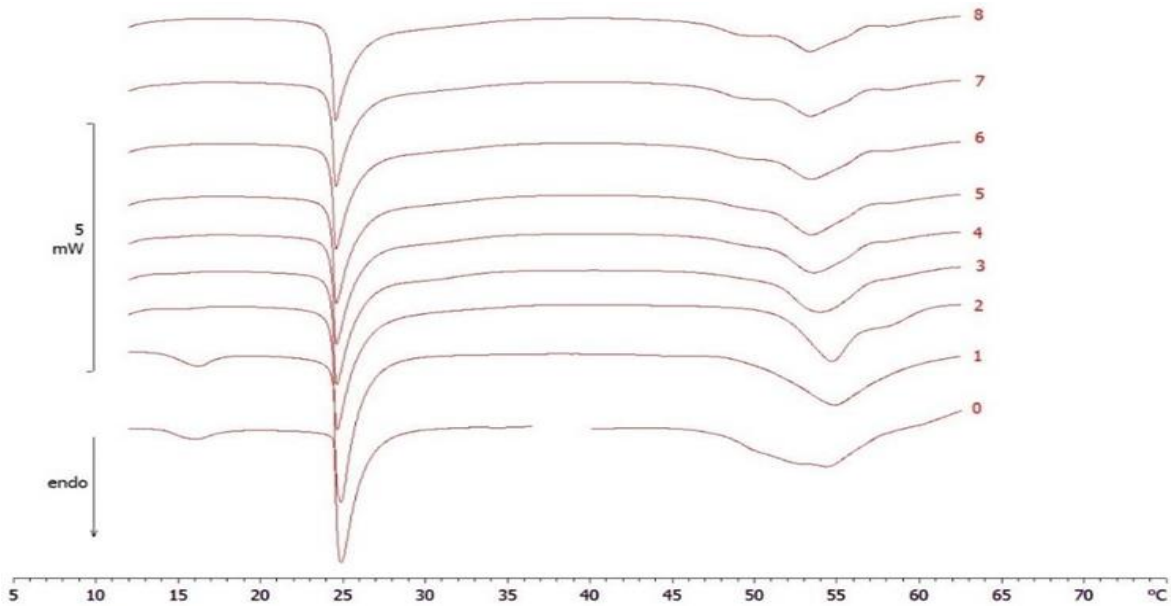

Figure 9: Calorimetric curves, in heating mode, of MLV put in contact with SLN-BXL at pH 5, at increasing incubation time. The numbers on the right side of the curves refer to the calorimetric scans. The curves 0 refer to the samples before contact.

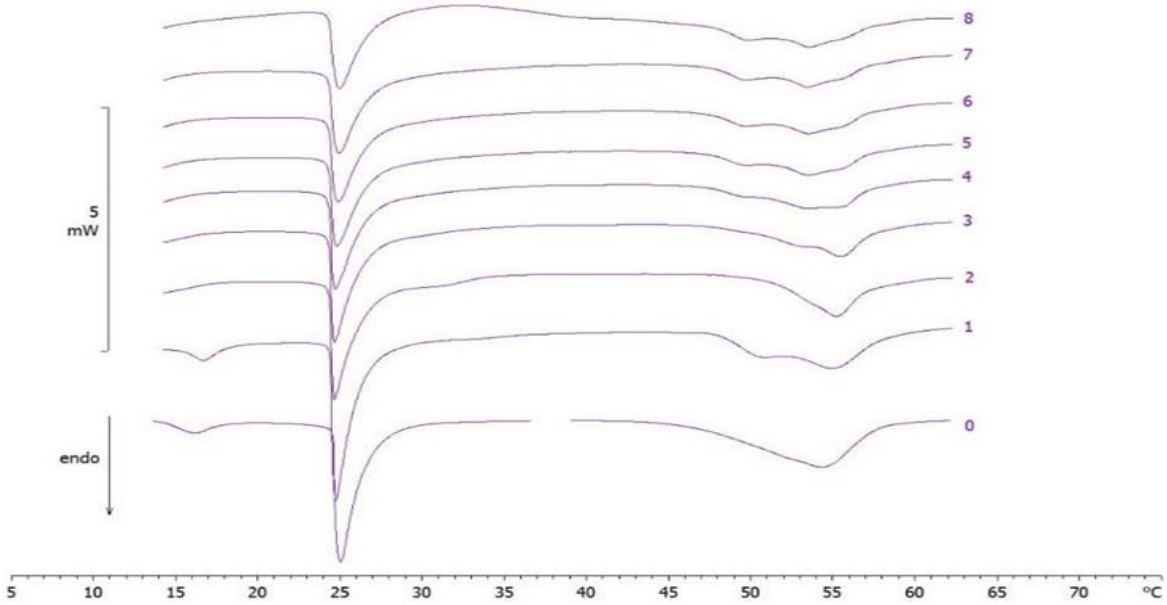

Figure 10: Calorimetric curves, in heating mode, of MLV put in contact with empty SLN, at pH 7.4, at increasing incubation time. The numbers on the right side of the curves refer to the calorimetric scans. The curves 0 refer to the samples before contact.

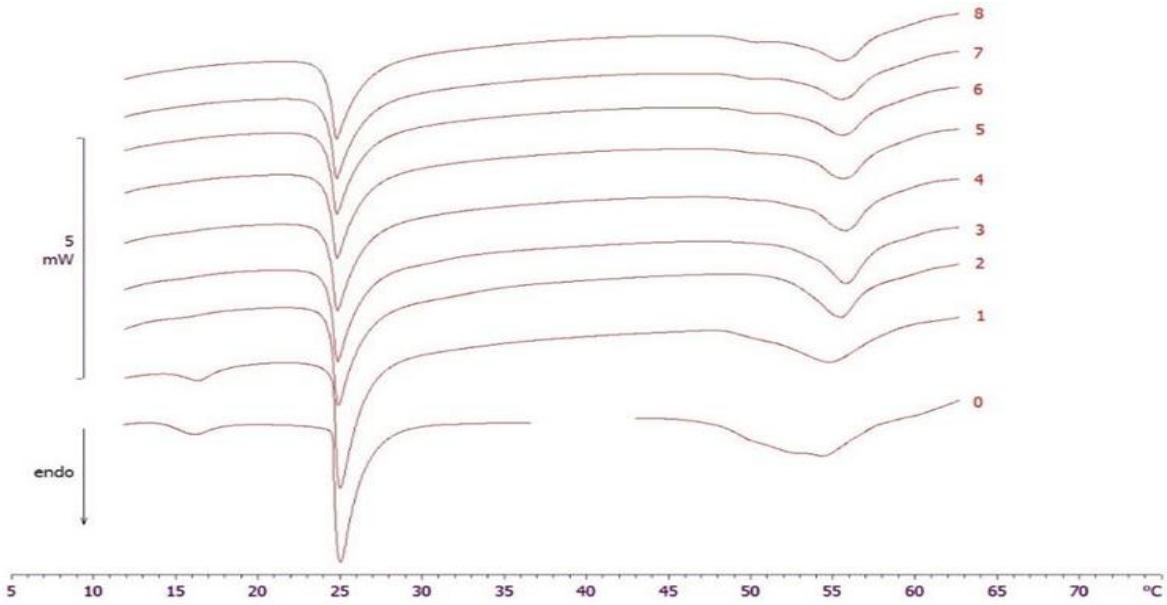

Figure 11: Calorimetric curves, in heating mode, of MLV put in contact with SLN-BXL, at pH 7.4, at increasing incubation time. The numbers on the right side of the curves refer to the calorimetric scans. The curves 0 refer to the samples before contact.

3.4. Conclusions

The aim of this research was to prepare solid lipid nanoparticles containing a benzo-[k,l]xanthene lignan possessing antioxidant properties to be used for topical application. In a precedent study [19], we obtained a SLN preparation with promising results in terms of physicochemical properties, but which did not display an optimal cytotoxicity assessment; for this reason, a new formulation, based on the same solid lipid, was developed.

SLN-BXL show a mean size around 200 nm, PDI of 0.2, and zeta potential of about -28 mV over a period of three months, and an encapsulation efficiency of 70%. SLN-BXL are able to penetrate and release the encapsulated compound into a biomembrane model and show relevant antioxidant activity in an in vitro cellular model, and also an optimal double-action release of BXL in the dialysis-bag experiment. Positively, the formulation does not influence the cellular viability, indicating its safety. In conclusion, based on these results, the formulation can be proposed as a candidate for preventive remedies against skin disorders induced by increased levels of ROS. In future research, given these promising results, we will assess the insertion of the formulation in a secondary pharmaceutical vehicle for topical delivery: we have already conducted some bibliographic scavenging and preliminary experiments that indicate that hydrogel could be a punctual solution, since it has high biocompatibility with human skin, and it has already been used successfully to contain and release SLN suspensions. The hydrogel we will propose is based on a very water-soluble variant of the Carbopol polymer with the addition of MilliQ water, glycerol, and triethanolamine. These components, in adequate ratios and experimental conditions, form a dense, viscoelastic gel with a rich hydrophilic matrix suitable for the entrapment of the SLN suspension. Preliminary tests show how the product has stable rheological parameters, such as viscosity, complex module, and extrapolated yield point, comparable with other well-studied polymeric hydrogel formulations already employed in SLN delivery; these first promising results will be further deepened in a dedicated study.

Supplementary Materials: The following supporting information can be downloaded at: https://www.mdpi.com/article/10.3390/molecules27185887/s1, Figure S1: Predicted Physicochemical properties and ADME parameters of BXL.

Author Contributions: Conceptualization, C.T., S.R. and M.G.S.; methodology, C.T., N.C., R.A., V.M., F.C. and M.G.S.; software, C.T., N.C., S.R., A.L.M., R.A. and V.M.; validation, R.A, V.M., and F.C.; formal analysis, C.T., N.C., S.R. and A.L.M.; investigation, C.T., S.R., R.A., V.M. and M.G.S.; resources: R.A., V.M. and M.G.S.; data curation, C.T., N.C. and S.R.; writing—original draft preparation, C.T. and M.G.S.; writing—review and editing, C.T., N.C., S.R., R.A., V.M. and M.G.S.; visualization, F.C.; supervision, C.T. and M.G.S.; project administration, M.G.S.; funding acquisition, V.M. All authors have read and agreed to the published version of the manuscript.

Funding: This research was funded by MIUR ITALY PRIN 2017 (Project No. 2017A95NCJ).

Institutional Review Board Statement: Not applicable.

Informed Consent Statement: Not applicable.

Data Availability Statement: Data were generated at the Department of Drug and Health Sciences and at the Department of Chemical Sciences, University of Catania. Data supporting the results of this study are available from the corresponding authors on request.

Acknowledgments: Authors thank Maria Grazia Saita and Danilo Aleo, Medivis srl, R&D Department, Italy, for rheological tests.

Conflicts of Interest: The authors declare no conflict of interest.

Sample Availability: Not applicable.

3.5. References

1. Khavkin, J.; Ellis, D.A.F. Aging Skin: Histology, Physiology, and Pathology. Facial Plast. Surg. Clin. 2011, 19, 229–234. [CrossRef] [PubMed]

2. Prow, T.W.; Grice, J.E.; Lin, L.L.; Faye, R.; Butler, M.; Becker, W.; Wurm, E.M.T.; Yoong, C.; Robertson, T.A.; Soyer, H.P.; et al. Nanoparticles and Microparticles for Skin Drug Delivery. Adv. Drug Deliv. Rev. 2011, 63, 470–491. [CrossRef] [PubMed]

3. Garcês, A.; Amaral, M.H.; Sousa Lobo, J.M.; Silva, A.C. Formulations Based on Solid Lipid Nanoparticles (SLN) and Nanostruc- tured Lipid Carriers (NLC) for Cutaneous Use: A Review. Eur. J. Pharm. Sci. 2018, 112, 159–167. [CrossRef]

4. Sala, M.; Diab, R.; Elaissari, A.; Fessi, H. Lipid Nanocarriers as Skin Drug Delivery Systems: Properties, Mechanisms of Skin Interactions and Medical Applications. Int. J. Pharm. 2018, 535, 1–17. [CrossRef] [PubMed]

5. Müller, R.H.; Radtke, M.; Wissing, S.A. Solid Lipid Nanoparticles (SLN) and Nanostructured Lipid Carriers (NLC) in Cosmetic and Dermatological Preparations. Adv. Drug Deliv. Rev. 2002, 54 (Suppl. 1), S131–S155. [CrossRef]

6. Pardeike, J.; Hommoss, A.; Müller, R.H. Lipid Nanoparticles (SLN, NLC) in Cosmetic and Pharmaceutical Dermal Products. Int. J. Pharm. 2009, 366, 170–184. [CrossRef]

7. Desai, P.; Patlolla, R.R.; Singh, M. Interaction of Nanoparticles and Cell-Penetrating Peptides with Skin for Transdermal Drug Delivery. Mol. Membr. Biol. 2010, 27, 247–259. [CrossRef] [PubMed]

8. Mardhiah Adib, Z.; Ghanbarzadeh, S.; Kouhsoltani, M.; Yari Khosroshahi, A.; Hamishehkar, H. The Effect of Particle Size on the Deposition of Solid Lipid Nanoparticles in Different Skin Layers: A Histological Study. Adv. Pharm. Bull. 2016, 6, 31–36. [CrossRef]

9. Bickers, D.R.; Athar, M. Oxidative Stress in the Pathogenesis of Skin Disease. J. Investig. Dermatol. 2006, 126, 2565–2575. [CrossRef] [PubMed]

10. Genovese, C.; Pulvirenti, L.; Cardullo, N.; Muccilli, V.; Tempera, G.; Nicolosi, D.; Tringali, C. Bioinspired Benzoxanthene Lignans as a New Class of Antimycotic Agents: Synthesis and Candida Spp. Growth Inhibition. Nat. Prod. Res. 2020, 34, 1653–1662. [CrossRef]

11. Tumir, L.-M.; Zonjic´, I.; Žuna, K.; Brkanac, S.R.; Jukic´, M.; Hud¯ek, A.; Durgo, K.; Crnolatac, I.; Glavaš-Obrovac, L.; Cardullo, N.; et al. Synthesis, DNA/RNA-Interaction and Biological Activity of Benzo[k,l]Xanthene Lignans. Bioorg. Chem. 2020, 104, 104190. [CrossRef]

12. Gerstmeier, J.; Kretzer, C.; Di Micco, S.; Miek, L.; Butschek, H.; Cantone, V.; Bilancia, R.; Rizza, R.; Troisi, F.; Cardullo, N.; et al. Novel Benzoxanthene Lignans That Favorably Modulate Lipid Mediator Biosynthesis: A Promising Pharmacological Strategy for Anti-Inflammatory Therapy. Biochem. Pharmacol. 2019, 165, 263–274. [CrossRef]

13. Vijayakurup, V.; Carmela, S.; Carmelo, D.; Corrado, T.; Srinivas, P.; Gopala, S. Phenethyl Caffeate Benzo [Kl] Xanthene Lignan with DNA Interacting Properties Induces DNA Damage and Apoptosis in Colon Cancer Cells. Life Sci. 2012, 91, 1336–1344. [CrossRef] [PubMed]

14. Capolupo, A.; Tosco, A.; Mozzicafreddo, M.; Tringali, C.; Cardullo, N.; Monti, M.C.; Casapullo, A. Proteasome as a New Target for Bio-Inspired Benzo[k,l]Xanthene Lignans. Chem. Weinh. Bergstr. Ger. 2017, 23, 8371–8374. [CrossRef] [PubMed]

15. Di Micco, S.; Mazué, F.; Daquino, C.; Spatafora, C.; Delmas, D.; Latruffe, N.; Tringali, C.; Riccio, R.; Bifulco, G. Structural Basis for the Potential Antitumour Activity of DNA-Interacting Benzo [Kl] Xanthene Lignans. Org. Biomol. Chem. 2011, 9, 701–710. [CrossRef] [PubMed]

16. Spatafora, C.; Barresi, V.; Bhusainahalli (Vedamurthy BM), V.; Micco, S.; Musso, N.; Riccio, R.; Bifulco, G.; Condorelli, D.; Tringali, C. Bio-Inspired Benzo[k,l]Xanthene Lignans: Synthesis, DNA-Interaction and Antiproliferative Properties. Org. Biomol. Chem. 2014, 12, 2686–2701. [CrossRef] [PubMed]

17. Daina, A.; Michielin, O.; Zoete, V. SwissADME: A Free Web Tool to Evaluate Pharmacokinetics, Drug-Likeness and Medicinal Chemistry Friendliness of Small Molecules. Sci. Rep. 2017, 7, 42717. [CrossRef]

18. Daina, A.; Michielin, O.; Zoete, V. ILOGP: A Simple, Robust, and Efficient Description of n-Octanol/Water Partition Coefficient for Drug Design Using the GB/SA Approach. J. Chem. Inf. Model. 2014, 54, 3284–3301. [CrossRef]

19. Torrisi, C.; Cardullo, N.; Muccilli, V.; Tringali, C.; Castelli, F.; Sarpietro, M.G. Characterization and Interaction with Biomembrane Model of Benzo[k,l]Xanthene Lignan Loaded Solid Lipid Nanoparticles. Membranes 2022, 12, 615. [CrossRef]

20. Gaspar, D.P.; Serra, C.; Lino, P.R.; Gonçalves, L.; Taboada, P.; Remuñán-López, C.; Almeida, A.J. Microencapsulated SLN: An Innovative Strategy for Pulmonary Protein Delivery. Int. J. Pharm. 2017, 516, 231–246. [CrossRef]

21. Shnoudeh, A.J.; Hamad, I.; Abdo, R.W.; Qadumii, L.; Jaber, A.Y.; Surchi, H.S.; Alkelany, S.Z. Chapter 15—Synthesis, Characterization, and Applications of Metal Nanoparticles. In Biomaterials and Bionanotechnology; Tekade, R.K., Ed.; Advances in Pharmaceutical Product Development and Research; Academic Press: Cambridge, MA, USA, 2019; pp. 527–612, ISBN 978-0-12-814427-5.

22. Barbosa, R.D.M.; Ribeiro, L.N.M.; Casadei, B.R.; da Silva, C.M.G.; Queiróz, V.A.; Duran, N.; de Araújo, D.R.; Severino, P.; de Paula, E. Solid Lipid Nanoparticles for Dibucaine Sustained Release. Pharmaceutics 2018, 10, 231. [CrossRef] [PubMed]

23. Çankaya, G.; Akyol, S.; Genç, C.O.; Arslan, B.Ö.; Gökalp, M.U. A Novel and an Alternative in Vitro Release Test for Hydrophobic Diflorasone Diacetate Ointment with Dialysis Method by Using Reciprocating Cylinder, USP Apparatus 3. Glob. J. Pharm. Pharm. Sci. 2021, 8, 1–5. [CrossRef]

24. Tomasello, B.; Malfa, G.A.; Acquaviva, R.; La Mantia, A.; Di Giacomo, C. Phytocomplex of a Standardized Extract from Red Orange (Citrus sinensis L. Osbeck) against Photoaging. Cells 2022, 11, 1447. [CrossRef]

25. Cao, C.; Xiao, Z.; Wu, Y.; Ge, C. Diet and Skin Aging-From the Perspective of Food Nutrition. Nutrients 2020, 12, 870. [CrossRef]

26. Bissett, D.L.; Chatterjee, R.; Hannon, D.P. Photoprotective Effect of Superoxide-Scavenging Antioxidants against Ultraviolet Radiation-Induced Chronic Skin Damage in the Hairless Mouse. Photodermatol. Photoimmunol. Photomed. 1990, 7, 56–62. [PubMed]

27. Walde, P. Preparation of Vesicles (Liposomes). In Encyclopedia of Nanoscience and Nanotechnology; American Scientific Publishers: Stevenson Ranch, CA, USA, 2004; Volume 8, pp. 43–79, ISBN 1-58883-001-2.

28. Pignatello, R.; Intravaia, V.D.; Puglisi, G. A Calorimetric Evaluation of the Interaction of Amphiphilic Prodrugs of Idebenone with a Biomembrane Model. J. Colloid Interface Sci. 2006, 299, 626–635. [CrossRef] [PubMed]

29. Sarpietro, M.G.; Accolla, M.L.; Puglisi, G.; Castelli, F.; Montenegro, L. Idebenone Loaded Solid Lipid Nanoparticles: Calorimetric Studies on Surfactant and Drug Loading Effects. Int. J. Pharm. 2014, 471, 69–74. [CrossRef] [PubMed]

30. Ricci, M.; Puglia, C.; Bonina, F.; Di Giovanni, C.; Giovagnoli, S.; Rossi, C. Evaluation of Indomethacin Percutaneous Absorption from Nanostructured Lipid Carriers (NLC): In Vitro and in Vivo Studies. J. Pharm. Sci. 2005, 94, 1149–1159. [CrossRef] [PubMed]

31. Daré, R.G.; Costa, A.; Nakamura, C.V.; Truiti, M.C.T.; Ximenes, V.F.; Lautenschlager, S.O.S.; Sarmento, B. Evaluation of Lipid Nanoparticles for Topical Delivery of Protocatechuic Acid and Ethyl Protocatechuate as a New Photoprotection Strategy. Int. J. Pharm. 2020, 582, 119336. [CrossRef]

32. Acquaviva, R.; Tomasello, B.; Di Giacomo, C.; Santangelo, R.; La Mantia, A.; Naletova, I.; Sarpietro, M.G.; Castelli, F.; Malfa, G.A. Protocatechuic Acid, a Simple Plant Secondary Metabolite, Induced Apoptosis by Promoting Oxidative Stress through HO-1 Downregulation and P21 Upregulation in Colon Cancer Cells. Biomolecules 2021, 11, 1485. [CrossRef] [PubMed]

33. Tomasello, B.; Di Mauro, M.D.; Malfa, G.A.; Acquaviva, R.; Sinatra, F.; Spampinato, G.; Laudani, S.; Villaggio, G.; Bielak- Zmijewska, A.; Grabowska, W.; et al. Rapha Myr®, a Blend of Sulforaphane and Myrosinase, Exerts Antitumor

and Anoikis- Sensitizing Effects on Human Astrocytoma Cells Modulating Sirtuins and DNA Methylation. Int. J. Mol. Sci. 2020, 21, 5328. [CrossRef] [PubMed]

34. Torrisi, C.; Di Guardia, M.; Castelli, F.; Sarpietro, M.G. Naringenin Release to Biomembrane Models by Incorporation into Nanoparticles. Experimental Evidence Using Differential Scanning Calorimetry. Surfaces 2021, 4, 295–305. [CrossRef]

35. Torrisi, C.; Morgante, A.; Malfa, G.; Acquaviva, R.; Castelli, F.; Pignatello, R.; Sarpietro, M.G. Sinapic Acid Release at the Cell Level by Incorporation into Nanoparticles: Experimental Evidence Using Biomembrane Models. Micro 2021, 1, 120–128. [CrossRef]

4. DESIGN OF NANOTECHNOLOGICAL CARRIERS FOR OCULAR DELIVERY OF MANGIFERIN: PREFORMULATION STUDY

Debora Santonocito[1,*], Maria Vivero-Lopez[2], Maria Rosaria Lauro[3], Cristina Torrisi[1], Francesco Castelli[1,4], Maria Grazia Sarpietro[1,4] and Carmelo Puglia[1,4]

[1]Department of Drug and Health Sciences, University of Catania, Viale Andrea Doria n 6, 95125 Catania, Italy; cristina.torrisi@phd.unict.it (C.T.); fcastelli@unict.it (F.C.); mg.sarpietro@unict.it (M.G.S.); capuglia@unict.it (C.P.)

[2]Departamento de Farmacología, Farmacia y Tecnología Farmacéutica, I+D Farma (GI-1645), Facultad de Farmacia and Health Research Institute of Santiago de Compostela (IDIS), Universidade de Santiago de Compostela, 15782 Santiago de Compostela, Spain; mariavivero.lopez@usc.es

[3]Department of Pharmacy, University of Salerno, Via Giovanni Paolo II, 84084 Fisciano, Italy; lauro@unisa.it

[4]NANO-i—Research Centre on Ocular Nanotechnology, University of Catania, 95125 Catania, Italy

*correspondence: debora.santonocito@unict.it;

Molecules 2022, 27, 1328.https://doi.org/10.3390/molecules27041328

4.1. Introduction

In recent years, intense research has been conducted to treat posterior ocular segment diseases using topical formulations able to overcome the complex anatomy of the eye [1]. The use of conventional eye drops is limited by precorneal drug removal mechanisms and physiological barriers [2,3] that oppose drug penetration, limiting the ocular bioavailability to 5–10% [4]. This means that the achievement of therapeutic effects requires frequent instillations, with consequent low patient compliance [5]. Other strategies are the use of ocular injections (peribulbar, retrobulbar and subconjunctival) and the application of ocular implants; however, both therapies show drawbacks due to high costs [6].

The advent of nanotechnology has made important innovations in the field of ophthalmology [7]. Over the years, two generations of lipid nanoparticles have been developed: the first generation consists of solid lipid nanoparticles (SLN) and the second generation consists of nanostructured lipid carriers (NLC). Drug encapsulation into these nanocarriers has been reported to increase drug solubility, stability, penetration, targeted cell uptake, tolerability and interaction with the ocular mucosa [8–12]. NLC present numerous advantages, such as controlled drug release, high drug loading and excellent tolerability [4,13]. NLC are made up of a mixture of lipid solid and liquid (oil), stabilized by a surfactant. The oily fraction is responsible for a distortion of the lipid crystals; this particular internal structure allows a high loading capacity and a remarkable physical stability. Therefore, NLC are currently studied as delivery systems for the treatment of the most important ocular disorders affecting the posterior eye segment [4–16].

Many eye diseases are related to oxidative stress, such as macular degeneration and diabetic retinopathy [17] as overproduction of reactive oxygen species (ROS) affects neurons and retinal vessels. Thus, the attention on antioxidants has been greatly increased in the field of ophthalmology. Ocular applications of antioxidants are hindered by stability and bioavailability problems, which can be overcome by encapsulation into nanocarriers [18]. Several studies pointed to mangiferin (MGN) for the potential treatment of eye diseases [19,20]. MGN (2-b-D-glucopyranosyl-1,3,6,7-tetrahydroxyxanthone) is a polyphenol compound (Figure1), primarily extracted from the leaves, stem barks and fruits of Mangifera indica L., exhibiting a variety of therapeutic effects, of which a strong antioxidant activity [21–24].

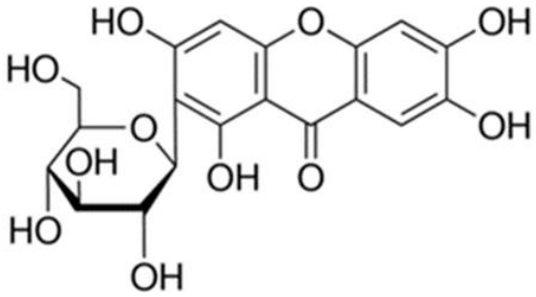

Figure 1: Chemical structure of mangiferin (MGN).

To overcome the stability and low aqueous solubility (0.111 mg/mL) limitations [25–27], the feasibility of encapsulating MGN in NLC was investigated in a previous paper [20]. In that work, NLC were obtained combining glyceryl monostearate, Gelucire 44/14, Mygliol 812, Labrasol and large proportions of Tween 80 surfactant, but the antioxidant activity of MGN was not investigated. Other nanotechnological systems have been developed in order to increase the solubility and bioavailability of MGN, such as self-assembled phytosomal soft nanoparticles encapsulated with a phospholipid complex (MPLC SNPs) [28] and polymeric nanoparticles [29,30], demonstrating the importance of the nanoencapsulation strategy.

The aim of this preliminary study was to design NLC for MGN using more biocompatible and safer surfactant and lipids and to elucidate their suitability for the potential treatment of posterior eye segment disorders using a variety of in vitro and in ovo approaches. Thus, Mygliol 812 was mixed with Compritol 888 ATO (COMP), a mixture of mono-, di- and triglycerides of behenic acid, which shows excellent regulatory and safety profiles [31]. Moreover, Lutrol F68 was used as a surfactant at a very low proportion (0.4% w/v). MGN-NLC were prepared by the high shear homogenization coupled with the ultrasound (HSH-US) method. MGN-NLC were characterized for their mean size, zeta- potential, size distribution and morphology. The mechanism by which NLC interact with a biomembrane model of multilamellar vesicles (MLV) was investigated using differential scanning calorimetry (DSC) [32] while the antioxidant activity of MGN was evaluated by the ORAC assay. Finally, the obtained formulations were analysed in terms of ocular tolerance. Therefore, MGN-NLC are a promising approach for treating retinal diseases as they are able to bypass the problems of MGN (low water solubility and instability) and administer it in the form of eye drops.

4.2. Materials and methods

4.2.1. Materials

Solid lipid Compritol 888 ATO (COMP, a mixture of mono-, di-, and triglycerides of behenic acid) was purchased from Gattefossè (Milan, Italy); oil Mygliol 812 (MIG, a mixture of medium-chain triglycerides) was obtained from Eigenmann & Veronelli S.p.A. (Milan, Italy) and Lutrol F68 (MW 8400 g/mol) was provided by BASF ChemTrade GmbH (Burgbernheim, Germany). Mangiferin (MGN, MW 422.33 g/mol), Trolox (MW 250.29 g/mol) and 2,2'-azobis(2-methylpropionamidine) dihydrochloride (AAPH, MW 271.19 g/mol) were obtained from Sigma-Aldrich (St. Louis, MO, USA). Fluorescein disodium salt (MW 332.31 g/mol) was purchased from Acros Organics (Milan, Italy). Triton X-100, propylene glycol and PBS commercial (10×) were purchased from Sigma-Aldrich (Madrid, Spain). Ultrapure water (18.2 Momega) was obtained by filtering through Millipore (MilliQ®, Millipore Ibérica, Madrid, Spain).

4.2.2. MGN-NLC preparation

MGN-NLC were prepared by high shear homogenization coupled with an ultrasound (HSH US) method [52] that was slightly modified. Briefly, the lipid phase containing MGN (0.1% *w/v*), COMP (0.6 g) and MIG (0.4 g) were first melted at 80 °C then uniformly mixed in the surfactant solution at the same temperature (Lutrol F68 0.4% w/v) by using a high-speed stirrer (Ultra-Turrax T25, IKA-Werke GmbH &Co. Kg, Staufen, Germany) for 10 min. The obtained pre-emulsion was ultrasonicated by a Labsonic 2000 (B. Braun, Melsunen, Germany) for 8 min. The hot dispersion was then cooled by dilution in 25 mL of additional water at 4 °C. Unloaded NLC was prepared by the same procedure without adding MGN.

4.2.3. MGN-NLC physical characterization

The average size (Z-Ave), polydispersity index (PDI) and the zeta potential (ZP, ξ) of MGN-NLC were assessed by dynamic light scattering (DLS) using a Zeta Sizer Nano-ZS90 (Malvern Instrument Ltd., Worcs, Malvern, UK). Experiments were carried out at 20 ± 0.2 °C and at a scattering angle of 90°. Samples (100 µL of NLC suspension) were diluted with distilled water (900 µL). Each formulation was measured at least in triplicate.

4.2.4. Transmission Electron Microscopy (TEM)

MGN-NLC morphology was investigated using TEM (JEOL JEM-101). The formulation was diluted 100 times with water and then deposited on the surface of a 200 mesh Formvar®-coated copper grid (TAAB Laboratories Equipment, Ltd., Aldermaston, UK). The acceleration voltage was set to 190 kV. After drying, the specimen was covered with chromium prior to imaging (Quorum Q150T ES East Grinstead, West Sussex, UK).

4.2.5. Encapsulation efficiency and drug loading

NLC formulation was diluted in H_2O, filtered through a 0.22 µm sterile syringe filter (TS-900-045-S, Test Scientific, Perugia, Italy) and freeze dried overnight. A defined amount of the lyophilized filtrate was solubilized in methanol, and the MGN content was measured by UV spectrophotometry at 257 nm ($T80^+$ UV/VIS Spectrometer, PG Instrument Ltd., Lutterworth, UK). Calibration curves of MGN were performed on six different concentrations (range 0.5–10 µg/mL). Each point was the average of three measurements. The entrapment efficiency (EE) of MGN in the NLC was calculated from Equation (1):

$$EE\% = [(mgMGN_{total} - mgMGN_{free})/mgMGN_{total}] \times 100 \quad (1)$$

The drug loading (DL) was calculated from Equation (2):

$$DL\% = [(mgMGN_{total} - mgMGN_{free})/\text{weight of lipids}] \times 100 \quad (2)$$

4.2.6. DMPC/MGN MLV preparation

DMPC/MGN MLV were prepared as follows. DMPC was dissolved in chloroform: methanol (1:1 *v*/*v*), and MGN was dissolved in methanol. Aliquots of a DMPC solution (0.010325 mmol) were delivered in glass vials, and aliquots of the MGN solution were added to have defined molar fractions of MGN with respect to DMPC (0.00, 0.03, 0.045, 0.06, 0.09, 0.12 and 0.15). The solvents were evaporated under a nitrogen flow at 37 °C. The obtained phospholipid films were freeze dried overnight to eliminate any solvent traces, and 50 mM of a Tris buffer solution at pH 7.4 was added to the films to reach 0.0614 mmoles DMPC/mL. The dispersions were kept at 37 °C for 1 min, vortexed three times for 1 min and then kept at 37 °C for 60 min.

4.2.7. Differential Scanning Calorimetry (DSC)

The DSC studies were carried out with a Mettler Toledo STAR^e system equipped with a DSC-822^e calorimetric cell and the Mettler TA-STAR^e software. The formulation was poured in aluminum (160 µL), which was sealed after filling. The reference pan contained a Tris buffer solution (50 mM). The maximum sensitivity obtainable by the calorimetric system was used. The procedure of the Mettler TA-STAR^e software was followed for the calibration of temperature and enthalpy changes; indium, stearic acid and cyclohexane were used.

4.2.7.1. MLV and NLC analysis

MLV (120 µL; 0.007375 mmoles of DMPC) were placed into the calorimetric pan and subjected to DSC heating and cooling scans: (1) a scan from 5 to 37 °C (2 °C/min) and (2) a scan from 37 to 5 °C (4 °C/min), both conducted at least three times to check the results' reproducibility. NLC (120 µL) were put into the calorimetric pan and subjected to the DSC analysis as follows: (1) a heating scan from 25 to 85 °C at a rate of 2 °C/min and then (2) a cooling scan from 85 to 5 °C at a rate of 4 °C/min; each scan was conducted at least three times to check the reproducibility of the results.

4.2.7.2. Kinetic experiments

Interaction between MLV and MGN

An amount of MGN corresponding to 0.5 molar fraction with respect to DMPC was weighed in the calorimetric pan, and 120 µL of a MLV sample was added. Then, the pan was hermetically sealed, and the interaction was monitored by the DSC analysis as follows: (i) a heating scan at a rate of 2 °C/min between 5 and 85 °C, (ii) a cooling scan at a rate of 4 °C/min between 85 and 37 °C, (iii) an isothermal period (1h) at 37 °C to allow the NLC to interact with and permeate the phospholipid bilayers of MLV and (iv) a cooling scan between 37 and 5 °C at a rate of 4 °C/min. This procedure was run at least eight times to follow eventual variations in the behaviour of the MLV made with DMPC (DMPC MLV) and of NLC due to the time-dependent interactions. Each experiment was repeated three times.

Interaction between MLV and NLC

Thirty microliters of MLV (0.245 mmoles DMPC/mL) were placed in the calorimetric pan, followed by the addition of 90 µL of NLC; the pan was hermetically sealed, and the interaction was monitored as described above.

4.2.8. Antioxidant activity: ORAC assay

The antioxidant activity of the MGN-NLC, MGN solution and unloaded NLC was measured using the ORAC assay [53]. Data were obtained using an OPTIMA FLUOstar microplates reader (BMG Labtech, Cary, North California, CA, USA). The assay was conducted at 37 °C, using AAPH (2,2-azobis (2-amidinopropane) dihydrochloride as the oxidant generator, Trolox (0.1 mM) as the control standard and phosphate buffer (pH 7.4) as the blank. A 96-well flat-bottomed black plate was used; the outer rows were filled with 200 µL of distilled water to avoid the evaporation due to the temperature effect. Samples (MGN-NLC, MGN solution and unloaded NLC) were diluted in phosphate buffer (1:1, 1:3, 1:10, 1:20, 1:50, 1:75, 1:100 and 1:150), and then they were deposited (70 µL) in triplicate in the well of the microplate with fluorescein solution (100 µL). Fluorescein solution (3 µM) was prepared in 75 mM phosphate buffer (pH 7.4). Moreover, eight calibration solutions using Trolox (3–100 µM, in phosphate buffer) were added in triplicate (70 µL). After incubation for 15 min at 37 °C, 30 µL of AAPH solution was added, and the fluorescence measurement started. The fluorescence was recorded every 2 min for 180 min (excitation 485 nm, emission 520 nm).

4.2.9. Ocular tolerability: HET – CAM assay

Ocular irritancy of unloaded and MGN-loaded NLC were evaluated through the Hen's Egg Test on Chorio-Allantoic Membrane (HET CAM), as previously described [18]. The eggshell of incubated (37 °C, 60% relative humidity, 9 days), fertilized hen's eggs (50–60 g, Coren, Spain) was pierced at the air chamber side using a rotatory saw (Dremel 300, Breda, The Netherlands), and the inner membrane was wet with 0.9% NaCl for 30 min (37 °C). Afterwards, the inner egg membrane was carefully removed to avoid any damage to the fine blood vessels of the chorioallantoic membrane.

Unloaded NLC and MGN-NLC (100 µL) (in duplicate) were dropped on the CAM. As negative and positive controls, 300 µL of 0.9% NaCl and 0.1 N NaOH solutions were placed on the CAM, respectively. Finally, the irritation score (IS) was calculated as

previously reported after observing the CAM for 5 min regarding hemorrhage, vascular lysis or coagulation [35].

4.2.10. Hemolysis assay

In vitro hemolysis assays were performed for unloaded NLC and MGN-NLC following a slightly modified method used by Chen et al. [54]. A hemolysis assay was performed using freshly drawn whole blood from anonymized healthy donors (Galician Blood Trans- fusion Center, Santiago de Compostela, Spain) [55,56]. Briefly, blood samples (5 mL) were diluted with 0.9% NaCl (145 mL). Samples (100 µL; dilution 1:5) were added in diluted blood (1 mL) while positive and negative controls were incubated with a Triton X-100 (4%) and a phosphate buffer (PBS commercial, 10), respectively. After incubation (37 °C) at 100 rpm for 1 h, the samples were centrifuged (Sigma 2-16P; Sigma Laboratory Centrifuges, Germany) at 10,000 rpm for 30 min. The release of hemoglobin was monitored by measuring the absorbance of the supernatant (150 µL) at 540 nm using a microplates reader (FLUOstar Optima, BMG Labtech, Cary, North California, USA). The percentage of hemolysis was calculated as follows Equation (3):

$$\%\, Hemolysis = \frac{A_S - A_N}{A_P - A_N} \times 100 \qquad (3)$$

where A_S is the absorbance of sample, A_N is the absorbance of negative control and A_P is the absorbance of positive control.

4.2.11. Statistical analysis

Statistical data analysis was performed using Student's t-test followed by a post hoc Bonferroni-Dunn test. A probability (p) of less than 0.05 was considered significant.

4.3. Results

4.3.1. NLC preparation and characterization

MGN-NLC showed a mean diameter of 148.9 ± 0.1 nm, a PDI value around 0.21 ± 0.02 and a zeta potential value of -23.5 mV (Table1), predicting a good long-term stability for the formulation [33]. The encapsulation efficiency, evaluated by UV/VIS spectrometry, was about 92%. The drug loading was about 4.7%.

Table 1. The values of size (Z-Ave), PDI and Z-potential for unloaded and MGN-NLC recorded at 25 °C.

Formulation	Z-Ave (nm ± SD)	PDI (–) ± SD	ZP (mV ± SD)
Unloaded NLC	123.1 ± 0.1	0.18 ± 0.10	−28.6 ± 0.3
MGN-NLC	148.9 ± 0.1	0.21 ± 0.02	−23.5 ± 0.2

4.3.2. Transmission Electron Microscopy (TEM)

The morphology of the MGN-NLC was performed using TEM (Figure 2). In agreement with the DLS data, the TEM images showed that the nanoparticles are suitable for ocular administration (particle size below 200 nm) [6,34–36] and are well structured.

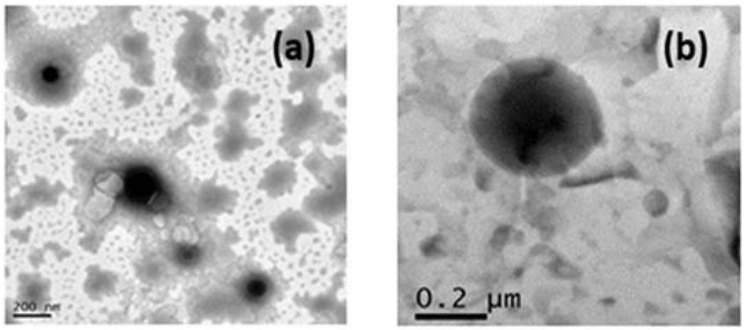

Figure 2: Transmission electron microscopy images of MGN-NLC. The scale bar represents 200 nm.

4.3.3. DSC analysis

4.3.3.1. NLC and MLV analysis

The thermotropic behaviour of unloaded NLC and MGN-NLC was evaluated by DSC. The calorimetric curves of the single components are shown in Figure S1 of the supporting information. Compritol, the solid lipid used to obtain NLC, showed a calorimetric peak centered at 71.57 °C, with an enthalpy variation of 124.76 J/g. The calorimetric curve of Lutrol was characterized by a peak centered at 52.49 °C, with an enthalpy variation of 122.93 J/g; Mygliol did not show any calorimetric peak but only a flat line. The calorimetric curves of NLC and MGN-NLC are shown in Figure 3. Unloaded NLC were characterized by a main peak centered at 64.24 °C and a shoulder at a higher temperature as well as an enthalpy variation of 66.13 J/g of Compritol. The NLC melting temperature was about 7 °C lower than that of Compritol, owing to an increase of surface area resulting from NLC colloidal sizes and from interactions between the solid lipid and MIG and surfactant molecules that led to a less ordered structure. The MGN-NLC run had a main peak at 64.68°C and a smaller one at 69.68 °C as well as an enthalpy variation of 65.08 J/g of Compritol. These results suggest that MGN affected the

thermotropic behaviour of the nanocarriers and, therefore, may interact with lipid constituents of the NLC formulation. The DSC analysis of MGN was also carried out. In accord with the literature data [37,38], MGN had an endothermic peak centered at 272.11 °C (Figure S1, supporting information). The effect of different molar fraction of MGN (0.03; 0.045; 0.06; 0.09; 0.12; 0.15) on the biomembrane model made of MLV of 1,2-dimyristoyl-sn-glycero-3-phosphocholine (DMPC) was also investigated by DSC (Figure 4) [31,39,40]. All recorded calorimetric curves were referred to those made of pure DMPC MLV. The latter one showed a pretransition peak at about 16 °C, related to the transition from the gel (ordered) to the ripple phase, and a main peak at 25 °C, due to the transition from the ripple to the liquid-crystalline (disordered) phase. Any foreign molecules in the lipid bilayer may act as impurities and cause variations of the thermodynamic parameters (Tm and ΔH). In the case of MGN, the pretransition peak decreased and finally disappeared as the amount of molar fraction increased while the main peak slightly shifted to a lower temperature, and its enthalpy variation remained almost unchanged. This result indicated that MGN exerted only a low effect on DMPC MLV.

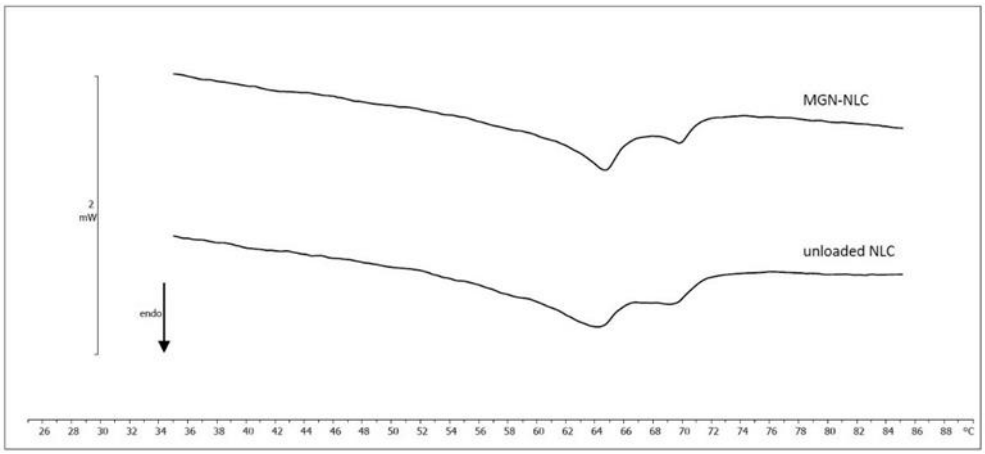

Figure 3: Calorimetric curves, in heating mode, of unloaded NLC and MGN-NLC.

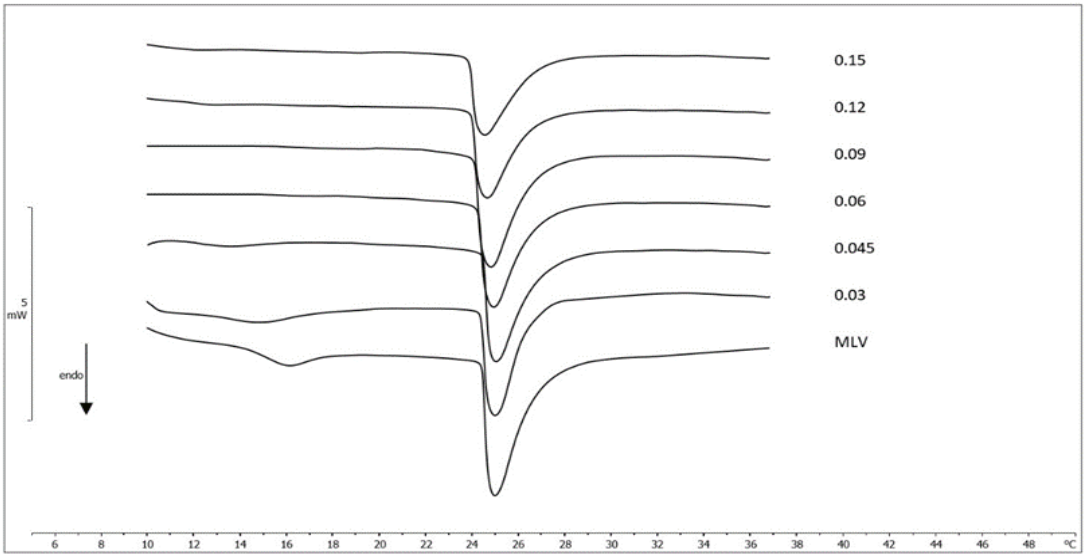

Figure 4: Calorimetric curves, in heating mode, of MLV containing a different molar fraction of MGN.

4.3.3.2. MLV/ MGN kinetic experiments

The ability of the MGN to be absorbed by the phospholipid membranes through an aqueous medium was studied by leaving an amount of the DMPC MLV dispersion in contact with a defined quantity of powdered compound. If the compound dissolves through the aqueous medium and is able to interact with the phospholipid bilayers, it is possible to observe a gradual variation of the calorimetric curve shape of DMPC MLV (reported as a reference). In this case, in all recorded calorimetric curves, the pretransition peak disappeared whereas the main peak did not show any variation (Figure 5). Therefore, MGN cannot be incorporated in the MLV structure, probably due to its low water solubility.

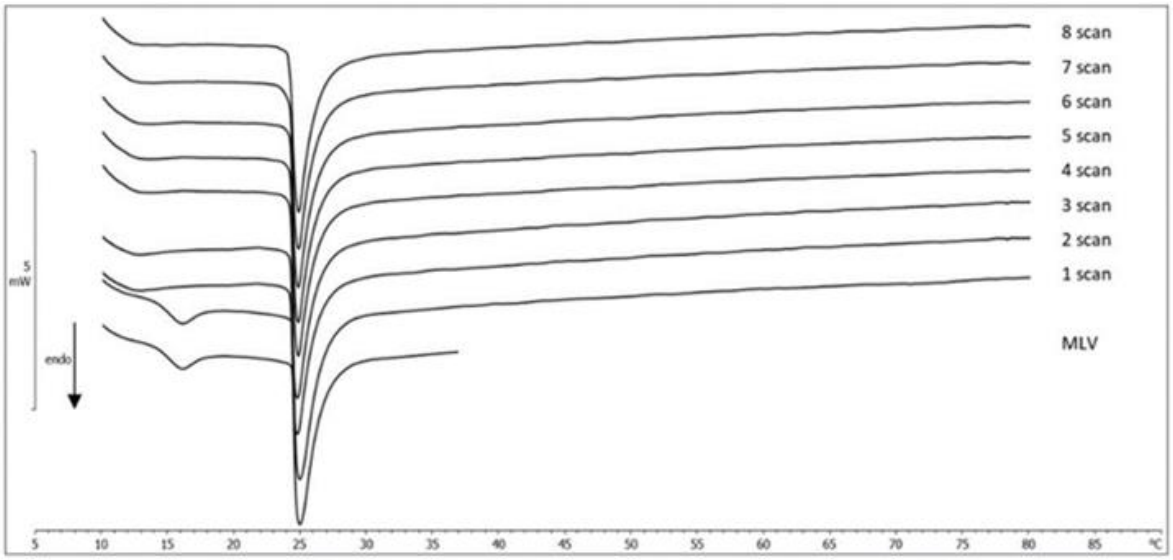

Figure 5: Calorimetric curves, in heating mode, of MLV left in contact with the solid MGN at increasing times.

4.3.3.3. MLV/NLC kinetic experiments

The interaction between DMPC MLV, used as biological membrane model, and NLC (unloaded NLC and MGN-NLC) was evaluated by DSC. An amount of DMPC MLV and NLC were put in contact, and the kinetic experiments were carried out. The calorimetric curves, recorded at one-hour intervals, were compared with the individual curves of samples (Figures 6 and 7, respectively). Regarding the first experiment, the pretransition peak of DMPC MLV gradually vanished while the main peak underwent variations in height and width, and the enthalpy variation gradually decreased (Table 2). Firstly, the calorimetric curve of NLC showed a main peak and a shoulder, characteristic of unloaded NLC; then, as the contact time increased, the peak merged with the shoulder, giving a unique peak at a higher temperature. This is clear evidence of the interaction between MLV and unloaded NLC; in particular, DMPC MLV maintained their structure while the NLC structure underwent marked variations. A similar behaviour can be seen in the DMPC MLV and MGN-NLC interactions. DMPC MLV lost the pretransition peak, and the main peak showed a reduction, associated with a gradual decrease of the enthalpy variation (Table 2). The shape of the MGN-NLC calorimetric curve, characterized by a well-defined two peaks structure, did not initially change, but the two peaks gradually merged in a unique peak that, in the last scans, was at 69.11 °C and remained stable. Therefore, there was an interaction between MLV and MGN-NLC. In order to confirm that the variations of the unloaded NLC and MGN-NLC were due to the interaction with MLV, simple experiments were carried out. Unloaded NLC and MGN-NLC were

separately submitted to the same calorimetric conditions of the kinetic experiments. The calorimetric curves did not show any variation over the time (data not shown), confirming the interaction between NLC and MLV. We can hypothesize that NLC can enter the MLV structure and release MGN.

Table 2. Enthalpy variation (ΔH) of MLV left in contact with NLC or MGN-NLC at increasing calorimetric heating scans.

Calorimetric Scan	NLC DH (J/mmol)	MGN-NLC DH (J/mmol)
0	30.30 ±0.50	30.30 ±0.50
1	30.30 ±0.52	29.60 ±0.51
2	25.35 ±0.54	23.30 ±0.72
3	25.20 ±0.61	23.30 ±0.73
4	23.19 ±0.91	22.32 ±0.64
5	20.07 ±0.83	20.38 ±0.80
6	19.88 ±0.74	20.16 ±0.82
7	19.65 ±0.70	19.39 ±0.90
8	19.51 ±0.73	18.92 ±0.72

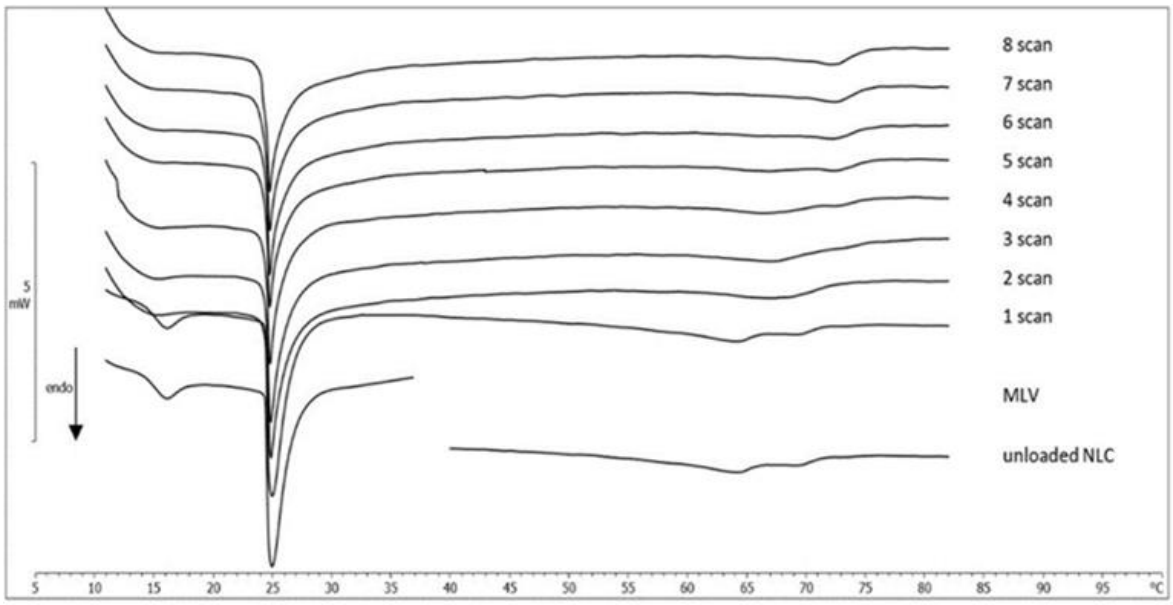

Figure 6: Calorimetric curves, in heating mode, of MLV left in contact with unloaded NLC at increasing times.

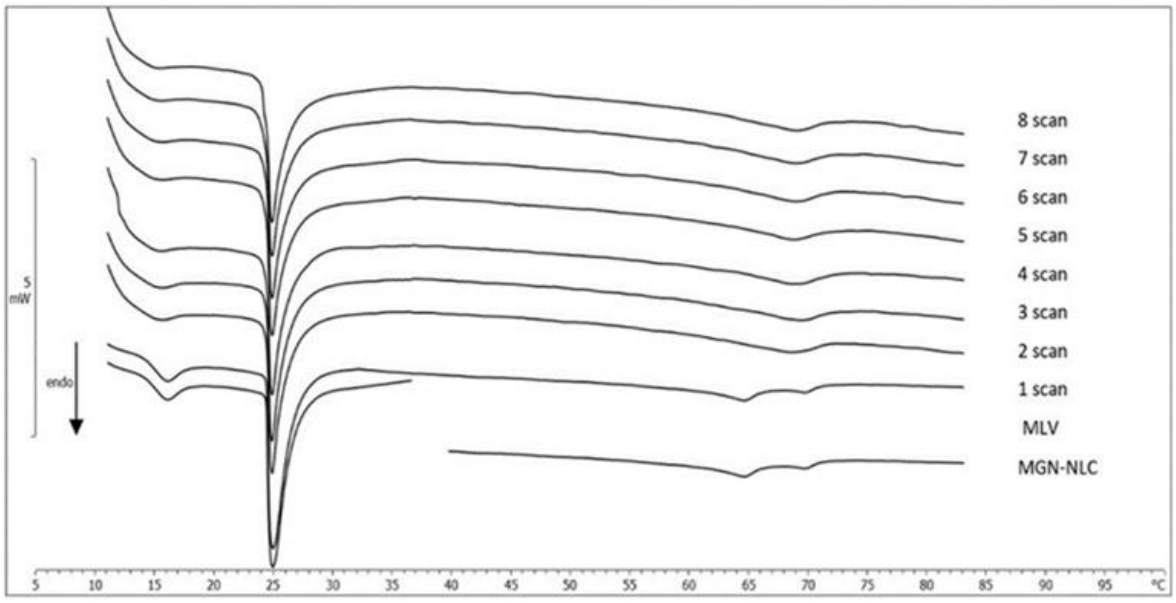

Figure 7: Calorimetric curves, in heating mode, of MLV left in contact with MGN-NLC at increasing times.

4.3.4. ORAC assay

During the ORAC assay, the decay of the fluorescence of fluorescein was monitored. A calibration curve was obtained by plotting the area under the curve (AUC) against a Trolox concentration (r^2 = 0.9913). The ORAC assay was applied to determine the antioxidant activity of the MGN-NLC (0.002 M) using unloaded NLC as a control and a MGN solution (free compound, 0.002 M), reaching values of 6494 ± 186, 769 ± 52 and 3521 ± 271 µM TE/g, respectively (Table 3). The obtained values showed that the antioxidant activity of MGN-NLC was higher than that of the free compound (MGN solution).

Table 3*. The antioxidant activity of unloaded NLC, MGN-NLC and MGN solution. Results are presented as the mean ± S.D., n = 3.*

Sample	Trolox-Equivs. (µM TE/g)
Unloaded NLC (1:50)	769 ± 52
MGN-NLC (1:75)	6494±186
MGN solution (1:50)	3521 ± 271

4.3.5. HET – CAM assay

HET CAM is an in ovo assay highly sensitive for predicting the ocular irritation effect [41]. Potential ocular irritation effects of MGN-NLC and unloaded NLC were determined on the chorioallantoic membrane (CAM) of fertilized hen eggs. No damage to the blood vessels on the CAM surface after a 5 min period of contact with MGN-NLC was detected,

as reported in Figure8. The IS was 0.0, as occurred with the negative control (0.9% NaCl). Thus, MGN-NLC can be classified as non-irritant (IS < 1) since no haemorrhage, lysis or coagulation were observed. The slight white halo observed in Figure 8C, D was due to the milky appearance of the tested formulations.

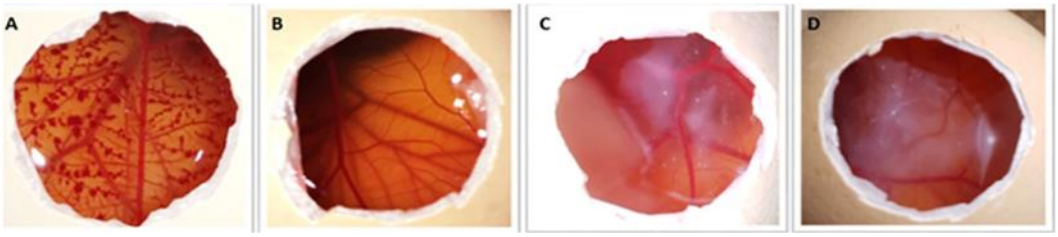

Figure 8: Pictures of chorioallantoic membrane (CAM) after the application of (A) 0.1 M NaOH solution (positive control), (B) 0.9 wt% NaCl solution (negative control), (C) unloaded NLC and (D) MGN-NLC.

4.3.6. Haemolysis assay

Investigation of the hemocompatibility profiles of tested formulations revealed that they had haemolysis effects of about 10%. The percentage of haemolysis for unloaded NLC and MGN-NLC were 11.16 ± 3.12% and 8.10 ± 0.95%, respectively.

4.4. Discussion

MGN-loaded NLC were formulated by high shear homogenization coupled with an ultrasound (HSH US) method using Compritol® 888 ATO and Mygliol 812® as the lipid phase and Lutrol F68® (Poloxamer 188) as the surfactant. The importance of this combination of HSH-US in controlling the size of lipid nanoparticles has been demonstrated [42]. Therefore, this method proved to be valid, highly reproducible and suitable for the formulation of ocular nanocarriers. DLS data showed good technological parameters, with a size below 200 nm (as confirmed by TEM images), a PDI around 0.2 and a zeta potential value approximately -20 mV, predicting a good long-term stability. This could be due to the presence of Poloxamer on the particle surface, thereby creating a stabilizer layer [43–45]. The choice of surfactant is very important because it controls the particle size and the stability, preventing their aggregation during storage [46,47]. In a previous report NLC prepared, combining glyceryl monostearate, Gelucire 44/14, Mygliol 812, Labrasol and large proportions of Tween 80 surfactant [20], there was a smaller size (50–70 nm), similar PDI and larger zeta potential (-30 to -36 mV). Calorimetric data demonstrated that MGN affects the thermotropic behavior of NLC; in fact, the one peak and one shoulder curve of unloaded NLC became a two peaks curve in

MGN-NLC, demonstrating that MGN was incorporated in NLC. The kinetic experiments, carried out to evaluate an interaction between MLV and unloaded NLC and between MLV and MGN-NLC, showed the variation both of the MLV as well as of the unloaded NLC and MGN-NLC peaks, indicating that unloaded NLC and MGN-NLC interacted with MLV [48]. The data were confirmed by the absence of variations in the calorimetric curves of unloaded NLC and MGN-NLC submitted to the same experimental conditions. The antioxidant activity of MGN-loaded NLC was determined by the ORAC assay using unloaded NLC as a control MGN-NLC and an MGN solution (free compound); the concentration of MGN was 0.002 M in both samples. The values obtained showed that the antioxidant activity of MGN-NLC (6494 ± 186 µM TE/g) was higher than that of the free compound (3521 ± 271 µM TE/g). This confirmed that the encapsulation of the drug was able to preserve and increase its activity [49]. The antioxidant activity against radicals ranked in the order MGN-NLC > MGN solution > unloaded NLC (control). In terms of safety, all the components used for the formulation of nanoparticles are safe [13,45,50,51] as confirmed by HET CAM test. This test is an alternative to the Draize test and provides information on the potential ocular irritancy of the formulations through the irritation score (IS). CAM is a vascular tissue that responds to harmful agents with a complete inflammatory process (hemorrhage, lysis or coagulation). The IS value was 0.0, which occurred with the negative control (0.9% NaCl), while the IS of the positive control was about 18.82. No damage to the blood vessels on the CAM surface after a 5 min period of contact with MGN-NLC was observed; therefore, it can be qualified as a nonirritating formulation. Moreover, MGN-NLC showed adequate hemocompatibility as the unloaded NLC.

The promising findings of the present work suggest future research directions to test in vivo the efficacy of MGN-NLC in the management of retinal diseases involving a deficit of antioxidant defenses (i.e., macular degeneration).

4.5. Conclusions

MGN has a wide range of pharmacological properties, including anti-inflammatory and antioxidant activities, and can be considered a good candidate for the potential treatment of eye diseases. Its use in ophthalmology is compromised due to its high lipophilicity. This obstacle has been overcome by encapsulating this compound in the NLC. MGN-NLC showed an appropriate particle size, good stability, and high ophthalmic tolerability.

The DSC studies indicate that MGN-NLC could enter the biomembrane model and release MGN, and further studies have been planned to prove this hypothesis. Furthermore, the antioxidant activity of MGN-NLC was higher than the free compound. This demonstrated that the carrier preserved the drug. Therefore, these findings suggest that the NLC system is a potential strategy to improve ocular bioavailability of lipophilic drugs.

Supplementary Materials: The following supporting information can be downloaded online. Figure S1: Calorimetric curves, in heating mode, of Compritol, Lutrol, Mygliol and MGN.

Author Contributions: Conceptualization, C.P., M.G.S. and D.S.; methodology, M.V.-L., M.G.S. and D.S.; software, C.T., D.S. and M.R.L.; validation, M.V.-L., M.G.S., F.C. and M.R.L.; formal analysis, C.T. and D.S.; investigation, C.P., M.G.S. and F.C.; resources, C.P.; data curation, C.T., D.S. and M.R.L.; writing—original draft preparation, M.V.-L., C.P., M.G.S. and D.S.; writing—review and editing, C.P., M.G.S. and D.S.; visualization, M.G.S. and D.S.; supervision, C.P. and F.C.; project administration, C.P.; funding acquisition, C.P. All authors have read and agreed to the published version of the manuscript.

Funding: This research was funded by Research Funding for University of Catania, under Project Piaceri "NanoRET"- "Patologie neurodegenerative retiniche: nuovi approcci farmacologici e nanotecnologici".

Data Availability Statement: Data is available on the request from the corresponding author.

Acknowledgments: C. Alvarez-Lorenzo is acknowledged for supervision of D.S. during a research stay at the University of Santiago de Compostela.

Conflicts of Interest: The authors declare no conflict of interest.

Sample Availability: Samples of the MGN, unloaded and MGN-NLC are available from the authors.

4.6. References

1. Cabrera, F.J.; Wang, D.C.; Reddy, K.; Acharya, G.; Shin, C.S. Challenges and opportunities for drug delivery to the posterior of the eye. *Drug Discov. Today* 2019, *24*, 1679–1684. [CrossRef] [PubMed]
2. Del Amo, E.M.; Urtti, A. Current and future ophthalmic drug delivery systems: A shift to the posterior segment. *Drug Discov. Today* 2008, *13*, 135–143. [CrossRef]
3. Bucolo, C.; Drago, F.; Salomone, S. Ocular drug delivery: A clue from nanotechnology. *Front. Pharmacol.* 2012, *3*, 188. [CrossRef]
4. Puglia, C.; Offerta, A.; Carbone, C.; Bonina, F.; Pignatello, R.; Puglisi, G. Lipid nanocarriers (LNC) and their applications in ocular drug delivery. *Curr. Med. Chem.* 2015, *22*, 1589–1602. [CrossRef]
5. Battaglia, L.; Serpe, L.; Foglietta, F.; Muntoni, E.; Gallarate, M.; del Pozo-Rodriguez, A.; Solinis, M.A. Application of lipid nanoparticles to ocular drug delivery. *Expert Opin. Drug Deliv.* 2016, *13*, 1743–1757. [CrossRef] [PubMed]
6. Puglia, C.; Santonocito, D.; Romeo, G.; Intagliata, S.; Romano, G.; Strettoi, E.; Novelli, E.; Ostacolo, C.; Campiglia, P.; Sommella, E.; et al. Lipid Nanoparticles Traverse Non-Corneal Path to Reach the Posterior Eye Segment: In Vivo Evidence. *Molecules* 2021, *26*, 4673. [CrossRef] [PubMed]
7. Pignatello, R.; Puglisi, G. Nanotechnology in Ophthalmic Drug Delivery: A Survey of Recent Developments and Patenting Activity. *Recent Patents Nanomed.* 2011, *1*, 42–54. [CrossRef]
8. Duan, Y.; Cai, X.; Du, H.; Zhai, G. Novel in situ gel systems based on P123/TPGS mixed micelles and gellan gum for ophthalmic delivery of curcumin. *Colloids Surf. B Biointerfaces* 2015, *128*, 322–330. [CrossRef]
9. Yu, S.; Wang, Q.-M.; Wang, X.; Liu, D.; Zhang, W.; Ye, T.; Yang, X.; Pan, W. Liposome incorporated ion sensitive in situ gels for opthalmic delivery of timolol maleate. *Int. J. Pharm.* 2015, *480*, 128–136. [CrossRef]
10. López, E.S.; Espina, M.; Doktorovova, S.; Souto, E.; García, M. Lipid nanoparticles (SLN, NLC): Overcoming the anatomical and physiological barriers of the eye—

Part II—Ocular drug-loaded lipid nanoparticles. *Eur. J. Pharm. Biopharm.* 2017, *110*, 58–69. [CrossRef]

11. Puglia, C. Cosmeceuticals: Nanotechnology-Based Strategies for the Delivery of Phytocompounds. *Curr. Pharm. Des.* 2019, *25*, 2314–2322. [CrossRef]

12. Puglia, C.; Pignatello, R.; Fuochi, V.; Furneri, P.M.; Lauro, M.R.; Santonocito, D.; Cortesi, R.; Esposito, E. Lipid Nanoparticles and Active Natural Compounds: A Perfect Combination for Pharmaceutical Applications. *Curr. Med. Chem.* 2019, *26*, 4681–4696. [CrossRef] [PubMed]

13. Araújo, J.; Nikolic, S.; Egea, M.A.; Souto, E.B.; Garcia, M.L. Nanostructured lipid carriers for triamcinolone acetonide delivery to the posterior segment of the eye. *Colloids Surf. B Biointerfaces* 2011, *88*, 150–157. [CrossRef]

14. Luo, Q.; Zhao, J.; Zhang, X.; Pan, W. Nanostructured lipid carrier (NLC) coated with Chitosan Oligosaccharides and its potential use in ocular drug delivery system. *Int. J. Pharm.* 2011, *403*, 185–191. [CrossRef]

15. Balguri, S.P.; Adelli, G.; Majumdar, S. Topical ophthalmic lipid nanoparticle formulations (SLN, NLC) of indomethacin for delivery to the posterior segment ocular tissues. *Eur. J. Pharm. Biopharm.* 2016, *109*, 224–235. [CrossRef] [PubMed]

16. Tronino, D.; Offerta, A.; Ostacolo, C.; Russo, R.; De Caro, C.; Calignano, A.; Puglia, C.; Blasi, P. Nanoparticles prolong N- palmitoylethanolamide anti-inflammatory and analgesic effects in vivo. *Colloids Surf. B Biointerfaces* 2016, *141*, 311–317. [CrossRef]

17. Beebe, D.C.; Holekamp, N.M.; Shui, Y.-B. Oxidative Damage and the Prevention of Age-Related Cataracts. *Ophthalmic Res.* 2010,*44*, 155–165. [CrossRef]

18. Alvarez-Rivera, F.; Fernández-Villanueva, D.; Concheiro, A.; Alvarez-Lorenzo, C. α-Lipoic Acid in Soluplus® Polymeric Na- nomicelles for Ocular Treatment of Diabetes-Associated Corneal Diseases. *J. Pharm. Sci.* 2016, *105*, 2855–2863. [CrossRef][PubMed]

19. Kim, S.-J.; Sung, M.-S.; Heo, H.; Lee, J.-H.; Park, S.-W. Mangiferin Protects Retinal Ganglion Cells in Ischemic Mouse Retina via SIRT1. *Curr. Eye Res.* 2016, *41*, 844–855. [CrossRef] [PubMed]

20. Liu, R.; Liu, Z.; Zhang, C.; Zhang, B. Nanostructured lipid carriers as novel ophthalmic delivery system for mangiferin: Improving in vivo ocular bioavailability. *J. Pharm. Sci.* 2012, *101*, 3833–3844. [CrossRef] [PubMed]

21. Engels, C.; Knödler, M.; Zhao, Y.-Y.; Carle, R.; Gänzle, M.; Schieber, A. Antimicrobial Activity of Gallotannins Isolated from Mango (*Mangifera indica* L.) Kernels. *J. Agric. Food Chem.* 2009, *57*, 7712–7718. [CrossRef] [PubMed]

22. Sá-Nunes, A.; Rogerio, A.P.; Medeiros, A.I.; Fabris, V.E.; Andreu, G.P.; Rivera, D.G.; Delgado, R.; Faccioli, L.H. Modulation of eosinophil generation and migration by Mangifera indica L. extract (Vimang®). *Int. Immunopharmacol.* 2006, *6*, 1515–1523. [CrossRef] [PubMed]

23. Joubert, E.; Richards, E.S.; Van Der Merwe, J.D.; De Beer, D.; Manley, M.; Gelderblom, W.C. Effect of Species Variation and Processing on Phenolic Composition and In Vitro Antioxidant Activity of Aqueous Extracts of *Cyclopia* spp. (Honeybush Tea). *J. Agric. Food Chem.* 2008, *56*, 954–963. [CrossRef]

24. Li, Y.; Huang, T.H.-W.; Yamahara, J. Salacia root, a unique Ayurvedic medicine, meets multiple targets in diabetes and obesity. *Life Sci.* 2008, *82*, 1045–1049. [CrossRef]

25. Tharanathan, R.N.; Yashoda, H.M.; Prabha, T.N. Mango (*Mangifera indica* L.), "The King of Fruits"—An Overview. *Food Rev. Int.*2006, *22*, 95–123. [CrossRef]

26. Pleguezuelos-Villa, M.; Nacher, A.; Hernández, M.J.; Buso, M.O.V.; Sauri, A.R.; Díez-Sales, O. Mangiferin nanoemulsions in treatment of inflammatory disorders and skin regeneration. *Int. J. Pharm.* 2019, *564*, 299–307. [CrossRef]

27. Acosta, J.; Sevilla, I.; Salomón, S.; Nuevas, L.; Romero, A.; Amaro, D. Determination of mangiferin solubility in solvents used in the biopharmaceutical industry. *J. Pharm. Pharmacogn. Res.* 2016, *4*, 49–53.

28. Telange, D.R.; Sohail, N.K.; Hemke, A.T.; Kharkar, P.S.; Pethe, A.M. Phospholipid complex-loaded self-assembled phytosomal soft nanoparticles: Evidence of enhanced solubility, dissolution rate, ex vivo permeability, oral bioavailability, and antioxidant potential of mangiferin. *Drug Deliv. Transl. Res.* 2021, *11*, 1056–1083. [CrossRef]

29. Razura-Carmona, F.F.; Pérez-Larios, A.; González-Silva, N.; Herrera-Martínez, M.; Medina-Torres, L.; Sáyago-Ayerdi, S.G.; Sánchez-Burgos, J.A. Mangiferin-Loaded Polymeric Nanoparticles: Optical Characterization, Effect of Anti-topoisomerase I, and Cytotoxicity. *Cancers* 2019, *11*, 1965. [CrossRef]

30. Samadarsi, R.; Dutta, D. Anti-oxidative effect of mangiferin-chitosan nanoparticles on oxidative stress-induced renal cells. *Int. J. Biol. Macromol.* 2020, *151*, 36–46. [CrossRef]

31. Santonocito, D.; Puglia, C.; Torrisi, C.; Giuffrida, A.; Greco, V.; Castelli, F.; Sarpietro, M.G. Calorimetric Evaluation of Glycyrrhetic Acid (GA)- and Stearyl Glycyrrhetinate (SG)-Loaded Solid Lipid Nanoparticle Interactions with a Model Biomembrane. *Molecules* 2021, *26*, 4903. [CrossRef] [PubMed]

32. Aburahma, M.H.; Badr-Eldin, S.M. Compritol 888 ATO: A multifunctional lipid excipient in drug delivery systems and nanophar- maceuticals. *Expert Opin. Drug Deliv.* 2014, *11*, 1865–1883. [CrossRef]

33. Müller, R.H.; Radtke, M.; Wissing, S.A. Nanostructured lipid matrices for improved microencapsulation of drugs. *Int. J. Pharm.*2002, *242*, 121–128. [CrossRef]

34. Amrite, A.C.; Edelhauser, H.F.; Singh, S.R.; Kompella, U.B. Effect of circulation on the disposition and ocular tissue distribution of 20 nm nanoparticles after periocular administration. *Mol. Vis.* 2008, *14*, 150–160. [PubMed]

35. Amrite, A.C.; Kompella, U.B. Size-dependent disposition of nanoparticles and microparticles following subconjunctival adminis- tration. *J. Pharm. Pharmacol.* 2005, *57*, 1555–1563. [CrossRef]

36. Sakurai, E.; Ozeki, H.; Kunou, N.; Ogura, Y. Effect of Particle Size of Polymeric Nanospheres on Intravitreal Kinetics. *Ophthalmic Res.* 2001, *33*, 31–36. [CrossRef]

37. Ma, H.; Chen, H.; Sun, L.; Tong, L.; Zhang, T. Improving permeability and oral absorption of mangiferin by phospholipid complexation. *Fitoterapia* 2014, *93*, 54–61. [CrossRef]

38. Liu, M.; Liu, Y.; Ge, Y.; Zhong, Z.; Wang, Z.; Wu, T.; Zhao, X.; Zu, Y. Solubility, Antioxidation, and Oral Bioavailability Improvement of Mangiferin Microparticles Prepared Using the Supercritical Antisolvent Method. *Pharmaceutics* 2020, *12*, 90. [CrossRef]

39. Bonaccorso, A.; Pellitteri, R.; Ruozi, B.; Puglia, C.; Santonocito, D.; Pignatello, R.; Musumeci, T. Curcumin Loaded Polymeric vs. Lipid Nanoparticles: Antioxidant Effect on Normal and Hypoxic Olfactory Ensheathing Cells. *Nanomaterials* 2021, *11*, 159. [CrossRef]

40. Sarpietro, M.G.; Accolla, M.L.; Puglisi, G.; Castelli, F.; Montenegro, L. Idebenone loaded solid lipid nanoparticles: Calorimetric studies on surfactant and drug loading effects. *Int. J. Pharm.* 2014, *471*, 69–74. [CrossRef]

41. ICCVAM. Test Method Evaluation Report: Current Validation Status of In Vitro Test Methods Proposed for Identifying Eye Injury Hazard Potential of Chemicals and Products.Availableonline: https://ntp.niehs.nih.gov/iccvam/docs/ocutox_docs/invitro-20 10/tmer-vol1.pdf (accessed on 10 December 2021).

42. Puglia, C.; Santonocito, D.; Ostacolo, C.; Sommella, E.M.; Campiglia, P.; Carbone, C.; Drago, F.; Pignatello, R.; Bucolo, C. Ocular Formulation Based on Palmitoylethanolamide-Loaded Nanostructured Lipid Carriers: Technological and Pharmacological Profile. *Nanomaterials* 2020, *10*, 287. [CrossRef]

43. Ghosh, I.; Bose, S.; Vippagunta, R.; Harmon, F. Nanosuspension for improving the bioavailability of a poorly soluble drug and screening of stabilizing agents to inhibit crystal growth. *Int. J. Pharm.* 2011, *409*, 260–268. [CrossRef]

44. Shimojo, A.A.M.; Fernandes, A.; Ferreira, N.R.E.; Sanchez-Lopez, E.; Santana, M.H.A.; Souto, E.B. Evaluation of the Influence of Process Parameters on the Properties of Resveratrol-Loaded NLC Using 22 Full Factorial Design. *Antioxidants* 2019, *8*, 272. [CrossRef] [PubMed]

45. Puglia, C.; Blasi, P.; Ostacolo, C.; Sommella, E.; Bucolo, C.; Platania, C.B.M.; Romano, G.L.; Geraci, F.; Drago, F.; Santonocito, D.; et al. Innovative Nanoparticles Enhance N-Palmitoylethanolamide Intraocular Delivery. *Front. Pharma- col.* 2018, *9*, 285. [CrossRef]

46. Mohammadi, M.; Pezeshki, A.; Abbasi, M.M.; Ghanbarzadeh, B.; Hamishehkar, H. Vitamin D3-Loaded Nanostructured Lipid Carriers as a Potential Approach for Fortifying Food Beverages; in Vitro and in Vivo Evaluation. *Adv. Pharm. Bull.* 2017, *7*, 61–71. [CrossRef] [PubMed]

47. Trotta, M.; Debernardi, F.; Caputo, O. Preparation of solid lipid nanoparticles by a solvent emulsification–diffusion technique. *Int. J. Pharm.* 2003, *257*, 153–160. [CrossRef]

48. Sarpietro, M.G.; Torrisi, C.; Di Sotto, A.; Castelli, F. Interaction of limonene, terpineol, and 1,8 cineol with a model of biomembrane: A DSC study. *Thermochim. Acta* 2021, *700*, 178938. [CrossRef]

49. Puglia, C.; Santonocito, D.; Musumeci, T.; Cardile, V.; Graziano, A.C.E.; Salerno, L.; Raciti, G.; Crascì, L.; Panico, A.M.; Puglisi, G. Nanotechnological Approach to Increase the Antioxidant and Cytotoxic Efficacy of Crocin and Crocetin. *Planta Med.* 2019, *85*, 258–265. [CrossRef]

50. Gökçe, E.H.; Sandri, G.; Egrilmez, S.; Bonferoni, M.C.; Güneri, T.; Caramella, C. Cyclosporine A-Loaded Solid Lipid Nanoparticles: Ocular Tolerance andIn VivoDrug Release in Rabbit Eyes. *Curr. Eye Res.* 2009, *34*, 996–1003. [CrossRef]

51. Leonardi, A.; Bucolo, C.; Romano, G.L.; Platania, C.B.M.; Drago, F.; Puglisi, G.; Pignatello, R. Influence of different surfactants on the technological properties and in vivo ocular tolerability of lipid nanoparticles. *Int. J. Pharm.* 2014, *470*, 133–140. [CrossRef]

52. Brugè, F.; Damiani, E.; Puglia, C.; Offerta, A.; Armeni, T.; Littarru, G.P.; Tiano, L. Nanostructured lipid carriers loaded with CoQ10: Effect on human dermal fibroblasts under normal and UVA-mediated oxidative conditions. *Int. J. Pharm.* 2013, *455*, 348–356. [CrossRef] [PubMed]

53. Lucas-Abellán, C.; Mercader-Ros, M.; Zafrilla, M.; Gabaldón, J.; Núñez-Delicado, E. Comparative study of different methods to measure antioxidant activity of resveratrol in the presence of cyclodextrins. *Food Chem. Toxicol.* 2011, *49*, 1255–1260. [CrossRef] [PubMed]

54. Chen, C.; Cheng, Y.C.; Yu, C.H.; Chan, S.-W.; Cheung, K.; Yu, P.H.F. In vitrocytotoxicity, hemolysis assay, and biodegradation behavior of biodegradable poly(3-hydroxybutyrate)-poly(ethylene glycol)-poly(3-hydroxybutyrate) nanoparticles as potential drug carriers. *J. Biomed. Mater. Res. Part A* 2008, *87*, 290–298. [CrossRef] [PubMed]

55. Caracciolo, P.C.; Rial-Hermida, M.I.; Montini-Ballarin, F.; Abraham, G.; Concheiro, A.; Alvarez-Lorenzo, C. Surface-modified bioresorbable electrospun scaffolds for improving hemocompatibility of vascular grafts. *Mater. Sci. Eng. C* 2017, *75*, 1115–1127. [CrossRef] [PubMed]

56. Weber, M.; Steinle, H.; Golombek, S.; Hann, L.; Schlensak, C.; Wendel, H.P.; Avci-Adali, M. Blood-Contacting Biomaterials: In Vitro Evaluation of the Hemocompatibility. *Front. Bioeng. Biotechnol.* 2018, *6*, 99. [CrossRef]

5. PREPARATION AND CHARACTERIZATION OF SOLID LIPID NANOPARTICLES (SLN) AND NANOSTRUCTURED LIPID CARRIERS (NLC) LOADED WITH BXL-A2

Cristina Torrisi[1, *], Maria Inês Teixeira[2,3], Nunzio Cardullo[4], Stefano Russo[1], Vera Muccilli[4], Paulo Jorge Costa[2,3] and Maria Grazia Sarpietro[1]

[1] Department of Drug and Health Sciences, University of Catania, Viale Andrea Doria 6, 95125 Catania, Italy;

[2] UCIBIO—Applied Molecular Biosciences Unit, MedTech—Laboratory of Pharmaceutical Technology, Department of Drug Sciences, Faculty of Pharmacy, University of Porto, Rua de Jorge Viterbo Ferreira, 228, 4050-313, Porto, Portugal;

[3]Associate Laboratory i4HB—Institute for Health and Bioeconomy, Faculty of Pharmacy, University of Porto, Rua de Jorge Viterbo Ferreira, 228, 4050-313, Porto, Portugal;

[4]Department of Chemical Sciences, University of Catania, Viale Andrea Doria 6, 95125 Catania, Italy

5.1. Introduction

Polyphenols are one of the largest and most widespread groups of secondary metabolites widespread in plant kingdom with marked biological activities. They are present in millions of different chemical structures and their characterization stands as a challenge[1]. In recent years, it is grown the interest in the isolation and identification of one of their subgroups: benzo[k,l]xanthene lignans (BXLs). The latter, unlike other polyphenols, have a limited availability in nature so, in 2009, a group of researchers developed a simple and biomimetic methodology for their synthesis [2], and a variety of synthetic benzoxanthenes have since been obtained and evaluated as antioxidant [3], anti-inflammatory [4], selective copper-chelators [5], antifungal [6], antiproliferative agents [7] and pro-apoptotic agents [8]. However, the lipophilic character of the xanthene core makes their use difficult in an aqueous medium, hindering their pharmacokinetic profile. One of the approaches to overcome this problem is the encapsulation of the molecules inside a carrier. In recent years, Solid Lipid Nanoparticles (SLN) and Nanostructured Lipid Carriers (NLC) have attracted the attention of numerous researchers as nanocarriers for lipophilic molecules such as BXLs[10]. SLN and NLC are colloidal systems stabilized by surfactants being the former one composed of solid lipids at room and body temperature and the second one composed of both solid and liquid lipids, as the core matrix. The presence of a liquid lipid allows to have a less organized lipid matrix and consequently a better drug encapsulation and limited drug expulsion during storage [11]. One of the major advantages of SLN and NLC is the nature of lipids, biocompatible and biodegradable, that make them safe and efficient as drug delivery systems. In this preliminary study, a bioactive benzoxanthene (BXL A2), reported in Figure 1, has been included in SLN and NLC. Unloaded and loaded SLN and NLC, have been prepared using hot high-pressure homogenization (HPH) method and characterized in terms of size, zeta potential, entrapment efficiency and stability. Moreover, their thermotropic behaviour and the possible drug-lipid interactions were evaluated by Differential Scanning Calorimetry (DSC) and Fourier-Transform Infrared spectroscopy (FTIR), respectively.

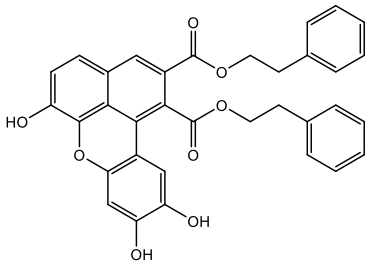

Figure 1: Structure of BXL A2.

5.2. Materials and methods

5.2.1. Materials

Precirol® ATO 5 (Glyceryl distearate) was kindly donated by Gattefossé (France). Tween® 80 (Polysorbate 80), was purchased from Sigma Aldrich Co (St. Louis, MO, USA). Mygliol® 812 (triglycerides of capric/caprylic acids) was acquired from Acofarma (Madrid, Spain). The ultrapure water used in all experiments was obtained from a Milli-Q® Direct 3 UV-R system (Millipore, Darmstadt, Germany). All the solvents used were of analytical grade and were purchased from Sigma-Aldrich (Steinheim, Germany).

5.2.2. Preparation of Solid Lipid Nanoparticles (SLN) and Nanostructured Lipid Carriers (NLC)

SLN and NLC were prepared by high-pressure homogenization technique (HPH)[9]. Precirol®ATO5 and Mygliol® 812 were used as solid and liquid lipids, respectively, while Tween 80 was used as non-ionic surfactant. Briefly, the lipid and the aqueous phases were heated to 70 °C, separately. When the two phases reached the same temperature, the aqueous phase was added drop by drop to the lipid phase. The prepared pre-emulsion was quickly transferred to the high-pressure hot homogenizing equipment (High-Pressure Homogenizer SPCH-10, Stansted Fluid Power, Essex, UK), being homogenized during three cycles at 350 bars, and then cooled and stored in a glass bottle at 25 °C. SLN-BXL A2 and NLC-BXL A2 were prepared with the same procedure. The compound was previously added to the lipid phase.

5.2.3. Characterization and stability studies of SLN and NLC

The lipid nanoparticles were characterized in terms of size, polydispersity index (PDI) and zeta potential (ZP). Z-Average size (Z-Ave) and PDI were determined by Dynamic Light Scattering (DLS) using a particle size analyzer with a light incidence angle of 90°

(Brookhaven Instruments, Holtsville, NY, USA). ZP was estimated by Electrophoretic Light Scattering (ELS) using the equipment previously reported. Before each measurement, all the samples were diluted in milli-Q water (dilution 1:100). To characterize and study the stability over time of the loaded and unloaded SLN and NLC, Z-Ave, PDI and ZP were monitored at different time points (day 0, day 3, day 7, day 15 and 1 month) after production and storage in closed glass vials at 25 ± 1 °C.

5.2.4. Encapsulation efficiency (EE)

The encapsulation efficiency (EE) was determined by ultrafiltration using centrifugal ultrafiltration tubes (Amicon® Ultra-4 filter 10 kDa cut-off, Millipore, Billerica, MA, USA). 1 mL of the SLN-BXL A2 and NLC-BXL A2 suspensions was diluted with 1 ml of ultrapure water, added to the upper chamber of the centrifugal tube and centrifuged at 5.000 g for 1 h at 4 °C using a Thermo Scientific TM Heraeus TM Multifuge X1R Refrigerated Benchtop Centrifuge (Waltham, MA, USA). The concentration of unentrapped BXL-A2 in the filtrate was subsequently determined by High-Performance Liquid Chromatography (HPLC) (Dionex UltiMate™ 3000, Thermo Scientific, Waltham, MA, USA). The chromatographic analysis was performed at 273 nm, using a BDS Hypersil TM C18 column (150 mm × 4.60 mm internal diameter, 5 µm particle size; Thermo Scientific, Waltham, MA, USA), and Acetonitrile/Water, 25:75 (v/v), as the mobile phase, eluted at a flow rate of 1 mL/min. Injections were made in triplicate (n = 3) with a sample volume of 10 µL. A calibration curve was built up by analysing independent standard solutions and fitting the respective data to the least squares linear regression, which gave a correlation coefficient (R) of 0.9994. BXL A2 entrapment efficiency (EE) was calculated by Eq. (1):

$$EE(\%) = \frac{W_t - W_e}{W_t}\, x\, 100 \qquad (1)$$

where *Wt* is the total amount of BXL A2 and *We* is the amount of the entrapped BXL A2.

5.2.5. Fourier Transform Infrared (FTIR) spectroscopy

To confirm the functionalization of the SLN and NLC with BXL A2, Fourier transform infrared spectroscopy (FTIR) was performed. The unloaded and loaded SLN and NLC were previously frozen overnight and lyophilized at −75 °C and 0.4 mBar using a LyoQuest freeze dryer (Telstar, Terrassa, Spain). The infrared spectra were obtained by

placing the samples (BXL A2, Precirol® ATO5, empty and loaded SLN and NLC) on a PerkinElmer Frontier™ FTIR Spectrometer (Waltham, MA, USA) equipped with a universal attenuated total reflectance (ATR) attachment and a diamond crystal. For each measurement, 32 scans at a resolution of 4 cm^{-1} were accumulated at frequencies between 4000 to 600 cm^{-1}.

5.2.6. DSC analysis

Calorimetric analysis was performed using a Mettler Toledo STARe thermoanalytical system (Greifensee, Switzerland) equipped with a DSC822 calorimetric cell. The calorimeter was calibrated using Indium (99.95%), based on the setting of the instrument. The sensitivity was automatically chosen as the maximum possible by the calorimetric system. 160 µl aluminum calorimetric pans were used. Enthalpy changes were calculated from the peak areas.

5.2.6.1. Empty and loaded SLN and NLC analysis

To evaluate the thermotropic behaviour of the formulations, they were submitted to DSC analysis under N_2 flow (70 ml/min) as follows: a heating scan from 5 to 85°C, at 2 °C/min, and a cooling scan from 85 to 5 °C, at 4 °C/min, for at least three times to confirm the reproducibility of data.

5.3. Results and discussions

5.3.1. Physicochemical characterization and stability studies

SLN and NLC in presence and in absence of BXL A2 were prepared and their Z Ave, PDI and ZP were determined. Stability studies were also performed by monitoring variations of these values for one month. As shown in Fig. 2, all the formulations have shown good values in terms of the above-mentioned analysis. Regarding the size (Fig. 2, a-b), the empty SLN have shown an initial value of 170 nm while the SLN-BXL A2 around 220 nm; so, the incorporation of BXL A2 exerted firstly an increment of size, which was stabilized over time at 150 nm for both formulations. The empty NLC and the NLC-BXL A2 have shown almost the same values of size (130 nm) all over the indicate period. PDI is as measurement of particles size distribution and the quality of nanoparticle systems; usually researchers consider PDI values of less than 0.5 as acceptable while 0.3 and below as optimum. Herein, as shown in Fig. 2 (c-d), SLN have exhibited a value of

0.3; this value increased significantly in SLN-BXL A2 at 15 days and in both empty and loaded SLN at 30 days. NLC have shown a PDI around 0.2, which increased slightly at 30 days for both formulations. Both SLN and NLC have good values in terms of polydispersity index. NLC can be considered less polydisperse with respect to SLN. ZP is another important parameter in evaluating the colloidal dispersion quality and its physical stability. In Fig. 2 (e-f) it is shown that there isn't a correlation in ZP values between empty and loaded nanoparticles, both for SLN and NLC; in general, the obtained values are an indication of stable formulations over the time.

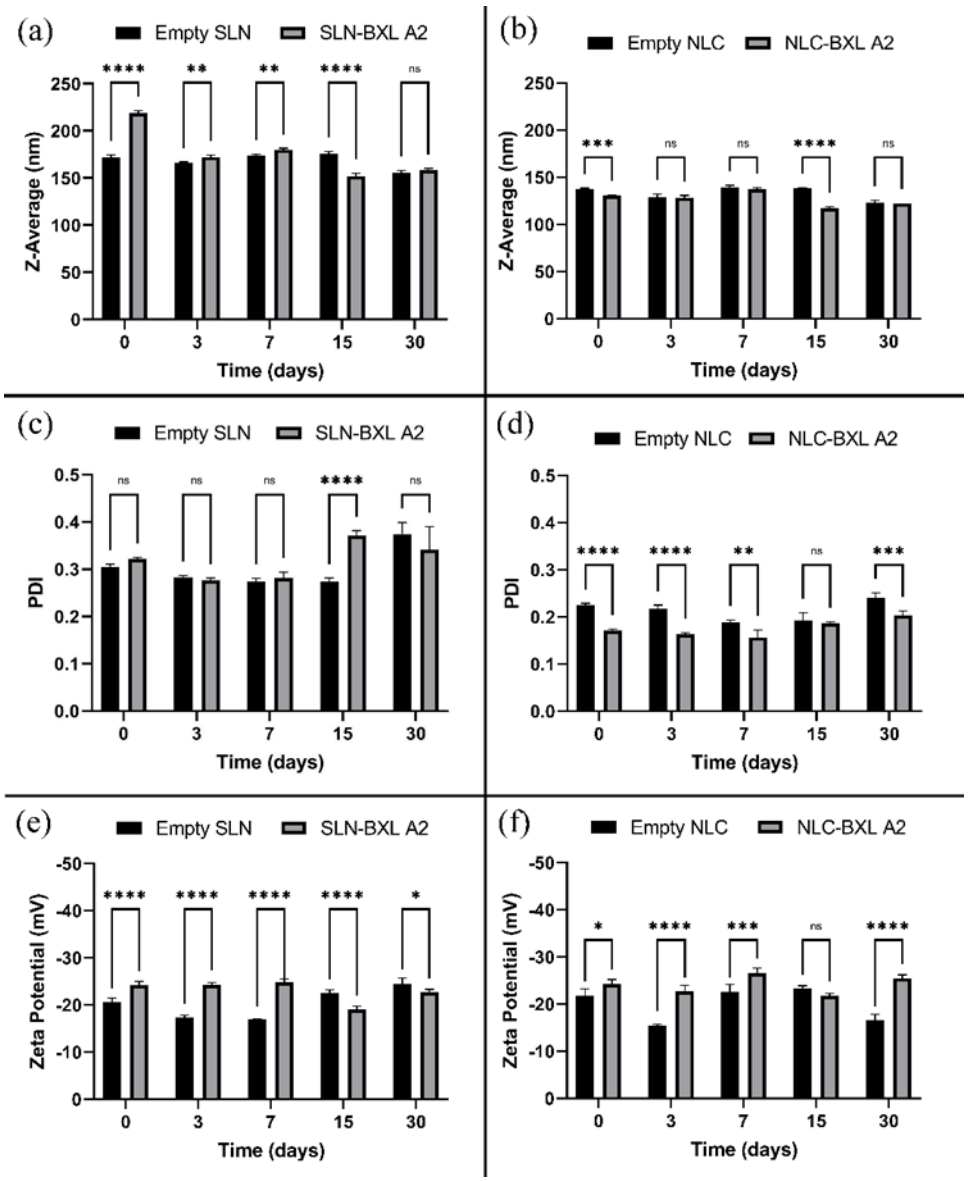

Figure 2: (a-b) Z-Ave, (c-d) PDI, (e-f) ZP of empty SLN and SLN-BXL A2 and empty NLC and NLC-BXL A2.

The entrapment efficiency, obtained with indirect method by using Amicon, was around 90%.

5.3.2. FTIR spectroscopy

To gain a better understanding on the state of the drug into the SLN and NLC, FTIR study is carried out. In Figure 3 (a) the spectra of bulk BXL A2, Precirol® ATO5, loaded and unloaded SLN and NLC are reported. Precirol® ATO5 presented several characteristic peaks, identified at 1470 cm^{-1} (C–C stretching), 1730 cm-1 (C=O stretching), and 2850 and 2914 cm^{-1} (C–H stretching), as reported elsewhere [12]. BXL A2 showed a broad peak from ≃ 3694 to 3024 cm^{-1} (O-H stretching) which partially overlaps multiple smaller, sharper peaks in the 3000-2800 cm^{-1} region (C-H stretching); these data confirm the presence of different phenol groups and the two alkyl ester chains. A strong sharp peak at 1696 cm^{-1}, with correlated overtone bands in the ≃ 1650-1480 cm^{-1} region, indicates the presence of an aromatic ester group, which is brought down to lower wavelengths due to the influence of an ortho ester group and of other three substituents on the aromatic ring. The 1300-800 cm^{-1} region is difficult to discriminate because it is crowded with multiple peaks, that can be roughly associated to: 1) C-O stretching of phenol and aromatic ester/ether groups; 2) C=C stretching of the various aromatic rings; 3) C-H stretching and bending (both in- and out-of-plane) of all the hydrocarburic moieties of the compound. The molecular signatures of SLN and NLC (empty and loaded) were comparable to that of Precirol® ATO5. This was to be expected, given the high lipid content compared to the drug but it is also a demonstration of successful entrapment of the drug into the lipid nanoparticles, since most of absorption bands ascribed to BXL A2 were not visible in the SLN and NLC spectra, as it is possible to see in Figure 3 (b).

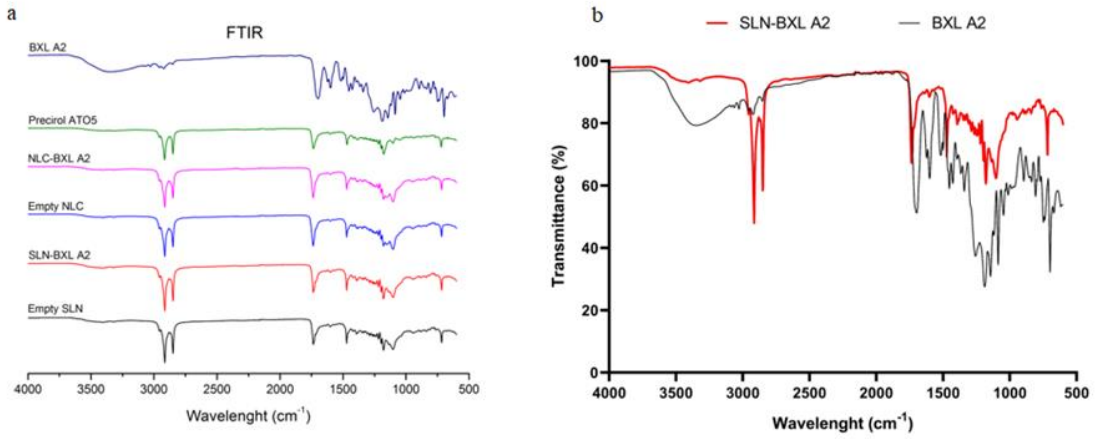

Figure 3: a - FTIR of bulk BXL A2, Precirol® ATO5, loaded and unloaded SLN and NLC;b - FTIR of SLN-BXL A2 and BXL A2

5.3.3. DSC studies

The thermotropic behaviour of the SLN and NLC (empty and containing BXL-A2) formulations was evaluated by DSC (Figure 4 - 5). The calorimetric curve of empty SLN is characterized by a main peak at 54.90 °C (characteristic of Precirol® ATO) and a small shoulder at lower temperature. In SLN BXL-A2 calorimetric curve, the shoulder of unloaded SLN becomes a peak at 51.80°C; a primary peak at 54.90°C can be observed. The discrete differences among the empty SLN and SLN BXL-A2 calorimetric curves suggest that BXL can be inside the SLN structure, affecting the thermotropic behaviour.

The calorimetric curve of empty NLC displayed a main peak at 54.50 °C and a broad peak at 47.80 °C. In NLC-BXL A2, the presence of the compound causes the shift of the main peak from 54.50 °C to 49.80 °C and the shift of the broad peak from 47.80 °C to 45.30 °C; in addition, this peak becomes sharper. The effect of BXL-A2 on the NLC is stronger with respect to SLN; probably because the compound is better distributed in the NLC structure.

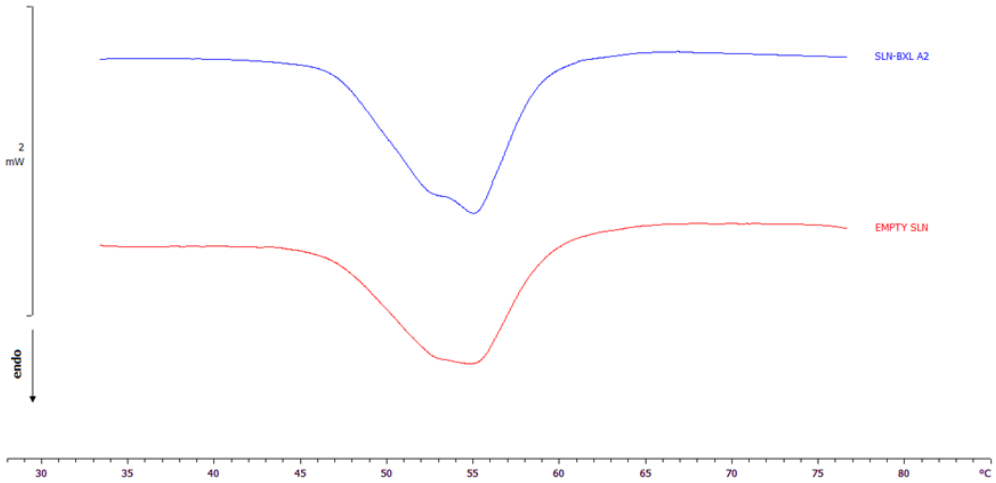

Figure 4: Calorimetric curves, in heating mode, of empty SLN and SLN-BXL A2

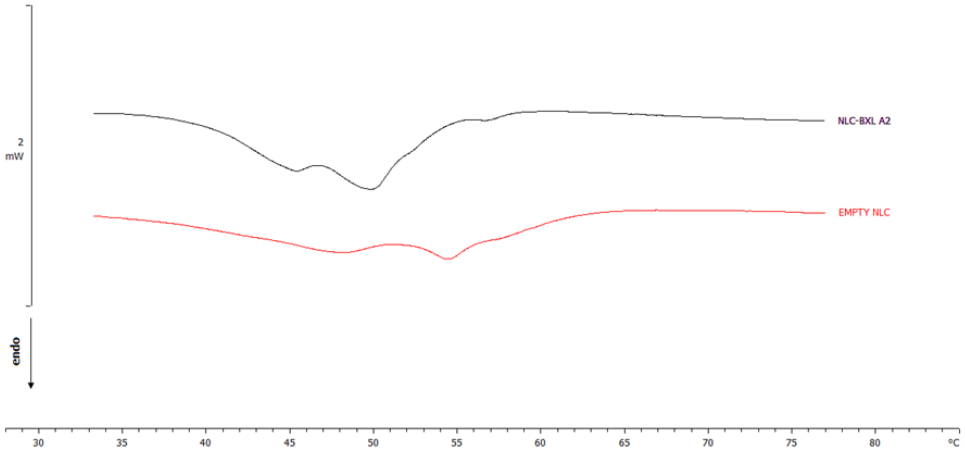

Figure 5: Calorimetric curves, in heating mode, of empty NLC and NLC-BXL A2

5.4. Conclusions

The high-pressure homogenization method permits to obtain SLN and NLC with promising physiochemical characteristics possessing good Z-Ave, PDI, ZP and being able to encapsulate around 90% of compound. FTIR and DSC studies confirmed the presence of BXL-A2 inside the nanoparticles. Other studies are ongoing to consolidate the obtained results; to evaluate the compound release; the interaction of the nanoparticles with biomembrane models; the in vitro and in vivo biological activity of BXL-A2 free or encapsulated in the nanoparticles will also be studied.

5.5. References

1. Rupasinghe, H. P. V. Application of NMR Spectroscopy in Plant Polyphenols Associated with Human Health. 91.

2. Daquino, C., Rescifina, A., Spatafora, C. & Tringali, C. Biomimetic Synthesis of Natural and "Unnatural" Lignans by Oxidative Coupling of Caffeic Esters. Eur J Org Chem 13 (2009).

3. Spatafora, C., Daquino, C., Tringali, C. & Amorati, R. Reaction of benzoxanthene lignans with peroxyl radicals in polar and non-polar media: cooperative behaviour of OH groups. 4 (2013).

4. Gerstmeier, J. Novel benzoxanthene lignans that favorably modulate lipid mediator biosynthesis_ A promising pharmacological strategy for anti-inflammatory therapy. Biochem. Pharmacol. 12 (2019).

5. Floresta, G., Cardullo, N., Spatafora, C., Rescifina, A. & Tringali, C. A Rare Natural Benzo[k,l]xanthene as a Turn-Off Fluorescent Sensor for Cu2+ Ion. Int. J. Mol. Sci. 21, 6933 (2020).

6. Genovese, C. et al. Bioinspired benzoxanthene lignans as a new class of antimycotic agents: synthesis and Candida spp. g. 11.

7. Micco, S. D. et al. Structural basis for the potential antitumour activity of DNA-interacting benzo[kl]xanthene lignans. 10 (2011).

8. Vijayakurup, V. Phenethyl caffeate benzo[kl]xanthene lignan with DNA interacting properties induces DNA damage and apoptosis in colon cancer cells. Life Sci. 9 (2012).

9. MuÈller, R. H., MaÈder, K. & Gohla, S. Solid lipid nanoparticles (SLN) for controlled drug delivery ± a review of the state of the art. Eur. J. Pharm. Biopharm. 17 (2000).

10. Muller, R. H., Radtke, M. & Wissing, S. A. Solid lipid nanoparticles (SLN) and nanostructured lipid carriers (NLC) in cosmetic and dermatological preparations. Adv. Drug Deliv. Rev. 25 (2002).

11. Selvamuthukumar, S. & Velmurugan, R. Nanostructured Lipid Carriers: A potential drug carrier for cancer chemotherapy. Lipids Health Dis. 11, 159 (2012).

12. Vitorino, C. et al. QbD-driven development of intranasal lipid nanoparticles for depression treatment. Eur. J. Pharm. Biopharm. 153, 106–120 (2020).

6. LIST OF PUBLICATIONS

1) Marrazzo A., Torrisi C., Barbaraci C., Amata E., Castelli F., Sarpietro M.G. Interaction of new sigma ligands with biomembrane models evaluated by differential scanning calorimetry and Langmuir-Blodgett studies. Colloids and Surfaces B: Bioint. Vol. 201, May 2021, 111643.

2) Sarpietro M.G., Torrisi C., Pignatello R., Castelli F., Montenegro L. Assessment of the technological properties of idebenone and tocopheryl acetate co-loaded lipid nanoparticles. Appl. Sci. 2021, 11, 3553.

3) Torrisi, C., Morgante, A., Malfa, G., Acquaviva, R., Castelli, F., Pignatello, R., Sarpietro, M.G. Sinapic Acid Release at the Cell Level by Incorporation into Nanoparticles: Experimental Evidence Using Biomembrane Models. Micro 2021, 1, 120–128.

4) Santonocito D., Puglia C., Torrisi C., Giuffrida A., Greco V., Castelli F., Sarpietro M.G. Calorimetric Evaluation of Glycyrrhetic Acid (GA)-and Stearyl Glycyrrhetinate (SG)-Loaded Solid Lipid Nanoparticle Interactions with a Model Biomembrane. Molecules 2021, 26, 4903.

5) Torrisi C., Di Guardia M., Castelli F. and Sarpietro M.G. Naringenin Release to Biomembrane Models by Incorporation into Nanoparticles. Experimental Evidence Using Differential Scanning Calorimetry. Surfaces 2021, 4, 295–305.

6) Santonocito D., Vivero-Lopez M., Lauro M.R., Torrisi C., Castelli F., Sarpietro M.G., Puglia C. Design of Nanotechnological Carriers for Ocular Delivery of Mangiferin: Preformulation Study. Molecules 2022, 27, 1328.

7) Torrisi C., Malfa G.A., Acquaviva R., Castelli F. and Sarpietro M.G. Effect of Protocatechuic Acid Ethyl Ester on Biomembrane Models: Multilamellar Vesicles and Monolayers. Membranes 2022, 12, 283.

8) Torrisi C., Cardullo N., Muccilli V., Tringali C., Castelli F. and Sarpietro M.G. Characterization and Interaction with Biomembrane Model of Benzo[k,l]xanthene Lignan Loaded Solid Lipid Nanoparticles. Membranes 2022, 12, 615.

9) Torrisi C., Cardullo N., Russo S., La Mantia A., Acquaviva R., Muccilli V., Castelli F. and Sarpietro M.G. Benzo[k,l]xanthene Lignan-Loaded Solid Lipid Nanoparticles for Topical Application: A Preliminary Study. Molecules 2022, 27, 5887.

7. CONFERENCES ATTENDED

- 7-9 November 2019, "CRS Italy Chapter Annual Workshop – Catania - Steering the Clinical Translation of Delivery Systems for Drugs and Health Products";
- 13-14 February, 2020, "MITO – un viaggio tra nanomedicina e direzionamento dei farmaci" (MITO - Between nanomedicine and targeting drugs) - Milan;
- 7-9 October 2022, "CRS Italy Workshop 2022 – Genoa – Unmet Medical Needs: Opportunities and Challenges for Drug Delivery Scientists".